République Algérienne Démocratique et Populaire

Ministère de l'Enseignement Supérieure et de la Recherche Scientifique

Université Mohamed Khider - Biskra

Faculté des Science et de la technologie

Département: chimie industrielle

Ref : ……..

Thèse Présentée en vue de l'obtention du Diplôme de

Doctorat en Génie des Procédés

Option : Génie des Matériaux

Optimisation des propriétés physico-chimiques et photocatalytiques des couches minces à base d'oxyde

Présentée par :

Hadjer Barkat

Soutenue publiquement le : 09/ 06/ 2025

Devant le jury compose de :

Pr. Abdallah ATTAF	**Professeur**	**Université de Biskra**	**Président**
Dr. Elhachmi GUETTAF TEMAM	**M.C.A**	**Université de Biskra**	**Encadreur**
Pr. Hachemi BEN TEMAM	**Professeur**	**Université de Biskra**	**Co Encadreur**
Pr. Abdelkrim MERZOUGUI	**Professeur**	**Université de Biskra**	**Examinateur**
Dr. Oussama BACHA	**M.C.A**	**Université de Ouargla**	**Examinateur**

Democratic and People's Republic of Algeria
Ministry of Higher Education and Scientific Research
Mohamed Khider University – Biskra

Faculty of Science and Technology
Department: industrial chemistry

Ref : ……..

Thesis Presented with a view to obtaining the Diploma of

Doctorate in Process Engineering
Option: Materials Engineering

Optimization of the physico-chemical and photocatalytic properties of oxide-based thin films

Presented by:
Hadjer Barkat

Publicly supported on: 09 / 06 / 2025

Before the jury composed of:

Pr. Abdallah ATTAF	**Professor**	**University of Biskra**	**President**
Dr. Elhachmi GUETTAF TEMAM	**M.C.A**	**University of Biskra**	**Supervisor**
Pr. Hachemi BEN TEMAM	**Professor**	**University of Biskra**	**Co Supervisor**
Pr. Abdelkrim MERZOUGUI	**Professor**	**University of Biskra**	**Examiner**
Dr. Oussama BACHA	**M.C.A**	**University of Ouargla**	**Examiner**

Dedication

I dedicate this thesis to the special people who deserve much respect and great love:

To my beloved family,

This achievement would not have been possible without your unwavering love, support, and encouragement. You have been my pillars of strength, guiding me through every challenge and celebrating each success along the way. Your belief in me has been my greatest motivation, and for that, I am eternally grateful.

Thank you for standing by my side through every step of this journey. This milestone is as much yours as it is mine.

To my friends and colleagues,

To all those who helped me without hesitation,

Thank you, a lot, indeed.

With all my love and appreciation,

Hadjer Barkat

Acknowledgments

*First and foremost, my deepest gratitude to **Allah**, who granted me the strength, perseverance, and confidence to complete this work.*

*I would like to express my sincere appreciation to my supervisor, **Dr. Elhachmi Guettaf Temam**, for his invaluable guidance, patience, and unwavering support throughout my research journey. His expertise and insightful advice have been instrumental in shaping this work, and I am truly grateful for the opportunity to learn under his mentorship.*

*I extend my profound thanks to my co-supervisor, **Prof. Hachemi Ben Temam**, for his continuous encouragement, constructive feedback, and invaluable contributions that greatly enriched the quality of this thesis.*

I am deeply grateful to the esteemed members of the examination committee for their time, effort, and valuable insights:

- ***Prof. Abdallah Attaf**, President of the Jury, for his thoughtful evaluation and valuable discussions that helped refine my research.*
- ***Prof. Abdelkrim Merzougoui**, Examiner, for his constructive critique and insightful comments, which have been essential in enhancing the scientific rigor of this work.*
- ***Dr. Oussama Bacha**, Examiner, for his detailed analysis, valuable suggestions, and encouragement throughout this process.*

*A special note of appreciation goes to **Prof. Saad Rahmane** and **Prof. Ouahab Abdelouahab** for their valuable guidance, insightful discussions, and support, which contributed to the refinement of my research.*

*I also extend my heartfelt thanks to **Mr. Gasmi Brahim** and all the engineers at the LPCMA laboratory for their technical support and assistance in carrying out the experimental work.*

*A special note of appreciation goes to **my family**, whose unwavering love, sacrifices, and encouragement have been my greatest motivation. Your support has been my foundation, and I dedicate this achievement to you.*

*Finally, I would like to thank **my friends**, **colleagues**, and **everyone** who has contributed, directly or indirectly, to the successful completion of this work. Your encouragement and guidance have been invaluable, and I am truly grateful for your support*

With sincere gratitude,
Hadjer Barkat

Table of Contents

Chapter II. Experimental Procedure: Synthesis and characterization techniques

Chapter III. SILAR-Processed ZnO Thin Films: Influence of Ba Doping Concentrations on Photocatalytic Degradation and Wettability

Chapter IV. Influence of SILAR Deposition Cycles on Ba-Doped ZnO Thin Films and their Photocatalytic Application

Chapter V. Influence of Annealing Temperature on Ba-Doped ZnO Thin Films and their Photocatalytic Application

Liste of Figures

Liste of Tables

General Introduction

General Introduction

Metal semiconducting oxides (MSOs) are highly regarded for their versatility in applications like solar cells and photocatalysis. Their ability to exist in various oxidation states, along with large surface areas, makes them ideal for addressing environmental issues and removing contaminants. With the growing concern over organic pollutants in wastewater, MSOs are poised to play a key role in environmental remediation. Their potential in mitigating environmental degradation is significant [1]. Moreover, the integration of metal oxide semiconductors in photocatalytic processes enhances pollutant degradation under visible light, overcoming a key limitation of traditional photocatalysts. Recent advancements, particularly through doping, have improved their photocatalytic activity and expanded their effectiveness in treating a wider range of wastewater contaminants [2].

Zinc oxide (ZnO) is a promising n-type semiconductor with a wide band gap and exceptional thermal and mechanical stability, making it suitable for various applications like photovoltaics, photocatalysis, and antimicrobial agents. Recent studies show that ZnO's photocatalytic efficiency can be significantly improved by doping with elements like barium (Ba). Ba doping enhances ZnO's properties by promoting grain growth, creating active sites, and improving stability, light absorption, and hydrophilicity[3][4]. This modification helps ZnO generate more reactive oxygen species under visible light, making it more effective in degrading organic pollutants and enhancing its potential for wastewater treatment and environmental remediation [5].

There are various physical and chemical techniques for synthesizing ZnO thin films [6], including physical vapor deposition (PVD), chemical bath deposition (CBD), sol–gel, spray pyrolysis, dip coating, and spin coating. Among these numerous techniques, the Successive Ionic Layer Adsorption and Reaction (SILAR) method stands out for its distinct advantages, such as simplicity, eco-friendliness, and cost-effectiveness. Additionally, it allows for precise control over film thickness and composition, is compatible with a wide range of substrates, and enables the fabrication of highly uniform films. This technique also requires minimal equipment, making it highly accessible for both research and industrial applications [7].

Hence, this work aims to demonstrate the optimal parameters for synthesizing ZnO thin films via the SILAR process for various applications. By varying the concentration of barium dopants,

the number of cycles, and the annealing temperature. The goal is to improve the structural, morphological, topographical, and optical properties of undoped and Ba-doped ZnO thin films and their utilization for fundamental study of the photocatalytic degradation of methylene blue dye under sunlight irradiation. Our experimental research was conducted at the Physics of Thin Films and Applications Laboratory (LPCMA), University of Biskra, Algeria.

This thesis is separates into five chapters ordered as follows:

The first chapter reviews thin films and their synthesis, particularly the SILAR process. We also discuss semiconductors and their classification. Furthermore, we highlight the unique properties of zinc oxide and their applications, focusing on the photocatalytic process.

The second chapter describes the SILAR deposition procedure, and details about the steps and conditions of the samples' preparation. Also, we notice the different films' characterization techniques, including X-ray diffractometer (XRD), scanning electron microscopy & energy dispersive X-ray spectroscopy (SEM & EDX), UV- vis spectrophotometer, and profilometer to determine structural, morphological, optical, and topographical properties respectively.

The third chapter investigates the effect of Ba-doping concentrations (1 wt.%, 3 wt.%, 5 wt.%, 7 wt.%) on ZnO thin films for photocatalytic degradation of methylene blue (MB) and wettability. It also provides an analysis and discussion of the results obtained.

The fourth chapter presents the impact of the deposition cycles (3, 6, 9, 12, and 15 cycles) on the Ba-doped ZnO films for the photodegradation of methylene blue (MB) and amoxicillin (AMX), alongside their wettability properties. Moreover, it interprets the results obtained.

The fifth chapter studies the influence of annealing at different temperatures (300 °C, 350 °C, 400 °C, and 450 °C) on the Ba-doped ZnO thin films and their photocatalytic application on methylene blue dye. We discuss and interpret the obtained results.

Finally, we give a general conclusion summarize of the main obtained results in this thesis.

References

[1] M. Hajji, M. Ajili, N. Jebbari, A. Garcia loreiro, N.T. Kamoun, Photocatalytic performance and solar cell applications of coupled semiconductor CuO– ZnO sprayed thin films: Coupling effect between oxides, Optical Materials, vol. 140, 2023, doi: https://doi.org/10.1016/j.optmat.2023.113798.

[2] W. Vallejo, C.E. Diaz-Uribe, F. Duran, Kinetic and thermodynamic study of methylene blue adsorption on TiO_2 and ZnO thin films, Materials, vol. 16, 2023, doi: https://doi.org/10.3390/ma16124434.

[3] A. Baig, M. Siddique, S. Panchal, A Review of fisible-light-active zinc oxide photocatalysts for environmental application, Catalysts, vol. 15, no.2, 2025, doi https://doi.org/10.3390/catal15020100.

[4] S. Kalpana, N. Senthilkumar, R. Jeyachitra, T.S. Senthil, Synthesis of barium-doped β-Bi_2O_3 photocatalyst with enhanced degradation of methylene blue and rhodamine-B dyes under UV–Vis light irradiation, Materials Science and Engineering: B, volume 306, 2024, doi: https://doi.org/10.1016/j.mseb.2024.117483.

[5] Y. Yang, T. Shao, Y. Zhang, Y. Lu, M. Li, H. Liu, Q. Xu, Y. Xia, Anionic S-doping of a $ZnMn_2O_4$/CNTs cathode material enhances its Zn^{2+} storage performance in aqueous zinc-ion batteries, Journal of Power Sources, vol. 564, 2023, doi: https://doi.org/10.1016/j.jpowsour.2023.232863.

[6] A. Murugan, V. Siva, A. Samad Shameem, S.A. Bahadur, Optimization of adsorption and reaction time of SILAR deposited Cu_2ZnSnS_4 thin films: Structural, optical and electrochemical performance, Journal of Alloys and Compounds, vol. 856, 2021 doi: https://doi.org/10.1016/j.jallcom.2020.158055.

[7] H. Barkat, E. Guettaf, T. Hachemi, B. Temam, N. Mokrani, S. Rahmane, Thickness - dependent photocatalytic performance and wettability of barium-doped ZnO thin films synthesized via SILAR technique, Transition Metal Chemistry, 2025, doi: https://doi.org/10.1007/s11243-025-00631-z.

Chapter I.

A bibliographic review

I.1 Introduction

Zinc oxide (ZnO) thin films are critical in modern technology, offering high transparency, a wide bandgap (3.37 eV), and excellent photocatalytic activity, making them ideal for optoelectronic devices, sensors, and photocatalysis. Their synthesis using methods such as physical vapor deposition (PVD), sputtering, and modified sol-gel techniques significantly influences their structural, electrical, and photocatalytic properties, with factors like deposition temperature playing a crucial role in enhancing nanorod orientation and defect reduction [1][2][3]. Photocatalytically, ZnO thin films generate electron-hole pairs under UV light, producing reactive oxygen species that degrade organic pollutants, with improvements seen in films treated with hot air for enhanced photo-corrosion resistance. Additionally, their optical and electrical properties enable their application in optoelectronic devices and sensors, such as ethanol detectors [3]. Despite these advancements, challenges remain in optimizing synthesis and deposition processes to further enhance their performance and broaden their applicability in emerging technologies.

This chapter provides a comprehensive exploration of thin films, emphasizing the remarkable attributes of ZnO. The discussion begins with an overview of thin films and their fundamental properties, followed by a detailed examination of the diverse growth techniques employed in their synthesis. The chapter also highlights ZnO's significant role in photocatalytic applications, showcasing its effectiveness in environmental remediation and clean energy production.

Through this detailed exposition, the chapter aims to:

- Introduce the concept of thin films.
- Highlight the unique properties of zinc oxide.
- Outline various ZnO thin-film growth techniques.
- Discuss the extensive applications of ZnO, with a focus on photocatalysis.

By achieving these objectives, the chapter seeks to establish a foundational understanding of ZnO thin films, paving the way for further discussions on their technological implications.

I.2 Thin films

I.2.1 Definition of thin films

Thin films are materials with grain sizes below 1000 nm, created by depositing a material onto a support called a "substrate." They are distinguished by their ultra-thin surface thickness,

ranging from a few nanometers (nm) to micrometers (μm) [4]. Factors such as substrate temperature, energy input, and chamber pressure significantly influence their growth and properties [5]. While thin films are not a recent innovation, they have gained renewed prominence due to their adaptability and effectiveness in advancing modern scientific and commercial applications.

I.2.2 Fabrication of thin films

Thin films are deposited onto substrates using various techniques, including thermal evaporation, chemical decomposition, or the vaporization of source materials through energetic particles or photons. The deposition process generally involves three key steps [6]:

- generating suitable atomic, molecular, or ionic entities,
- transporting these entities to the substrate,
- condensing them to form a solid layer, either directly or via electrochemical or chemical processes.

The characteristics of thin films, such as their structure and performance, are influenced by preparation conditions, including the type of substrate, post-deposition annealing temperature, and the specific deposition technique employed [7].

I.3 Semiconductors material

I.3.1. Definition

Semiconductors are solid materials that are structurally sensitive in electric conduction and usually have comparatively low energy band-gaps and their resistivity lies intermediate between the conductors and insulators [8]. **Figure I.1** summarized the semiconductors in part of the periodic table from Group II to Group VI [8].

II	III	IV	V	VI
${}_{4}\mathrm{Be}$ $2s^2$	${}_{5}\mathrm{B}$ $2s^2 2p$	${}_{6}\mathrm{C}$ $2s^2 2p^2$	${}_{7}\mathrm{N}$ $2s^2 2p^3$	${}_{8}\mathrm{O}$ $2s^2 2p^4$
${}_{12}\mathrm{Mg}$ $3s^2$	${}_{13}\mathrm{Al}$ $3s^2 3p$	${}_{14}\mathrm{Si}$ $3s^2 3p^2$	${}_{15}\mathrm{P}$ $3s^2 3p^3$	${}_{16}\mathrm{S}$ $3s^2 3p^4$
${}_{30}\mathrm{Zn}$ $3d^{10}$ $4s^2$	${}_{31}\mathrm{Ga}$ $3d^{10}$ $4s^2 4p$	${}_{32}\mathrm{Ge}$ $3d^{10}$ $4s^2 4p^2$	${}_{33}\mathrm{As}$ $3d^{10}$ $4s^2 4p^3$	${}_{34}\mathrm{Se}$ $3d^{10}$ $4s^2 4p^4$
${}_{48}\mathrm{Cd}$ $4d^{10}$ $5s^2$	${}_{49}\mathrm{In}$ $4d^{10}$ $5s^2 5p$	${}_{50}\mathrm{Sn}$ $4d^{10}$ $5s^2 5p^2$	${}_{51}\mathrm{Sb}$ $4d^{10}$ $5s^2 5p^3$	${}_{52}\mathrm{Te}$ $4d^{10}$ $5s^2 5p^4$

Figure I.1 The periodic table from Group II to Group VI

In transparent conducting oxides (TCOs), the nonmetal component denoted as B consists of oxygen. When they are incorporated with different metals or metal combinations denoted as A, they form a compound known as semiconductors (AyBz) with various opto-electrical properties. It is possible to modify and optimize these characterizations by doping with metals, metalloids, or nonmetals [9]. Further, the introducing of dopants (donors) into the films aims to stabilize their conductivity by increasing the concentration of impurity donors instead of depending only on oxygen vacancies [10]. Furthermore, this addition of impurities to semiconductors changes their properties without changing their crystalline structure [11]. Several oxides materials have been employed as conducting coatings on glasses such as indium oxide ln_20_3, magnesium oxide MgO, Tin dioxide $Sn0_2$, and Zinc oxide ZnO which are attracted the attention of the global research for many decades.

I.3.2 Classification of Semiconductors

Semiconductors can be classified as:

- Intrinsic semiconductor

An intrinsic semiconductor refers to a semiconductor material of high chemical purity in which the conduction band's quantity of holes (positive carriers) is equivalent to the quantity of electrons (negative carriers) [12].

- Extrinsic semiconductor

An extrinsic semiconductor refers to the introduction of a very small quantity of impurity atoms, which are named “dopants,” into an intrinsic semiconductor (pure silicon Si or pure

germanium Ge) to ameliorate the conductivity. Usually, the concentration of doping atoms is approximately equivalent to 0.01 ppm [12][13]. An extrinsic semiconductor can be further categorized into:

- N-type Semiconductor

In this type the majority charge carriers are electrons. This is accomplished by addition donor impurities into the semiconductor crystal lattice. Specifically, when an intrinsic semiconductor (Silicon or Germanium) is doped by pentavalent impurity from the Group V in the periodic table, then, four electrons out of five valence electrons bonds with the four electrons of Ge or Si. The fifth electron of the dopant is set free and transfer it to the conduction band. Because this electron is already in excess, it does not create a corresponding hole in the valence band. Consequently, the impurity atom donates a free electron for conduction in the lattice and is referred to as "Donor " which creates a n-type semiconductor [13].

- P-type Semiconductor

In this type, the majority of charge carriers are holes. This is accomplished by adding acceptor impurities to the semiconductor crystal lattice. In particular, when a pure semiconductor is doped by trivalent impurities from Group III in the periodic table, then the three valence electrons of the impurity bond with three of the four valence electrons of the semiconductor create an absence of electrons and formation of holes in the impurity that are ready to accept bonded electrons are called "acceptors, which create a p-type semiconductor [12].

I.3.3 Criteria selection of transparent conducting oxides

Transmission and electrical conductivity are considered the most crucial properties when selecting an organic transparent conductor (OTC) and should ideally be maximized. However, other factors are significant, including thermal stability, chemical durability, mechanical resistance, minimum deposition temperature, toxicity, and production cost. The variety of applications for transparent conductors clearly shows that no single material is ideal for every use. The choice of a material depends on which property is deemed most critical for the specific application. **Table I.1** summarize some of the key criteria that can impact the choice of a transparent conducting material [14].

Table I.1 Property of some transparent conducting material.

Property	*Material*
Highest transparency	ZnO:F, Cd_2SnO_4
Highest conductivity	In_2O_3:Sn
Best thermal stability	SnO_2:F, TiN, Cd_2SnO_4
Best chemical durability	SnO_2:F
Least toxic	ZnO:F, SnO_2:F
Lowest cost	SnO_2:F

I.3.4 Applications of transparent conducting oxides

Transparent conducting oxides (TCOs) have diverse applications, including solar cells, flat-panel displays, photovoltaic panels, gas sensors, automotive windshield defrosters, static electricity dissipators in photocopiers, touch-panel controls, low-emissivity windows in buildings, heated transparent mirrors, and electrochromic windows. TCOs also play a crucial role in optoelectronic devices such as light-emitting diodes, organic light-emitting diodes, thin film transistors, and organic thin film transistors [15].

I.3.5 Semiconductors as Photocatalysts

A photocatalyst is defined as a material that accelerates a reaction when it absorbs photons without being consumed in the process [16].

Semiconductor compounds exhibit critical functionality as photocatalytic materials, facilitating their pivotal role in a wide array of advanced oxidation processes for clean energy generation and environmental remediation.

Semiconductors possess the ability to act as sensitizers for light-induced redox processes owing to their unique electronic band structure. This structure is characterized by a filled valence band (VB) and an empty conduction band (CB) separated by an energy gap known as the bandgap (Eg) [17]. In addition, an ideal semiconductor photocatalyst should be highly photo-active and photo-stable, making TiO_2 and ZnO being the most commonly utilized materials for this purpose [18].

I.4 Zinc oxide (ZnO)

Researchers have studied zinc oxide, an inorganic compound with the chemical formula ZnO, as a versatile semiconductor material for over 80 years, and it is applicable in vast optoelectronics applications, including light-emitting diodes, lasers, photodetectors, etc. In its solid state, ZnO appears as an odorless, off-white to pale yellow powder, characterized by its insolubility in water but being soluble in acids and alcohols. A notable advantage of ZnO is its abundance and cost effectiveness, which renders it an attractive semiconductor candidate for many applications across various technological domains [4].

I.4.1 The choice of ZnO

The most attractive characteristics of zinc oxide are noted below [19] [9] [20] [21] [22] [23]:

- ZnO is a non-toxicity compound and abundance presence on the earth.
- ZnO possesses an exceptionally high exciton binding energy of 60 meV and large band gap (Eg ~ 3.37 eV).
- High transparency in the visible range.
- ZnO has a good electron-donating property in its pure state, owing to its intrinsic electrical characteristics.
- Have a high catalytic performance.
- ZnO is eco-friendly, and it is not dangerous when eliminated at the end of its life cycle.

I.4.2 Properties of zinc oxide

- Structural and crystallographic properties

Generally, ZnO has three different forms of crystallization, as shown in **Figure I.2**: hexagonal wurtzite structure, cubic zinc blende, and rock salt [6]. The most common crystal structure of ZnO is the hexagonal wurtzite structure (B4 type) with lattice parameters a = 0.325 nm and c = 0.521 nm, which is thermodynamically stable at normal conditions (ambient temperature and pressure) [24]. However, when ZnO is deposited at high pressures on certain substrates with cubic symmetry, it synthesizes according to the cubic blende B3 (B3 type). Furthermore, when the wurtzite structure of ZnO is exposed to high hydrostatic pressure (10^{-15} GPa), it changes into the metastable rocksalt (B1 type) [23].

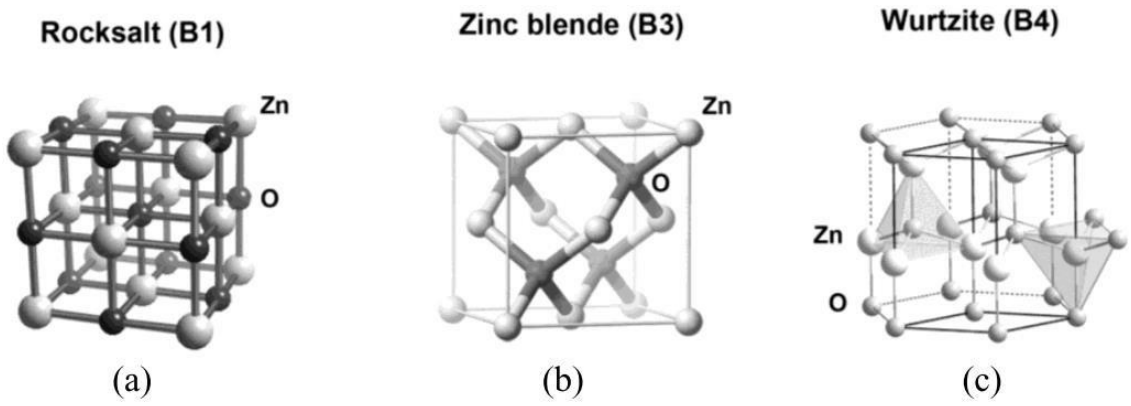

Figure I.2. Different structural of Zinc oxide [25]

Overall, there is no center of inversion in wurtzite, which is composed of alternating planes of zinc and oxygen atoms. wurtzite is intrinsically asymmetric along the c-axis, or the (001) direction, thus being an anisotropic crystal. This structure lattice is fourfold coordinated. That is, each atom has four nearest neighbor atoms, the zinc ion surrounded by tetrahedral oxygen ions and vice versa. Certainly, this type of tetrahedral coordination in ZnO forms a non-central symmetric structure with polar symmetry along the hexagonal axis. This not only contributes to the presence of piezoelectricity and spontaneous polarization but also plays a significant role in crystal growth, etching, and defect formation in ZnO [25] [26].

- optical properties

Zinc oxide presents compelling electrical properties that render it highly valuable for various technological applications. ZnO thin films have a low electrical resistivity and a high transmittance around 80-90%, in the visible and near-ultraviolet range. This making them a good candidate for various applications requiring transparency, such as solid state display devices, optical coatings heaters chemical sensors, hybrid and heterojunction solar cells, light emitting diodes, bioimaging, and conductive transparent layer for photovoltaic applications. Additionally, ZnO has a wide direct optical bandgap of approximately 3.3 eV at room temperature [27] [28][29].

- Chemical and catalytic properties

Zinc oxide exhibits diverse chemical properties that contribute to its versatility and widespread use in various industrial and technological applications. ZnO is recognized for its simple manufacturing techniques, cost-effectiveness, minimal toxicity, and large surface area compared with other chemical materials [30]. Additionally, ZnO shows high thermal stability, decomposing

at temperatures above 1975°C, which makes it suitable for high-temperature applications. These chemical natures and surface properties make ZnO a valuable catalyst. Specifically, zinc oxide is utilized in gas sensing applications for detecting hydrogen sulfide (H_2S), carbon dioxide (CO_2), hydrogen (H_2), and methane (CH_4). Additionally, ZnO is used for the efficient photocatalytic degradation of organic dyes, antibiotics, and antibacterial agents [7].

- Electromechanical properties

ZnO possesses notable piezoelectric properties due to its wurtzite crystal structure, allowing for a bidirectional interaction between electric and mechanical fields. ZnO electrically polarizes when subjected to mechanical stress (direct effect) due to the displacement of ions within the crystal, creating a separation of charges. Conversely, it deforms when an electric field is applied (inverse effect), altering its physical dimensions. These properties arise from the crystal structure of ZnO. Due to the crystal's anisotropy, the piezoelectric constants, which define the relationship between mechanical stress and electrical polarization as well as between the electric field and mechanical deformation, vary according to the crystal's orientation. This anisotropy is crucial for optimizing piezoelectric devices such as sensors, transducers, and actuators by aligning the crystals in specific orientations to maximize performance. Thus, understanding the directional properties of ZnO enables the development of advanced technologies in various fields, ranging from electronics to renewable energy [23].

- Photocatalytic properties

ZnO exhibits exceptional photocatalytic characteristics, especially when compared to TiO_2. Notably, ZnO nanostructures are also nontoxic in contrast to TiO_2 and other inorganic photocatalytic materials, making them highly desirable materials for a wide range of applications in both biological and environmental settings. With its strong adsorption and wide bandgap (3.37 eV), ZnO efficiently absorbs UV light irradiation, generating electron-hole pairs that drive redox reactions on its surface. These reactions enable the degradation of organic pollutants and their possibility for environmental protection [31][32].

I.5 Different growth techniques of thin films

Numerous thin-film growing methods have been investigated in the research publications, each technique offers unique advantages and characteristics, making them suitable for a range of

applications in optoelectronics, sensors, and photocatalysis. **Figure I.3** summarizes an overview of various methods of growing thin films:

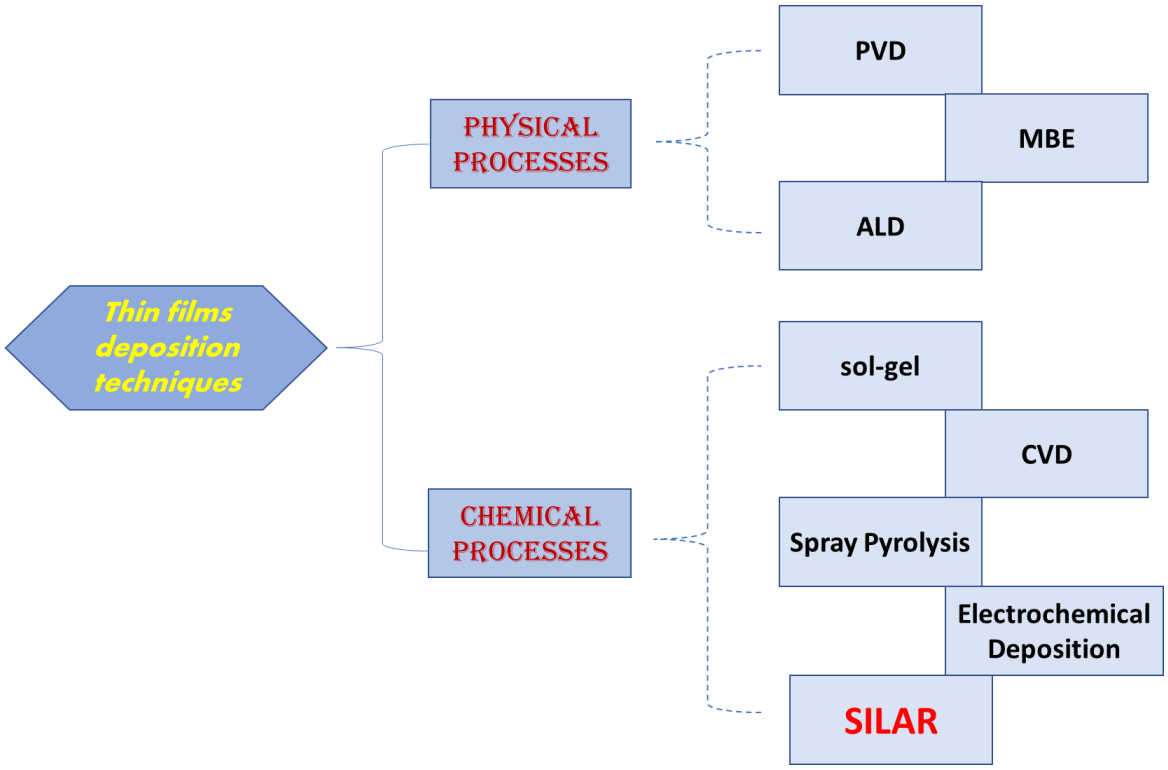

Figure I.3. Thin film deposition technologies

I.5.1. Successive ionic layer adsorption and reaction (SILAR) process

The successive ionic layer adsorption and reaction (SILAR) method was initially proposed by Y.K Nicolau in 1985 for the deposition of ZnS and CdS. This process has been employed in synthesizing diverse thin film semiconductors. Additionally, the SILAR technique is extensively utilized at the laboratory scale due to its relative cost-effectiveness, simplicity, and ease of use, as it does not require advanced equipment, making it highly flexible and reproducible. Furthermore, SILAR has recently garnered the attention of scientific researchers for several reasons, as outlined below [33]:

- Thin films are typically fabricated on a simply cleaned and rigid planar substrate that imposes no dimensional limitations, and its possibility of being established on large surface substrates.

- Deposition rates and film thickness can be precisely controlled by monitoring the reactant precursors, which typically consist of desired cationic and anionic salts dissolved in solvents.
- The thicknesses of the thin films can be also controlled by adjusting the number of deposition cycles and concentration of precursors solution.
- SILAR fabrications are highly convenient and energy-efficient since it is applicable at room temperature. If necessary, the as-deposited coatings can be subjected to post-deposition annealing to promote grain growth, crystallization, and other desired properties.

Therefore, the SILAR technique's advantages make it a promising choice for industrial-scale thin film fabrication, especially in the semiconductor industry.

I.5.2. Description the protocol of SILAR technique

In this process, the substrate is alternately immersed in two different precursor solutions, immersion in deionized water between each rinsing to remove loosely bound species. A typical SILAR cycle involves the adsorption of cationic precursors, then immersing in DI water, and adsorption of anionic precursors. The cations and anions adhere to the substrate surface and react to form the final product. This cycle is repeated multiple times to achieve the desired film thickness. Key parameters such as the concentration of the precursors and the immersion time in each solution can be adjusted to tailor the composition and thickness of the materials [34]. **Figure I.4** describes the successive ionic layer adsorption and reaction method:

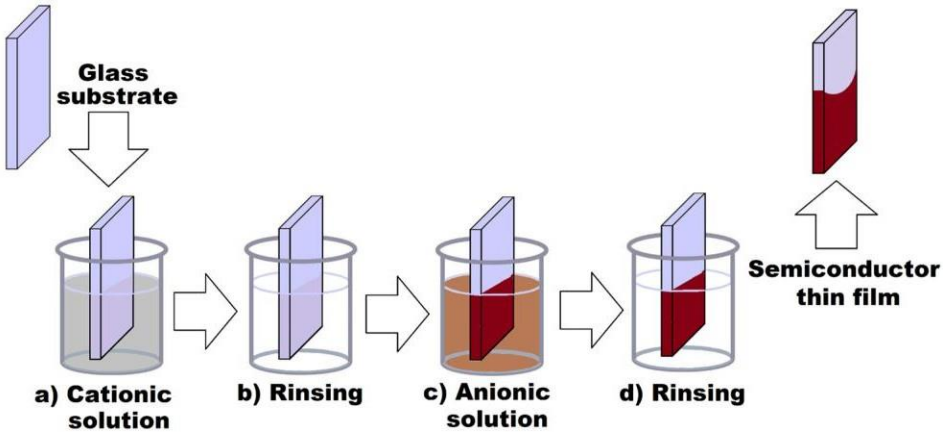

Figure I.4. SILAR process [35]

I.5.3. Factors affecting SILAR deposition

SILAR deposition is influenced by several factors that develop the effectiveness and quality of the thin films. These factors collectively impact the fabrication rate as well as the structural, optical, electrical, and photocatalytic properties of the thin films. A detailed discussion on the role of these parameters, which have been extensively investigated in the SILAR literature [36], will be presented below:

- Impact of doping

To maximize the number of charge carriers participating in the material's functionality, a material with low activation energy is essential, allowing electrons to easily transition from the valence band to the conduction band. Doping is one of the most effective methods for tuning this structure. In many instances, incorporating cation dopants is a highly effective strategy to enhance electrical conductivity. By reducing the bandgap, electron transfer between the valence and conduction bands is increased, leading to an increase in electrode capacitance for energy storage devices [33].

- Type of Precursor

The precursor used in the SILAR process greatly influences the properties of the resulting materials. Different precursors such as zinc nitrate, zinc acetate, and zinc chloride influence the crystallinity, morphology, bandgap energy, and photocatalytic activity of the resulting ZnO nanoparticles. The best crystallinity and surface morphology was observed in films produced by zinc chloride according to S. P. Ratnayake [36]. The precursor type also affects the particle size, aspect ratio, and organic material content, consequently influencing the photocatalytic efficiency of ZnO nanoparticles [37]. Furthermore, the choice of precursor in the synthesis of ZnO/TiO_2 heterostructures impacts the crystal growth, carrier mobility, and photoelectrochemical performance of the resulting composite materials. Overall, the type of precursor plays a crucial role in tailoring the properties of ZnO nanoparticles for various applications, including photocatalysis and nanocomposite materials.

- Concentration of solution

The concentration of the precursor solution is a critical factor influencing the properties and performance of SILAR-grown thin films. Higher concentration solutions tend to produce coatings with larger grain sizes and increased surface roughness. Conversely, employing multiple SILAR

cycles with lower concentration precursor solutions can yield smoother, thinner, and potentially without holes in films. By meticulously controlling precursor solution concentration, it is possible to advance the structural and surface characteristics of thin films, thereby enhancing their overall quality and suitability for various advanced applications [36].

- Cycles number

The number of cycles in SILAR method is pivotal in defining the properties of thin films. Research on various materials, including zinc oxide has demonstrated that increasing the number of deposition cycles results in notable changes in crystal size, film thickness, structural, and optical properties [19]. Typically, an increase in cycles leads to a reduction in crystal size, an increase in film thickness, and alterations in optical properties such as transmittance and absorbance. However, there is an optimal range of cycles, beyond which the properties can degrade, as observed in BiOI, where photovoltaic performance declined after exceeding a certain number of cycles. These findings underscore the importance of optimizing the number of cycles in SILAR processes to achieve the desired thin film characteristics.

- Annealing temperature

Annealing is a highly effective post-deposition treatment in the SILAR approach, used to modify the properties of thin films. Typically, high-temperature annealing leads to an increase in crystallite size and surface roughness, which is consistent with thermally induced grain growth [38]. Furthermore, annealing can reduce defects in the films and eliminate the hydroxide phase along with the recrystallization. Careful optimization of annealing parameters is essential to achieve the desired film properties for various functional applications.

- pH of solution

The pH of the precursor solution is a critical parameter in SILAR depositions, as it influences the speciation, reactivity, and solubility of the involved species. Changes in pH can significantly impact supersaturation conditions, nucleation rates, and growth mechanisms, resulting in variations in film morphology, crystallinity, and composition. For example, in the deposition of ZnO thin films, Sakthivelu and colleagues observed that the grain size of ZnO increased with higher pH levels of the precursor solution. Additionally, they reported a decrease in the bandgap with increasing pH [39]. Thus, precise control of pH in SILAR processes is essential to tailor the properties of thin films for specific applications.

I.6. Doping of ZnO

Doping ZnO involves introducing foreign ions to alter its physical properties for various applications. It has been demonstrated that the doping of different metals into the ZnO lattice significantly affects its physical and chemical properties. Doping strategies impact the optical response and photocatalytic performance of ZnO nanomaterials, highlighting the significance of doping concentration and preparation conditions [26]. Additionally, ZnO doping can occur through the introduction of impurities or native defects in the lattice.

I.6.1. Native defects

Doping is an important process in many semiconductor technologies; however, it can be significantly impacted by native point defects. The control of defects and associated charge carriers is of critical importance in applications that exploit the diverse range of characteristics of materials since the defects have great effects on doping, minority carrier life time and luminescence efficiency, and may be directly involved in the diffusion mechanisms linked to the growth process [6].

In the case of ZnO material, there are many intrinsic defects with various ionization energies. The energy levels of the native defects in ZnO film are shown in **Figure I.5**, which depicts that there are numerous defect states within the band gap and the defect ionization energies range from 0.05 to 2.8 eV. The donor defects are: $Zn_i^{\bullet\bullet}$, $Zn_i^{\bullet}$, Zn_i^{x}, $V_o^{\bullet\bullet}$, $V_o^{\bullet}$, V_o and the acceptor defects i ' are:V''_{Zn}, V'_{Zn}. The predominant ionic defect types in ZnO are Zn interstitials and oxygen vacancies which have been mentioned as sources of n-type conductivity. Due to the different ionization energies, the relative concentrations of the various defects depend strongly on temperature [40].

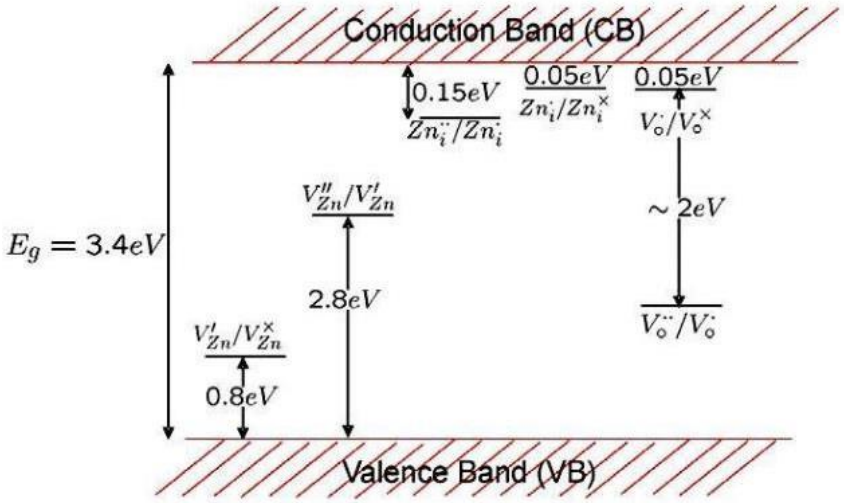

Figure I.5. Energy levels of native defects in ZnO[40]

I.6.2. Impurity doping

ZnO possesses a relatively open structure characterized by a hexagonal close-packed lattice where zinc atoms occupy half of the tetrahedral sites, leaving all octahedral sites vacant. This structural feature provides numerous sites for accommodating both intrinsic defects and extrinsic dopants. The ability to introduce selective element doping offers a method to fine-tune ZnO's properties, which is crucial for enhancing its performance in various applications. This capacity to modify its properties through doping is essential for optimizing ZnO's use in fields such as optoelectronics, photocatalysis, and sensor technology. Topically, there are four main interests in doping ZnO are maintained below [26]:

- Doping with donor impurities to achieve n-type conductivity
- Doping with acceptor impurities to achieve p-type conductivity
- Doping with rare-earth elements to achieve desired optical properties
- Doping with transition metals to achieve desired magnetic properties.

Various types of doping of ZnO with various elements, such as rare earth metals, transition metals, noble metals, and alkaline metals, have been extensively studied to enhance its properties for a wide range of applications. The effectiveness of doping indeed depends on the ease with which heteroatoms can be incorporated into the zinc substitutional sites within the ZnO lattice [41].

I.6.2.1. Barium doped zinc oxide

Barium is one of the perfect alkaline metals that have been chosen as dopants in ZnO. Recently, many researches have extensively studied barium-doped zinc oxide films due to their unique properties. Moreover, the selection of barium as a dopant for ZnO is due to its similar valence states to zinc, allowing it to easily diffuse into the Zn lattice. Although barium has the same valence electrons as zinc, its ionic radius enables it to substitute into the ZnO lattice during the doping process. Incorporating Ba in ZnO enhances the dielectric constant and AC conductivity, indicating improved charge carrier mobility. Ba-doped ZnO forms crystalline structures with smooth surfaces and low density, capable of absorbing internal stress. This doping reduces the energy bandgap and increases charge separation in ZnO nanoparticles, enhancing their electronic and optical properties. Additionally, Ba doping improves interfacial electron transfer processes at the surface, increasing surface reactivity. The reduced bandgap and high surface reactivity positively impact photocatalytic activity [42][43][44].

I.7. photocatalytic activity

I.7.1. Introduction

Over the past few decades, population growth and significant industrial development have led to widespread contamination of sewage and drinking water resources with organic pollutants (e.g., pharmaceuticals, hydrocarbons, dyes), heavy metals (e.g., chromium, mercury, lead), and inorganic compounds (e.g., nitrite, nitrate, arsenic), and various other complex substances, which present in **Figure I.6**. Several of these pollutants are toxic, carcinogenic, mutagenic, or have endocrine-disrupting effects [45]. The United Nations' World Water Development Report (2020) highlights that alterations in the water cycle will threaten food security, human health, and energy production. Consequently, there is an urgent need for environmental protection and the generation of green energy [46]. Additionally, the traditional biological-physical wastewater treatment methods are generally not realizable for the removal of large amounts of these pollutants. Today, solar energy, radiant light, and heat from the sun, is the most abundant clean energy source available. As a result, the scientific community became very interested in the photocatalysis process, which uses solar energy, as the most promising solution to environmental issues [47].

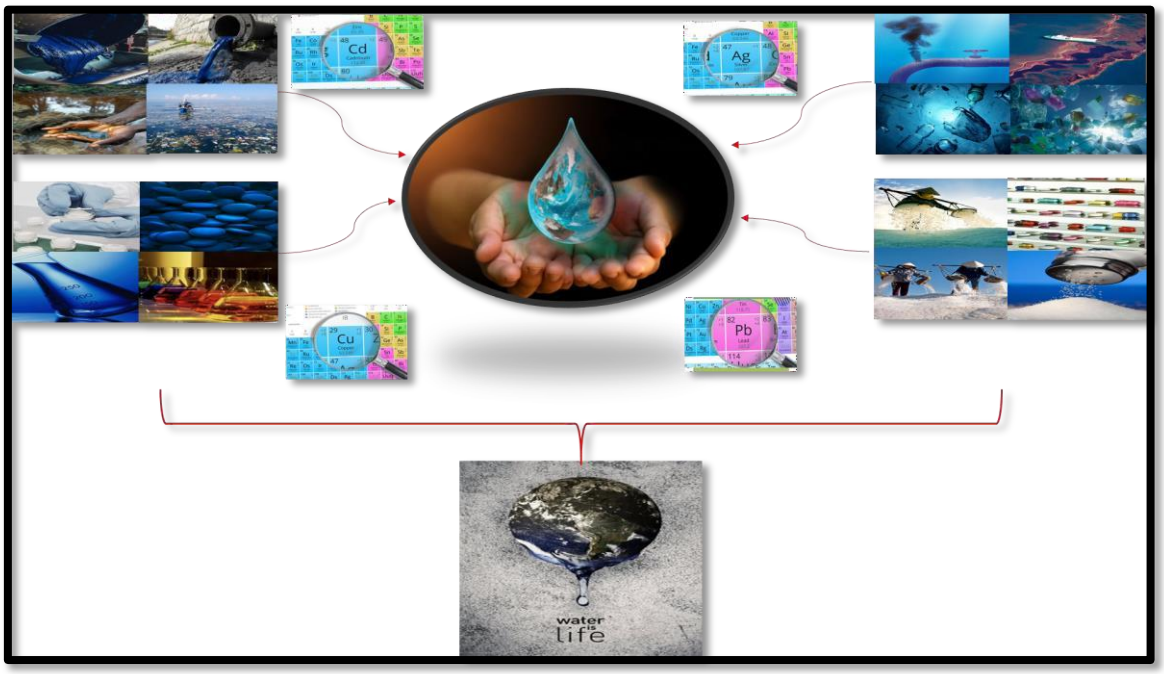

Figure I.6. Different organic and inorganic sources of water pollution in the environment

I.7.2. Definition of Photocatalysis

The term photocatalysis merges the concepts of photochemistry and catalysis, and it refers to the acceleration of a photoreaction in the presence of a catalyst (semiconductor). An ideal photocatalyst should possess several key properties: it must be highly photoactive, chemically and biologically inert, resistant to photo corrosion, non-toxic, cost-effective, and capable of activation by solar light [47][45]. Photocatalysis is referred to as heterogeneous when the catalyst is in a different physical state (solid) than the pollutants (liquid or gas) [48]. First-generation photocatalysts include various materials, including ZnO and TiO2, the first semiconductors to be investigated and used in photocatalytic applications[45].

I.7.3. Semiconductor photocatalysis mechanism

In an optimal photocatalytic process, organic pollutants are mineralized into CO_2, H_2O, and mineral acids in the presence of ZnO particles and reactive oxidizing agents such as oxygen or air [47]. **Figure I.7** presents the mechanism steps of the process; whereas the first step is the generation of photoelectrons (e^-) in the conduction band (CB) and holes (h^+) in the valence band (VB) of the semiconductor upon exposure to light with a wavelength equal to or greater than the energy of the bandgap ($h\nu \geq Eg$) [49]. The second step illustrates the separation of photogenerated

electrons and holes. However, the bulk charge carriers often recombine, producing phonons or heat, which decreases the number of excited charge carriers. This rapid recombination, occurring within a few nanoseconds, adversely affects the photocatalytic efficiency of catalysts in water decontamination. Then, for photocatalysis to be effective, the recombination phenomenon must be reduced to a minimum or eliminated. Furthermore, surface modifications including adding metals, and dopants, or combining them with another semiconductor can reduce electron-hole recombination rates and enhance efficiency. Doping ZnO with transition metals (Cu, Fe…) improves electron and hole trapping, decreasing recombination [23]. Photogenerated electrons often act as reductants, directly reducing heavy metal ions. The separated holes may react with hydroxyl ions (OH^-) or water molecules to produce hydroxyl radicals (·OH), which are highly oxidizing and play a crucial role in oxidative decomposition. This reaction is the primary pathway for ·OH production. Additionally, the separated electrons can react with dissolved oxygen in water to form superoxide radicals ($\cdot O_2^-$), which further decompose to produce ·OH. Contaminants in water are first adsorbed onto the surface of the catalytic material, enhancing charge mobility and redox ability. Subsequently, a series of chemical reactions occur with the active species generated by the catalyst, leading to the degradation of pollutants. All the redox reactions mentioned in the explanation are listed below (**Eq I. (1)–(9)**) [46]:

$$Semiconductor + hv \rightarrow h^+ + e^- \quad \textbf{(Eq I.1)}$$

$$e^- + O_2 \rightarrow \cdot O_2^- \quad \textbf{(Eq I.2)}$$

$$\cdot O_2^- + H^+ \rightarrow \cdot OOH \quad \textbf{(Eq I.3)}$$

$$2 \cdot OOH \rightarrow O_2 + H_2O_2 \quad \textbf{(Eq I.4)}$$

$$H_2O_2 + \cdot O_2^- \rightarrow \cdot OH + OH^- + O_2 \quad \textbf{(Eq I.5)}$$

$$H_2O_2 + hv \rightarrow 2 \cdot OH \quad \textbf{(Eq I.6)}$$

$$h^+ + H_2O \rightarrow \cdot OH + H^+ \quad \textbf{(Eq I.7)}$$

$$h^+ + OH^- \rightarrow \cdot OH \quad \textbf{(Eq I.8)}$$

$$Pollutants + (\cdot OH, h^+, e^-, \cdot OOH \text{ or } \cdot O_2^-) \rightarrow degradation\ products \quad \textbf{(Eq I.9)}$$

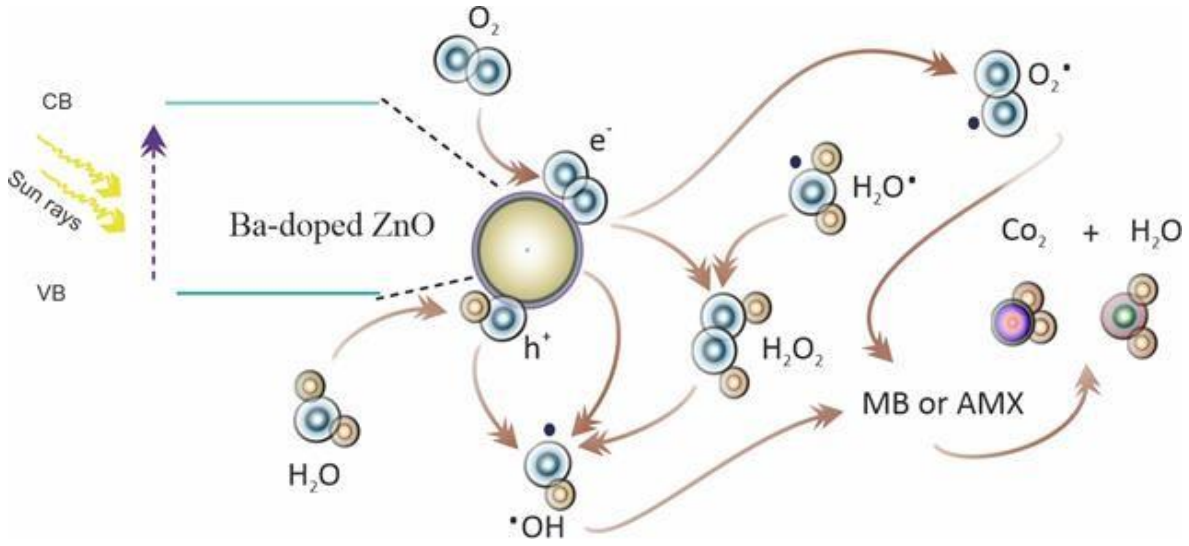

Figure I.7. Photocatalytic processes over a heterogeneous photocatalyst

The photocatalytic performance of catalysts is indeed significantly influenced by the physical-chemical characteristics of the catalyst and the chemical composition of the pollutant [50].

I.7.4. Kinetic of photocatalytic reaction

The kinetics of photocatalytic degradation of pollutants are studied by employing the Langmuir-Hinshelwood model. This model is utilized to monitor the degradation rate of pollutants at different concentrations and for characterizing solid catalytic reactions which consists of four steps [51]:

- adsorption of molecules on a catalytic surface;
- dissociation of adsorbed molecules;
- reactions of dissociated molecules to produce products:
- desorption of products.

Additionally, Langmuir–Hinshelwood mechanism is based on the following five key assumptions [48]:

- The number of adsorption sites is fixed at equilibrium;
- Each adsorption site accommodates only one substrate molecule;
- Only molecules adsorbed on the surface react;
- Adsorption occurs quickly relative to the secondary reactions of the substrate in the solution;

- The adsorption energy is the same across all adsorption sites and is independent of the rate of surface coverage.

In the case of these hypotheses, they are accepted, and according to the rate law of chemical reactions, the rate of degradation is expressed as follows:

$$r = -\frac{dC}{dt} = k\theta \qquad \textbf{(Eq I.10)}$$

Where r, C, k, and t indicate the speed of degradation, the concentration of reagent, apparent reaction rate constant, and the irradiation time, respectively.

For a low initial concentration C_0 of the reactant ($C_0 < 10^{-3}$ M), the above equation can be simplified to a pseudo first order equation:

For an initial reactant concentration C_0 lower than 10^{-3} M, the above equation can be simplified to a pseudo-first-order equation:

$$ln(C_o/C_t\ ) = K.t \qquad \textbf{(Eq I.11)}$$

At high concentrations, the reaction rate reaches its maximum, indicating that the reaction becomes zero-order.

$$(C_o - C) = K.t \qquad \textbf{(Eq I.12)}$$

I.7.5. Factors affecting the photocatalytic process

The effectiveness of photocatalytic activity is depending on several principal factors presented below:

- Initial concentration of organic pollutant

At low pollutant concentrations, the reaction rate rises significantly due to the abundance of available active sites on the catalyst. However, as the concentration of the pollutant increases, the reaction rate begins to show an asymptotic behavior. This is because the catalyst surface becomes saturated, so that an increase in the substrate concentration hardly increases the reaction rate. This saturation occurs when the catalyst sites are occupied either by reactants at high concentrations or by reaction products. The Langmuir–Hinshelwood model effectively interprets this behavior [50].

- Photocatalyst concentration

The concentration of the photocatalyst is one of the key elements influencing the photocatalytic efficiency. Typically, higher catalyst loading provides more surface-active sites and generates more electron-hole pairs, thus enhancing photocatalytic activity. However, excessively increasing the photocatalyst concentration can reduce the reaction rate due to the reflection and scattering of incident radiation, preventing catalyst particles from absorbing more photons. Therefore, optimizing the photocatalyst concentration is essential to maximize the photodegradation rate [52].

- Temperature

Photocatalytic reactions are generally not highly sensitive to temperature changes since their activation is driven by photon absorption, and the rate constant is not so dependent on temperature as established by Hoff-Arrhenius equation (**Eq I.13)** for conventional thermally activated reactions. In photocatalytic processes, temperature primarily influences the adsorption-desorption dynamics of reactants, intermediates, and products. Therefore, the effect of temperature is contingent on the surface properties of the photocatalytic material and the reactant to be decomposed [50]. Additionally, increasing temperature can enhance the adsorption capacity of photocatalysts, thereby improving the photocatalytic degradation rate of organic compounds. This effect has been observed in various studies, such as with Orange G within the range of 20–50 °C, Indigo Carmine between 20–40 °C, and Rhodamine B from 30–50 °C [51].

$$k(t) = k_o \exp(-\frac{E_a}{RT}) \qquad \textbf{(Eq I.13)}$$

- Light wavelength

The effect of light wavelength on photocatalytic degradation is a critical factor in determining the efficiency of pollutant removal processes. For optimal catalyst activation, it is essential that the pollutants do not absorb light in the same wavelength range as the catalyst [48]. Research indicates that different wavelengths of light can significantly influence the degradation rates of contaminants. Specifically, the UV-A range spans wavelengths from 315 to 400 nm (3.10-3.94 eV), the UV-B range covers 280 to 315 nm (3.94-4.43 eV), and the germicidal UV-C range includes wavelengths from 100 to 280 nm (4.43-12.4 eV) [47].

- Solution pH

The solution pH is a critical factor in the photocatalytic degradation process, as demonstrated by various studies. The pH of the precursor solution significantly influences the photocatalytic

activity of zinc oxide and tin oxide nano powders. Notably, samples prepared at pH 9 exhibit remarkable dye degradation efficiency and enhanced biological activities. Herrmann et al. [53] found that increasing the pH above 10 enhances the reaction rate due to the increased formation rate of OH radicals. However, depending on the nature of the organic compound, adsorption is disadvantaged and the photocatalytic efficiency is greatly reduced. In another hand, the positively charged of the surface of photocatalyst at pH =4 will enhance the electrostatic interaction between the dye and photocatalyst and will also be promoted the hydroxyl radical formation. additionally, reduced pH levels increase the creation of more H^+ ions in the hydrogen evolution reaction, which is advantageous for the process [52].

- Morphology of the photocatalyst

Photocatalysts with different morphologies generally exhibit variations in their photocatalytic performance due to the diverse active facets, unique active sites, and the corresponding adsorption-desorption ability to reactant [54]. Further, the structure of ZnO plays a crucial role in its photocatalytic degradation efficiency. Various ZnO structures, including nanorods, nanotubes, hexagonal shapes, and wurtzite structures, have demonstrated enhanced photocatalytic performance [55]. Furthermore, ZnO nanoparticles with a hexagonal structure exhibit superior photocatalytic property due to their high crystallinity and optimal bandgap energy, resulting in efficient degradation of organic pollutants. Studies have shown that ZnO nanorods with a higher specific surface area achieve better photodegradation efficiency compared to those with a lower surface area [47].

- Charge-Carrier Scavengers

Scavengers are employed in photocatalytic processes to remove undesirable reaction products, such as oxygen, to prevent unwanted reactions, and to evaluate photocatalytic activity by deactivating reactive species. Frequently used scavengers in photocatalytic reactions include ammonium oxalate and disodium ethylenediaminetetraacetate (EDTA-2Na) for capturing holes, dimethyl sulfoxide (DMSO) and $AgNO_3$ for capturing electrons, 1,4-benzoquinone (BQ) for capturing $\bullet O_2^-$, and methanol, 2-propanol (IPA), and tert-butanol (t-BuOH) for capturing OH radicals [52].

I.7.6. Advantages and disadvantages of heterogeneous photocatalysis

Heterogeneous photocatalysis offers several advantages, including [23]:

- heterogeneous photocatalysts are non-hazardous, efficient, eco-friendly process, and reusable, making them ideal for various applications.
- Achieves total mineralization: generates H_2O, CO_2, and various other species.
- Enables the utilization of solar energy.
- It is applicable at room temperature and pressure.

Heterogeneous photocatalysts face limitations such as [56]:

- The recombination of photogenerated charges can reduce the process's efficiency.
- It requires energy consumption (UV irradiation), limiting the technology's efficiency in the visible spectrum.

I.7.7. Application of Heterogeneous Photocatalysis

Heterogeneous photocatalysis has emerged an effective strategy for several applications, including organic transformations, wastewater treatment, selective hydrogenation reactions, and the degradation of pollutants. **Figure I.8** illustrates the various applications of this process in environmental, medical and structural applications.

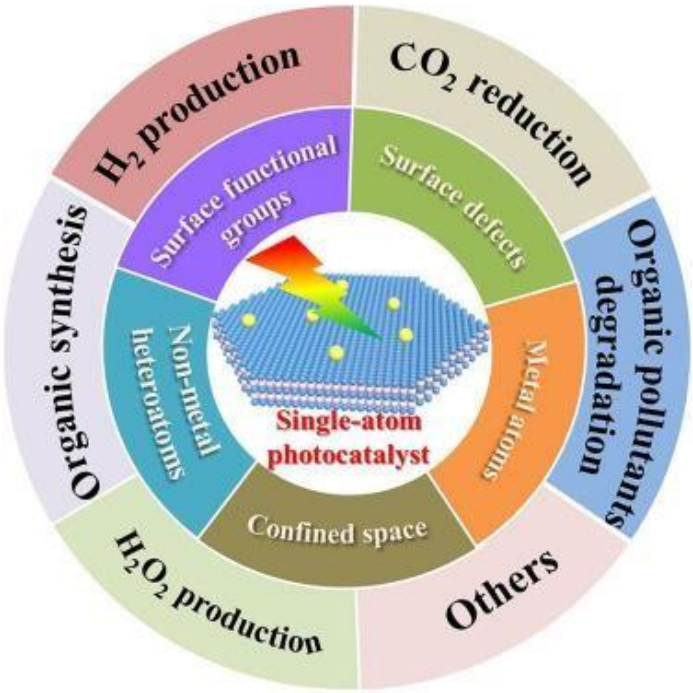

Figure I.8. The potential uses of heterogeneous photocatalysis in environmental, medical, and structural applications

- Photoelectrochemical H_2 Production from Water Splitting

In recent year, the utilization of solar energy, which is an abundant and renewable resource, presents an exceptionally promising to achieving green energy production. A particularly exciting and innovative approach is the applicable of photocatalytic mechanisms for the generation of hydrogen (H_2) through water splitting. Recent technological advancements have resulted to the development of various photocatalysts specifically to enhance the efficiency of this process [57]. Hydrogen can be produced through photoelectrochemical (PEC) water splitting on semiconductor photocatalysts that are characterized by nanostructures with high surface-to-volume ratios and superior light absorption ability. In a conventional PEC cell setup, there are two half-reactions that occur simultaneously: (a) the oxygen evolution reaction (OER), which is usually occurs on an n-type semiconductor serving as a photoanode, and (b) the hydrogen evolution reaction (HER), which is occurs on a cathode functioning as a counter electrode, as shown in **Figure I.9**.[52]

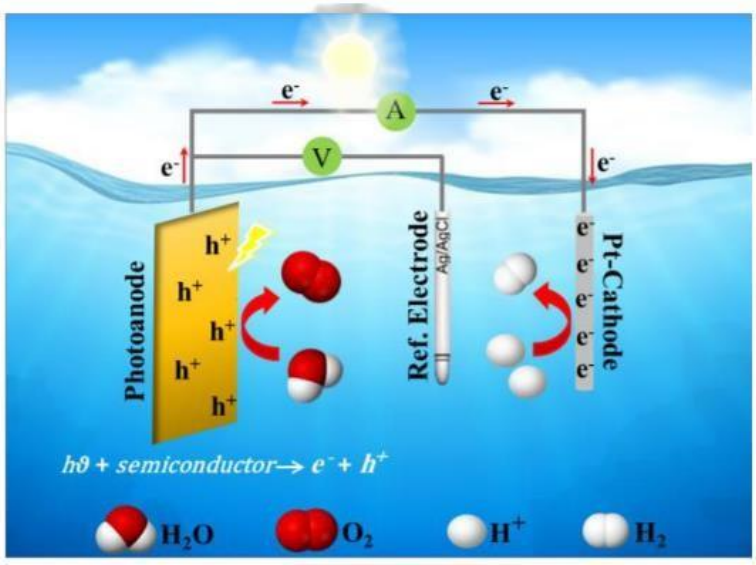

Figure I.9. A schematic of a typical photoelectrochemical (PEC) cell [52]

- Photocatalytic CO_2 Reduction

Photocatalytic CO_2 reduction is a promising approach for converting carbon dioxide into valuable small-molecule chemicals or energy fuels such as CO, CH_4, HCOOH, and other chemicals through photocatalytic technology. This strategy can solve the problems of the environment and public health, such as global warming and climate changes, sea-water acidification, and the upsurge of ocean levels. These issues are caused by the overuse of fossil

fuels including petroleum, gas, and coal, which release substantial amounts of CO_2 into the atmosphere upon combustion [52][58].

- Photocatalytic Dye/Drug Degradation

Despite the significant economic importance of the textile, leather, food, and paper industries in the world, this is a major source of water pollution in both toxicological and aesthetic qualities. Approximately half a ton of dyestuffs are discharged every day into the environment. Several synthetic dyes used in textiles, including both cationic dyes such as safranin O (SO), rhodamine B (RhB), malachite green (MG), rhodamine 6G (Rh6G), methylene blue (MB), and crystal violet (CV), as well as anionic dyes like eosin Y (EY), Eriochrome black T (EBT), phenol red (PR), methylene orange (MO), and Congo red (CR), are hazardous and toxic organic contaminants that will impede the photosynthesis process of aquatic plants and harm human health via the channels of food and drinking water supply.

In other hand, chemical and pharmaceutical industries produce other organic wastes that are detrimental to both society and the environment. Especially, with the increasing of the production and usage of pharmaceutical products, which notably increased due to the COVID-19 pandemic in recent years. Pharmaceutical contaminants are found in water at concentrations as trace as $ng.L^{-1}$ to $\mu g.L^{-1}$. But even at these low concentration levels, because of their physical and chemical properties, they can be a major danger to living organisms' health. Given the severe problems resulting from water pollution caused by dye and pharmaceutical pollutants, the degradation of these organic pollutants by photocatalysis, in a sustainable development option, has become one of the alternative modern techniques for wastewater treatment, particularly when using a renewable energy source, as well as regarding the significant advantages of photocatalysis processes in eliminating harmful pollutants from water [52][59].

I.8. Self-Cleaning Function

The application of nanotechnology in self-cleaning was investigated by measuring the water contact angle, which is defined as the angle formed between the solid surface and the tangent line of the liquid phase [60]. Based on wettability, these surfaces can exhibit hydrophilic properties when the contact angle is less than 90°, or hydrophobic properties, similar to lotus leaves when the contact angle exceeds 90° [61].

I.9. Conclusion

In this chapter, we first provide a definition of thin films and their synthesis, with a particular focus on the SILAR process. We also present a study on semiconductors and their classification. Furthermore, we discuss the general properties of zinc oxide, with a specific emphasis on its optical and structural properties. In general, ZnO exhibits good optical transmission. Additionally, we explore the effect of barium-doping concentration, the number of deposition cycles, and annealing temperature on the properties of the films. The key characteristic of this material is its potential for large-scale industrial applications, particularly in self- cleaning and the photocatalytic degradation of organic pollutants. In the next chapter, we will describe the technique used to form our thin films and the characterization methods employed in this study.

References

[1] J. Gonzalez. Cuadra, A. Lahlahi, S. Porcar, R. Cadena, S. Toca, Zinc oxide thin films: Synthesis and photocatalytic applications, e-book, 2024, doi: 10.5772/intechopen.115470.

[2] R. Gegova.Dzhurkova, D. Nesheva, I. Stambolova, K. Zaharieva, V. Dzhurkov, I. Miloushev, Enhanced photocatalytic performance under ultraviolet and visible light illumination of ZnO thin films prepared by modified Sol-Gel method, Molecules, vol. 29, no.17, 2024,doi: https://doi.org/10.3390/molecules29174005.

[3] S. Basavaraj, N. A. Pattanashetti, A. B. Yadav, Effect of deposition temperature on growth of Zinc oxide nanorods on Zinc oxide thin film for optoelectronics and sensing applications, Interactions, vol. 245, no.113, 2024, doi: https://doi.org/10.1007/s10751- 024-01952-8.

[4] B. Safa, Synthesis and characterization of thin films based on functional metal oxides, Doctoral thesis, University of Kasdi Merbah, Ouargla, Algeria, 2024.

[5] M. Depaz, Processing and characterization of zinc oxide thin films, Doctoral thesis, University of South Florida, 2007, doi: https://digitalcommons.usf.edu/etd/694.

[6] B.Youcef, Elaboration and characterization of thin layers of zinc oxide (ZnO) deposited by ultrasonic spray for photovoltaic and optoelectronic applications, Doctoral thesis, University of Mohamed Khider, Biskra, Algeria, 2019, doi: http://thesis.univ-biskra.dz/id/eprint/4150.

[7] S. Benramache, Elaboration et caractérisation des couches minces de ZnO dopées cobalt et indium, Doctoral thesis, University of Mohamed Khider, Biskra, Algeria, 2012, doi: http://thesis.univ-biskra.dz/id/eprint/4166.

[8] S. Katsumoto, Physics of Semiconductors, Institute for Solid State Physics, University of Tokyo, Japan, chapter. 1, pp. 1–15, 2021, Site: https://note-collection.issp.u-tokyo.ac.jp/katsumoto/semicon2021/note1-14_en.pdf.

[9] F. Bouaichi, Deposition and analysis of Zinc Oxide thin films elaborated using spray pyrolysis for photovoltaic applications, Doctoral thesis, University of Mohamed Khider, Biskra, Algeria, 2019, doi: http://thesis.univ-biskra.dz/id/eprint/4533.

[10] F. Alexander James Crawford, Deposition of zinc oxide by spray pyrolysis, Doctoral thesis, University of Durham, 1993, doi: http://etheses.dur.ac.uk/6108/.

[11] L.H.S. Lacerda, S.R. De Lazaro, R.A.P. Ribeiro, Theoretical investigation of optical and structural properties of Ba-doped ZnO material, IOP Conference Series: Materials Science and Engineering, vol. 97, no.1, 2015, doi: 10.1088/1757-899X/97/1/012005.

[12] M.d. Atikur Rahman. A Review on Semiconductors Including Applications and Temperature Effects in Semiconductors. American Scientific Research Journal for

Engineering, Technology, and Sciences, vol. 7, no.1, pp. 50–70, 2014, site: http://asrjetsjournal.org/

[13] N. Balkan, A. Erol, Graduate Texts in Physics, Semiconductors for Optoelectronics: Basics and Applications, eBook, ISSN 1868-4521, Edition Number. 1, pp. 292, 2021, Original Turkish edition published by Seçkin Yayıncılık, Ankara, doi: https://doi.org/10.1007/978-3-319-44936-4.

[14] R.G.Gordon, Criteria for choosing transparent conductors materials properties relevant to transparent conductors optical and electrical performance of transparent conductors, MRS Bulletin, vol. 25, no. 8, pp. 52–7, 2000, doi: https://doi.org/10.1557/mrs2000.151

[15] A. Adjimi, Elaboration des oxydes transparents conducreurs par voie Sol-Gel, Doctotal thesis, University of Freres Mentouti, Constantine 1, Algeria,2022.

[16] B. Korkmaz. Erdural, Photocatalytic antimicrobial and self-cleaning properties of titania- silica mixed oxide thin films, Doctoral thesis, University of Middle East Technical, 2012.

[17] M.R. Hoffmann, S.T. Martin, W .Choi, D.W. Bahnemann, Environmental Applications of Semiconductor Photocatalysis, Chemical Reviews, vol. 95, no. 1, pp. 69–96, 1995, doi: https://doi.org/10.1021/cr00033a004.

[18] C. AVŞAR, Electrodeposition of ZnO thin films: Effect of vandium doping, Doctoral thesis, University of Middle East Technical, 2013.

[19] Y. Khadraoui, E. Guettaf .Temam, S. Rahmane, H. Barkat, Effect of film thickness on the electrical and the photocatalytic properties of ZnO nanorods grown by SILAR technique, Physica Scripta, vol. 98, no. 12, pp. 1–40, 2023, doi: 10.1088/1402-4896/ad0ae7.

[20] S. Wongrerkdee, S. Krobthong, Synthesis, Characterization, and Photocatalytic Property of Ba-Doped ZnO Nanoparticles Synthesized Using Facile Precipitation, Integrated Ferroelectrics, vol. 224, no. 1, pp.192–204, 2022, doi: https://doi.org/10.1080/10584587.2022.2035609.

[21] A. Ouhaibi, N. Saoula, M. Ghamnia, M.A. Dahamni, L. Guerbous, Effect of deposition temperature on morphological, optical, and Photocatalytic properties of ZnO thin films synthesized by ultrasonic Spray Pyrolysis method, Crystal Research and Technology, vol. 57, no. 8, 2022, doi: 10.1002/crat.202100224.

[22] Z.W. Zena, D.M. Andoshe, L.T. Tufa, A.B. Gemta, F. B. Dejene, High Performance Co3O4/ Sn-ZnO Nanocomposite Photocatalyst for removal of methylene blue dye, Physica Scripta, vol. 99, no. 4, 2024, doi: 10.1088/1402-4896/ad2f8f.

[23] A. Herzi, Elaboration et caractérisation des couches minces du semi-conducteur ZnO non dopé et dopé par l'Argent, Doctoral thesis, University of Freres Mentouti, Constantine 1, Algeria, 2020.

[24] G. Neumark, Y. Gong, I. Kuskovsky, Doping aspects of Zn-based wide-Band-gap semiconductors, Electronic and Photonic Materials, vol. 13, no. 12, pp. pp 843–854. 2006, doi: https://doi.org/10.1007/978-0-387-29185-7_35.

[25] J. Luke. Wilson, Nanowires: Synthesis, electrical properties and uses in biological systems, Series: Nanotechnology science and technology, e-book, ISBN: 978-1-63117-855-9, pp. 173, nova publishers, New York, 2014, Web Site: http://www.novapublishers.com.

[26] S. Marouf, Propriétés Optiques des Nanostructures d'oxide de zinc (ZnO), Doctoral thesis, University of Ferhat Abbas Sétif 1, Algeria, 2017.

[27] M .Rasheed, R .Barillé, Room temperature deposition of ZnO and Al:ZnO ultrathin films on glass and PET substrates by DC sputtering technique, Optical and Quantum Electronics, vol.49, no. 5, 2017, doi: 10.1007/s11082-017-1030-7.

[28] A. U. R. Khan, M. Ramzan, M. Imran, M. Zubair, S. Shahab, S.J. Ahmed, F. Ferreira, M.F. Iqbal, Tailoring the structural, optical and electrical properties of zinc oxide nanostructures by zirconium doping, Coatings, vol. 13, no. 1, pp. 1-15, 2023, doi: https://doi.org/10.3390/coatings13010034.

[29] V. J. Shukla, Synthesis and characterization of pure and doped ZnO thin films by colloidal solution route, Doctoral thesis, University of Gujarat Technological, 2022.

[30] Z.H. Khan, Materials Horizons: From Nature to Nanomaterials Nanomaterials for Innovative Energy Systems and Devices, e-book, ISSN 2524-5392, 2022, doi: https://doi.org/10.1007/978-981-19-0553-7.

[31] S. AbouZeid, A. Perez, S. Bastide, M. Le Pivert, S. Rossano, H. Remita, N. Hautière, Y. Leprince.Wang, Antibacterial and Photocatalytic Properties of ZnO nanostructure decorated coatings, Coatings, vol. 14, no. 1, pp. 1-18, 2024, doi: https:// doi.org/10.3390/coatings14010041.

[32] X. Shu, Research on Photoelectric Properties of ZnO-based semiconductor material, Journal of Physics: Conference Series, vol. 2541, no.1, 2023, doi:10.1088/1742-6596/2541/1/012060.

[33] M. A. M. Patwary, Thin films processed by SILAR method, Thin Films, e-book, ISBN: 978-1-80356-456-2, pp. 222, 2023, doi: http://dx.doi.org/10.5772/intechopen.106476.

[34] S. Sanchez, Réalisation de cellules solaires nanostructurées à base de nanofils de ZnO Matériaux et Propriétés, Doctoral thesis, University of Grenoble, France, 2012.

[35] M. Calixto.Rodriguez, J.S. Valdez. Martínez, M.A. Meneses. Arcos, J. Ortega. Cruz, E. Sarmiento.Bustos, A. Reyes. Mayer, M. González. Castañeda, R.O. Domínguez. García, Design and development of software for the SILAR control process using a low-cost embedded system, Processes, vol. 9, no. 967, pp. 1–19, 2021, doi: https:// doi.org/10.3390/pr9060967.

[36] S. Ratnayake, J. Ren, E. Colusso, M. Guglielmi, A. Martucci, E. Della.Gaspera, SILAR deposition of metal oxide nanostructured films, Small, vol. 17, no. 49, 2021, doi: 10.1002/smll.202101666.

[37] J.D. Harris, E.A. Wade, E.G. Ellison, C.C. Pena, S.C. Bryant, N.L. McKibben, J. Allison, O. Kevin. Laughlin, E. A. Harris, V. K. Goettsche, E. C. Larson, Zinc–Acetate–Amine Complexes as Precursors to ZnO and the effect of the amine on nanoparticle morphology, size, and Photocatalytic activity, Catalysts, vol. 12, no. 10, 2022, doi: https://doi.org/10.3390/ catal12101099.

[38] K. Patel, D. V. Shah, V. Kheraj, Influence of deposition parameters and annealing on Cu_2ZnSnS_4 thin films grown by SILAR, Journal of Alloys and Compounds, vol. 622, pp. 942-947, 2015, doi: http://dx.doi.org/10.1016/j.jallcom.2014.11.019.

[39] A. Sakthivelu, S. Valanarasu, J.J. Prince, Effect of pH on SILAR deposited ZnO thin films, International Journal of Chemical Sciences, vol. 7, no. 4, pp. 2463-2469, 2009.

[40] I. Ameur, Fabrication and characterization of oxides, Doctoral thesis, University of Freres Mentouri, Constantine, Algeria, 2021.

[41] N. Rauf, Recent progress of ZnO-based nanoparticle: Synthesizing methods of various dopant and applications, Jurnal Fisika Flux, vol. 20, no.1, 2023, doi: https://doi.org/10.20527/flux.v20i1.16044.

[42] A. Modwi, K.K. Taha, L. Khezami, A.S. Al-Ayed, O.K. Al-Duaij, M. Khairy, M. Bououdina, Structural and electrical characterization of Ba/ZnO nanoparticles fabricated by co-precipitation, Journal of Inorganic and Organometallic Polymers and Materials, vol. 30, no. 7, pp. 2633–2644, 2020, doi: https://doi.org/10.1007/s10904-019-01425-4.

[43] A.R. Jayakrishnan, K. V. Alex, A.T. Tharakan, K. Kamakshi, J.P.B. Silva, M.S. Prasad, K. C. Sekhar, M. J. M. Gomes, Barium-doped zinc oxide thin films as highly efficient and reusable Photocatalysts, ChemistrySelect, vol. 5, no. 9, pp. 2824–2834, 2020, doi: 10.1002/slct.201904943.

[44] C.C. Okorieimoh, U. Chime, A.C. Nkele, A.C. Nwanya, I.G. Madiba, A.K.H. Bashir, S. Botha, P. U. Asogwa, M. Maaza, F. I. Ezema, Room-temperature synthesis and optical properties of nanostructured Ba-doped ZnO thin films, Superlattices and Microstructures, vol. 130, no. 1, pp. 321–331, 2019, doi: 10.1016/j.spmi.2019.05.010.

[45] S. Garg, A. Chandra, Green Photocatalytic Semiconductors: Recent Advances and Applications, e-book, ISSN. 2196-6982, 2022, doi: https://doi.org/10.1007/978-3-030-77371-7.

[46] G. Ren, H. Han, Y. Wang, S. Liu, J. Zhao, X. Meng, Z. Li, Recent Advances of Photocatalytic Application in Water Treatment: A Review, Nanomaterials,vol. 11, no. 7, 2021, doi: https://doi.org/10.3390/nano11071804.

[47] K.M. Lee, C.W. Lai, K.S. Ngai, J.C. Juan, Recent developments of zinc oxide based photocatalyst in water treatment technology: A review, Water Research, vol. 88, pp.428–448, 2016, doi: http://dx.doi.org/10.1016/j.watres.2015.09.045.

[48] O. Beldjebli. Élaboration et caracterisation des materiaux pour la photocatalyse, obtenus par la voie Sol-Gel, Doctoral thesis, University of Freres Mentouri, Constantine, Algeria, 2021.

[49] N. Bouhssira, Elaboration des filmes minces d'oxyde de zinc par evaporation et par pulverisation magnetron et etude de leurs proprietes, University of Freres Mentouri, Constantine, Algeria, 2013.

[50] J.C. Garc, L.A. Gonz, J.B. Nájera, M. García-Roig, Study of influence factors in the evaluation of the Performance of a Photocatalytic fibre reactor (TiO_2/SiO_2) for the removal of organic pollutants from water, Catalysts, vol. 12, no. 122 ,2022, doi: https:// doi.org/10.3390/catal12020122.

[51] H.D. Tran, D.Q. Nguyen, P.T. Do, U.N.P. Tran, Kinetics of photocatalytic degradation of organic compounds: a mini-review and new approach, RSC Advances, vol. 13, no. 25, pp. 16915, 16925, 2023, doi:10.1039/d3ra01970e.

[52] N. Goodarzi, Z. Ashrafi-peyman, E. Khani, A.Z. Moshfegh, Recent progress on semiconductor heterogeneous photocatalysts in clean energy production and environmental remediation, Catalysts, vol. 13, no. 1102, pp. 1–55, 2023, doi: https://doi.org/10.3390/ catal13071102.

[53] J. Herrmann, C. Guillard, P. Pichat, Heterogeneous photocatalysis: an emerging technology for water treatment, Catalysis Today, vol. 17, no. 1-2, pp. 7–20, 1993, doi: https://doi.org/10.1016/0920-5861(93)80003-J.

[54] J. Kou, C. Lu, J. Wang, Y. Chen, Z. Xu, R. S. Varma, Selectivity enhancement in heterogeneous Photocatalytic transformations, Chemical reviews, vol. 117, pp. 1445−1514, 2017, doi: 10.1021/acs.chemrev.6b00396.

[55] A.K. Alsharyani, L. Muruganandam, Fabrication of zinc oxide nanorods for photocatalytic degradation of docosane , a petroleum pollutant , under solar light simulator, RSC Advances, vol. 14, pp. 9038-9049, 2024, doi: 10.1039/d4ra00672k.

[56] Y. Subramanian, A. Dhanasekaran, L.A. Omeiza, M.R. Somalu, A.K. Azad, A Review on heteroanionic-based materials for Photocatalysis applications, Catalysts, vol. 13, no. 1, 2023, doi: https://doi.org/ 10.3390/catal13010173.

[57] X. Zhang, Z. Cheng, C. Bo, Y. Sun, L. Piao, The photocatalytic wastewater hydrogen production process with superior performance to the overall water splitting, Journal of Colloid And Interface Science, vol. 677, pp. 189–197, 2025, doi: https://doi.org/10.1016/j.jcis.2024.06.039

[58] F. Deng, J. Peng, X. Li, X. Luo, P. Ganguly, S.C. Pillai, B. Ren, L. Ding, D. Dionysiou, Metal sulfide-based Z-scheme heterojunctions in photocatalytic removal of contaminants, H_2 evolution and CO_2 reduction: Current status and future perspectives, Journal of Cleaner Production, vol. 416, 2023, 137957, doi: https://doi.org/10.1016/j.jclepro.2023.137957.

[59] F. Bourfa, Deposition of ZnO Thin Films for Treatment of Water, Doctoral thesis, University of Freres Mentouri, Constantine, Algeria, 2020.

[60] Z. Madiha, D. Radouane, B. Boudjema, D. Bouras, Effect thickness of copper oxide thin films on structural, optical, electrical, and hydrophobic properties for use in self-cleaning technique, Journal of Nanomaterials and Biostructures, vol. 18, no. 4, pp.1371-1384, 2023, doi: https://doi.org/10.15251/DJNB.2023.184.1371.

[61] A. Seifi, D. Salari, A. Khataee, B. Çoşut, L.Ç. Arslan, A. Niaei, Enhanced photocatalytic activity of highly transparent superhydrophilic doped TiO_2 thin films for improving the self-cleaning property of solar panel covers, Ceramics International, vol. 49, no. 2, pp. 1678–1689, 2023, doi: https://doi.org/10.1016/j.ceramint.2022.09.130.

Chapter II.

Experimental Procedure: Synthesis and characterization techniques

II.1. Introduction

This chapter focuses on the experimental synthesis and characterization of barium-doped ZnO thin films, fabricated using the Successive Ionic Layer Adsorption and Reaction (SILAR) method. The aim is to optimize their photocatalytic efficiency and self-cleaning applications by systematically exploring parameters such as dopant concentration, SILAR deposition cycles, and annealing temperature. This study investigates the influence of these variables on the structural, morphological, optical, and photocatalytic properties of the thin films.

In addition to detailing the experimental protocols for film synthesis, the chapter also covers the methodologies employed for characterizing the films, including X-ray diffraction (XRD), scanning electron microscopy (SEM), atomic force microscopy (AFM), and UV-Vis spectrophotometry. These techniques are essential to understand the films' crystallinity, morphology, optical behavior, and functional performance.

This experimental foundation sets the stage for a deeper understanding of how barium doping enhances ZnO thin films' properties, providing insights into their potential for addressing critical challenges in environmental sustainability and green technology development.

The objectives of this study are to optimize and characterize the performance of barium-doped ZnO films synthesized via the SILAR process for photocatalytic and self-cleaning applications. To achieve these objectives, the following specific goals are addressed:

- Identifying the optimal Ba dopant concentration for enhanced performance.
- Determining the ideal number of SILAR deposition cycles.
- Establishing the most effective annealing temperature for film stability and functionality.

II.2. Materials

A thoughtful selection of solvents and additive agents was employed to ensure the best performance of films fabricated. The materials utilized in this experimental work included the following: glass slides (MICROSCOPE SLIDES, NO.7102) with dimensions of (25.4*76.2*1 mm) as depicted in **Figure II.1**, zinc chloride dihydrate ($ZnCl_2$. $2H_2O$, 99 %), barium nitrate $Ba(NO_3)_2$,99 %), ammonium hydroxide (30%- 33%), deionized water, ethylene glycol ($C_2H_6O_2$, 99 %), and acetone (C_3H_6O). These substances were utilized as precursors, additives, solvents, and detergents to remove any possible impurities,

respectively, and these selections were made based on their characteristics and compatibility with the synthesis process. All chemicals were sourced from Sigma-Aldrich and were utilized without further purification.

Figure II.1. Glass substrates

In this work, the selection of the glass substrate was based on several specific reasons [1] [2]:

- Due to their transparency, these are highly suitable for the optical characterization of films in the visible.
- Since it is an insulator, it will not affect the conductivity measurement.
- Its thermal expansion is almost the same as that of ZnO ($\alpha_{glass} = 10^{-6}$ K^{-1}, $\alpha_{ZnO} = 7.2$ 10^{-6} K^{-1}, to promote good adhesion and reduces thermal stresses at the layer-substrate interface.
- For economic cost reasons and availability.

The photocatalytic process was investigated by degrading two compounds: the organic pollutant methylene blue (MB) and the antibiotic amoxicillin (AMX) during sunlight irradiation.

The following subsections summarize the key protocols used in the synthesis of barium-doped and undoped ZnO thin films via the SILAR process.

II.3. SILAR-Processed ZnO Thin Films: Influence of Ba-Doping on Photocatalytic Degradation and Wettability

II.3.1. Synthesis of Ba/ZnO thin films

Undoped and ZnO thin films doped with different concentrations (1 wt. %, 3 wt. %, 5 wt. %, and 7 wt. %) of Ba were deposited on glass substrates.

Before the deposition process, the glass substrates were cleaned in soapy water, distilled water, and rinsing in acetone for a duration of 30 minutes to eliminate any possible impurities and contaminations, and then dried with a light-cleaning paper.

For the successful Ba/ZnO thin films deposition, successive ionic layer adsorption and reaction (SILAR) method was employed.

The cationic solutions were prepared by dissolving 2.195 g of zinc chloride dihydrate ($ZnCl_2$, $2H_2O$, 99 %) in 100 ml of distilled water, which served as the pure solution. To introduce doping, specific amounts of barium nitrate $Ba(NO_3)_2$,99 %) was added into the zinc chloride solution to achieve a dopant concentrations of 1 wt. %, 3 wt. %, 5 wt. %, and 7 wt. %. These doping levels have the potential to significantly alter ZnO's structural and functional characteristics.

We added ammonium hydroxide (NH_4OH, 30%-33%) to adjust the pH value of the cationic solution maintained at 11. The pH level was precisely selected to ensure the stability and the homogeneity of the solution, avoid the precipitation of metal ions, and dictate the growth of Ba/ZnO thin films.

The deionized water was chosen as an anionic solution, maintained at 80 °C [3], which is the ideal temperature condition for SILAR reaction.

The SILAR deposition procedure was involved three steps. Initially, the substrates were immersed in the prepared cationic complex solution $Zn((NH_3)_4)^{2+}$ for 30 seconds at a temperature range of 80-90 °C. This complex decomposes to form $Zn(OH)_2$. The samples were then rinsed in a hot anionic solution for 30 seconds, allowing the adsorbed zinc ions to react with the anions present in the solution, resulting in the formation of ZnO. Last immersion, the substrates are rinsed with deionized water at room temperature for 30 seconds. All the prepared films underwent 30 SILAR dip cycles, alternating between cationic and anionic solutions. Finally, samples were dried in air after deposition, and then annealed at 450 °C in a muffle furnace for 90 minutes to ensure

the oxidation process, stabilize the thin films, and enhance their crystallinity. **Figure II.2** illustrates the comprehensive experimental setup for one SILAR cycle.

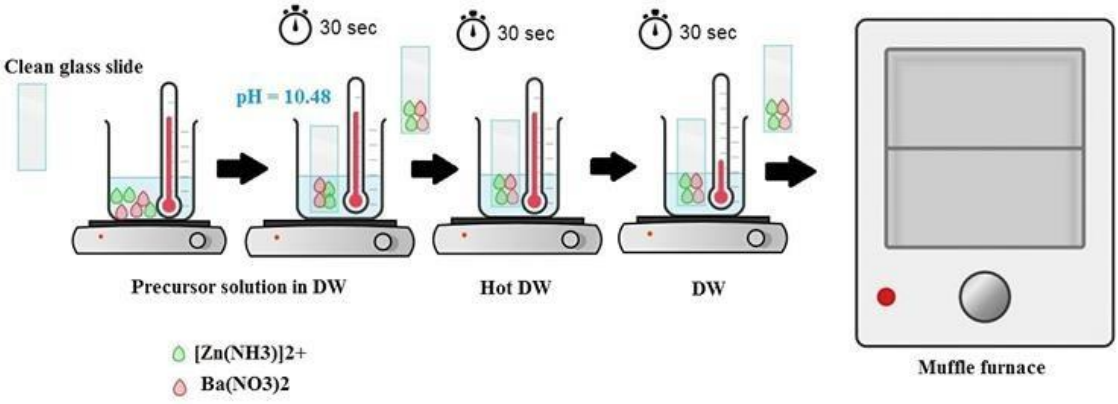

Figure II.2 Procedure of SILAR process for Ba-doped ZnO thin films

The chemical reaction presented by the equations (**Eq II.1 to Eq II.4**) below is related to the un-doped ZnO:

$$Zn(CH_3\,COO)_2\,.2H_2O \rightarrow Zn^{2+} + 2CH_3COO^- + 2H_2O \quad \textbf{(Eq II.1)}$$

$$NH_4OH \rightarrow NH_4^+ + OH^- \quad \textbf{(Eq II.2)}$$

$$Zn^{2+} + 2OH^- \rightarrow Zn(OH)_2 \quad \textbf{\textit{(Eq II.3)}}$$

$$Zn(OH)_2 \rightarrow ZnO + H_2O \quad \textbf{\textit{(Eq II.4)}}$$

II.4. Influence of SILAR Deposition Cycles on Ba-Doped ZnO Thin Films and their Photocatalytic Application

II.4.1. Preparation of Ba-doped ZnO films at different SILAR deposition cycles

The precursor solution was prepared by dissolving 0.1 M $ZnCl_2$. $2H_2O$ (99.5%) in 100 ml of ethylene glycol ($C_2H_6O_2$, 99%), with 25% concentrated ammonium hydroxide (NH_4OH, 99%) added under stirring to adjust the pH to approximately 11. To synthesize 5 wt.% Ba-doped ZnO, barium nitrate ($Ba(NO_3)_2$) was introduced into the initial solution.

The SILAR method was chosen for the deposition of Ba-doped ZnO films, utilizing varying reaction cycles (3, 6, 9, 12, and 15) based on previous experimental findings [4] [5]. For more details of SILAR deposition see **figure II.2**.

II.5. Influence of Annealing Temperature on Ba-Doped ZnO Thin Films and their Photocatalytic Application

II.5.1. Experimental procedure

The Ba/ZnO films were deposited on clear and clean glass substrates by the SILAR method, as presented in **Figures II.1**. A barium concentration of 5 wt. % was utilized over 15 SILAR deposition cycles. After deposition, the samples were annealed in a furnace at the different temperatures: 300 °C, 350 °C,400 °C, and 450 °C for 90 minutes. The technique followed is consistent with previously described experimental procedures.

II.6. Film Characterizations

The crystal structure of semiconductors was studied using X-ray diffraction (XRD), which provides detailed information about the crystalline phase, quality, orientation, lattice parameters, defects, stress, and strain of samples. Crystals are defined as atoms arranged in regular arrays, with parallel planes separated by a distance d.

The XRD technique was employed to characterize the structural properties of all Ba-doped ZnO thin films using a Bruker diffractometer (D8 Advance model) with CuKα radiation (λ = 1.5406 Å). The XRD analyses were taken at room temperature and the values of diffracted angle 2θ were ranged from 20° to 80° at 0.03 s^{-1} rate.

The structural parameters for all films including crystallites size, lattice strain, dislocation density, and number of crystallites, were recognized according to the most intense peaks for each sample using X'Pert High Score.

The crystallites size was determined by applying the Williamson-Hall method represented by **Eq II.5** [6] [7]:

$$\beta\ cos\theta = (k\ \lambda)/D + (4\ \varepsilon\ sin\theta) \qquad \textbf{(Eq II.5)}$$

Where, β is the full width at half maximum (FWHM), θ is the Bragg diffraction angle, k is a constant (0.94), λ is the wavelength of the incident X-ray (λ = 1.5406 Å), ε denote the lattice strain,

and D is the crystallite size.

The values of D and ε were determined from the intercept of the linear fit of a plot of β cosθ as a function of 4 sinθ. The intercept of the plot on the y-axis corresponds to the crystallite size.

The d-spacing values was computed by using the **Eq II.6 and 7** [8].

$$n.\lambda = 2.d.sin\theta \qquad \textbf{(Eq II.6)}$$

$$(\frac{1}{\mathrm{d}^2}) = \frac{4}{3}\,[\frac{\mathrm{h}^2+\mathrm{hk}+\mathrm{k}^2}{a^2}] + (l^2/\mathrm{c}^2) \qquad \textbf{(Eq II.7)}$$

Dislocation density (δ) was computed through the **Eq II.8** [9]:

$$\delta = 1/D^2 \qquad \textbf{(Eq II.8)}$$

The number of crystallites was obtained by the **Eq II.9**) [10]:

$$N = t/D^3 \qquad \textbf{(Eq II.9)}$$

Herein N the number of crystallites, t is the film thickness (nm).

The 3D surface topography and the surface roughness of Ba/ZnO films were characterized using a mechanical profilometer type (Tencor P-7), a high-resolution imaging technique that allows for imaging and measuring samples at the nanoscale. Since it moves a tip or stylus across the surface of the film, recording the vertical displacement along a specific path.

Scanning electron microscopy (SEM) is a highly effective technique for examining nanoscale surface morphology. It is extensively employed in various scientific disciplines for the analyzes of thin films, nanomaterials, and nanostructures.

The surface morphology and elemental composition of Ba-doped ZnO thin films was studied by SEM (JEOL JSM 5800) and energy-dispersive X-ray spectroscopy (EDX), respectively. The thickness values of the films were confirmed by SEM analysis of cross-sections of the samples and via the gravimetric weighing method (**Eq II.10**) [11]:

$$t = \frac{m}{\rho * A} \qquad \textbf{(Eq II.10)}$$

where m is the mass of the films (g), ρ is the density of the material, taken as 5.71 g/cm^3, and A is the surface area of the deposited film (cm^2). The mass of the deposited films was determined by measuring the glass substrate's weight before and after deposition and calculating the difference.

It was found that the values of thickness measurement obtained using different methods yielded approximately similar results.

To analyze the optical transmission spectra and calculate the band gap of undoped and barium-doped zinc oxide samples, a JASCO V-770 UV-Vis spectrophotometer was used, operating over a wavelength range of 280 nm to 1200 nm. Additionally, it was included Tauc and Menth equation (**Eq II.11**) for a direct optical band gap. In this method, the absorption coefficient α (cm^{-1}) was initially calculated (**Eq II.12**) [12]:

$$(\alpha\, h\upsilon)^2 = A\,(h\upsilon - Eg) \qquad \textbf{(Eq II.11)}$$

$$\alpha = \frac{1}{t}\, ln\,(\frac{100}{T}) \qquad \textbf{(Eq II. 12)}$$

Here, t is the film thickness (cm), T is the transmittance (%), α is the absorption coefficient (cm^{-1}), hυ is the incident photon energy (eV).

It is important to highlight that all these characterizations of Ba/ZnO thin films were conducted at the **LPCMA Laboratory**, University of Biskra, Algeria.

II.6.1. Water droplet contact angle measurements

The water droplet contact angle (WCA) measurements of thin film surfaces were performed by a simple homemade technique at room temperature, to detect the hydrophobicity/hydrophilicity film surfaces. To calculate the medium value of the WCA, IC Measure software was used. For each sample, the drops were applied five times using a micropipette (SCILOGEX-ISO 9001/13485), with the volume consistently maintained at 10 µl. The average values of WCA was calculated by taking the average of the left and right angles using the following equation **(Eq II.13)**, as shown in **Figure II.3**:

$$\theta = (\theta_1 + \theta_2)/2 \qquad \textbf{(Eq II.13)}$$

With θ_1 is the angle on the left of the droplet (◦) and θ_2 is the angle on the right (°), θ denotes the average angles of θ_1 and θ_2 in degrees.

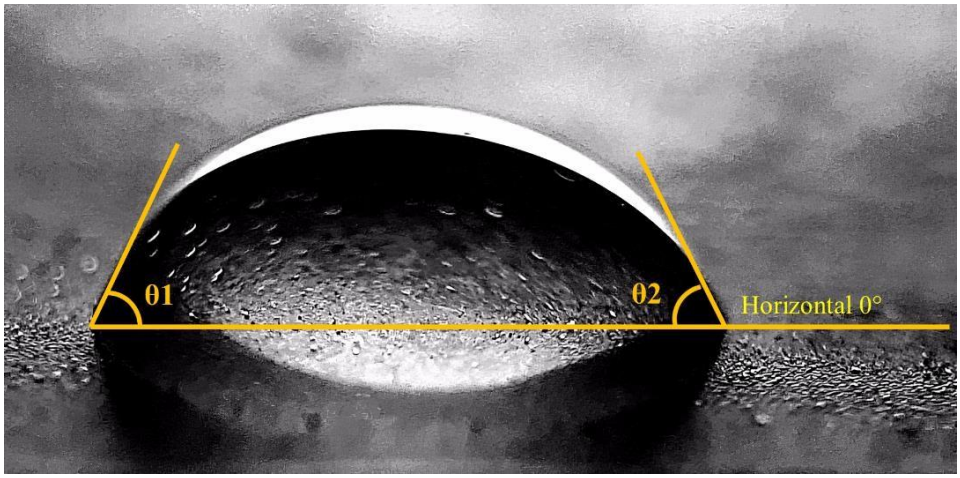

Figure II.3. Illustrates the calculation of a water droplet's contact angle

II.6.2. Photocatalytic degradation Procedure for methylene blue

In order to evaluate the photocatalytic performance of the prepared film samples, the methylene blue (MB) was employed as a photocatalytic reactant pollutant model. To investigate the photocatalytic activity of undoped and Ba-doped zinc oxide films, the photocatalyzed discoloration of MB was measured under sunlight irradiation. **Figure II.4** describes the photocatalytic process.

Figure II.4. Photocatalytic process of Ba-doped ZnO thin films under sunlight

Methylene blue (MB) is an aromatic organic heterocyclic basic cationic dye, with a molecular

formula $C_{16}H_{18}N_3ClS$, and having λ_{max} of 663 nm. The chemical name of MB is [3,7-bis(dimethylamino) phenothiazine chloride tetra methylthionine chloride], according to the International Union of Pure and Applied Chemistry. The molecular structure model of MB is shown in **Figure II.5**. MB is found in the nature as a solid, odorless, dark green powder that dissolved in the water to form a blue solution [2][13]. The hazardous effects of MB to human health and environment is presented in **Figure II.6** [14]**.**

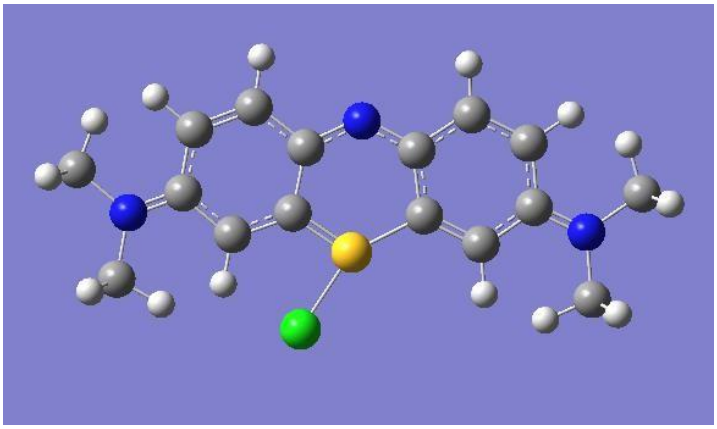

Figure II.5. The molecular structure model of MB dye

Figure II.6. The hazardous effects of MB to human health and environment

To prepare the MB dye solution, 0.004 g of MB powder was dissolved in 1 L of distilled water. The solution was subjected to magnetic stirring for one hour. Then, the photocatalyst was kept in 100 ml of MB solution in a dark place for 30 min to achieve the adsorption/desorption equilibrium.

The photocatalytic degradation tests were conducted for 5 hours under sunlight irradiations with the atmosphere conditions of this day in Algeria, Biskra city. During the reaction, 3 ml of reaction mixture was taken every hour and the absorbance was tested by a spectrophotometer (UV-VIS JASCO V-770) in wavelength range of 270–800 nm. The degradation performance of the photocatalysts can be evaluated using the following equation (**Eq II.14**) [15]:

$$degradation\ performance = \left(\frac{C_0 - C_t}{C_0}\right) * 100\% \qquad \textbf{(Eq II.14)}$$

Where C_0 is the initial concentration of MB dye solution, C_t is the concentration of dye solution after irradiation.

To confirm the performance of undoped and barium-doped zinc oxide thin films for the degradation of MB dyes, a control experiment was tested by first placing 100 ml of the MB solution in the dark and then exposing it to sunlight without any films for 5 hours.

The kinetics of the photocatalytic process were examined by applying the pseudo-first-order kinetics model using the Langmuir–Hinshelwood equation (**Eq II.15**) [16], which is used to determine the constant rate (K) and the correlation coefficient (R^2).

$$r = Ln\left(\frac{Co}{Ct}\right) = K\,.\,t \qquad \textbf{(Eq II.15)}$$

where r represents the rate of the reaction, k denotes the pseudo first-order rate constant (h^{-1}), and t is the irradiation time (h).

By employing this equation, the reaction rate can be determined by monitoring the change in concentration as a function of time. The apparent rate constant (K) represents the reaction's progression rate, while the correlation coefficient (R^2) reflects the relationship between the rate and the concentration. This approach facilitates the determination of K constant and provides a deeper understanding of the reaction kinetics under investigation.

Reusability in photocatalytic degradation refers to the ability of a photocatalyst to maintain its effectiveness and stability over multiple cycles of use. In photocatalytic processes, a catalyst is

used to accelerate the degradation of MB pollutants when exposed to sunlight irradiation for 5 hours. For practical applications, it is important that the photocatalyst can be reused several times without significant loss in activity.

The reusability of a photocatalyst is evaluated by testing its performance in repeated cycles of photocatalytic degradation. After each cycle, the catalyst is usually recovered, washed, and reused in the subsequent degradation process. A photocatalyst with good reusability will exhibit stable or only slightly reduced photocatalytic efficiency over multiple cycles, making it cost-effective and practical for large-scale or long-term applications in environmental cleanup, wastewater treatment, or air purification [17].

II.3. Conclusion

In this chapter, we described the experimental techniques and methods used for the synthesis of our films. We then presented the various techniques employed for the structural, topographical, morphological, and optical characterization of the thin films produced. Additionally, we provided an overview of the photocatalytic tests and wettability measurements of our films. The following chapter will focus on studying the impact of Ba-doping concentrations on the films' performance and interpreting the results obtained.

References

[1] B. Saadi, Synthèse et caractérisations d'oxyde semiconducteurs de type p en couches minces par chimie douce pour des applications photovoltaiques, Doctoral thesis, University of Mohamed Khider, Biskra, Algeria, 2024.

[2] I. Ameur, Fabrication and characterization of oxides, Doctoral thesis, University of Freres Mentouri, Constantine, Algeria, 2021.

[3] I. Benaicha, Y. Ait-alla, J. Mhalla, R. Bakkali, O. Daoudi, I. Jelall, K. Nouneh, M. Fahoume, A. Qachaou, SILAR‑engineered ZnO thin films: exploring the impact of Ni, Co, and Fe dopants on structural, optical, and electronic properties, Journal of Materials Science: Materials in Electronics, vol. 35, pp.919, 2024, doi: https://doi.org/10.1007/s10854-024-12678-2.

[4] M. Rashid, N.M. Ahmed, A. Mebdir, F.K. Yam, M.Z. Al-abri, M.A. Almessiere, B.A. El-badry, M.A. Ibrahem, O.A. Aldaghri, K. Hassan, Photoconversion efficiency of In2S3/ZnO core-shell heterostructures nanorod arrays deposited via controlled SILAR cycles, Heliyon, vol. 8, 2022, doi: https://doi.org/10.1016/j.heliyon.2022.e09959.

[5] L. Wei, J. Zhang, M. Ruan, Combined CdS/In_2S_3 heterostructures with cocatalyst for boosting carriers separation and photoelectrochemical water splitting, Applied Surface Science, vol. 541, 2021, doi: https://doi.org/10.1016/j.apsusc.2020.148431.

[6] H. Naseer, N. Al-Zaqri, T. Iqbal, M. Yousaf, S. Afsheen, M.S. Sultan, I. Warad, M. Farooq, A. Masood, Investigation of Mg doped ZnO nanoparticles decorated with Ag for efficient photocatalytic degradation, Journal of Inorganic and Organometallic Polymers and Materials, vol. 33 pp. 2790–2802, 2023, doi: https://doi.org/10.1007/s10904-023-02722-9.

[7] S. Sahu, P.K. Samanta, Microstructural study and crystallite size analysis of chemically grown bougainvillea flower-like zinc oxide nanostructures, Materials Today: Proceedings, vol. 65, pp. 2502–2505, 2022, doi: https://doi.org/10.1016/j.matpr.2022.04.474.

[8] K. Abdelkarem, R. Saad, A.M. Ahmed, M.I. Fathy, M. Shaban, H. Hamdy, Efficient room temperature carbon dioxide gas sensor based on barium doped CuO thin films, Journal of Materials Science, vol. 58, pp. 11568–11584, 2023, doi: https://doi.org/10.1007/s10853-023-08687-x.

[9] O. Ben Messaoud, A. Ouahab, S. Rahmane, S. Hettal, A. Kater, M. Sayad, H. Attouche, N. Gherraf, Optoelectronic and dielectric properties of tenorite CuO thin films Sprayed at various molar concentrations, Periodica Polytechnica Chemical Engineering, vol. 68 pp. 93–105, 2024, doi: https://doi.org/10.3311/PPch.22136.

[10] A.H. Omran Alkhayatt, A.H. Ali, Influence of cycles number and time on the structural, surface morphology and some optical properties of CuO nanostructure thin film prepared by SILAR method, Sensor Letters, vol. 16 pp. 64–70, 2018, doi: https://doi.org/10.1166/sl.2018.3907.

[11] H. Barkat, E. Guettaf Temam, H. Ben Temam, N. Mokrani, S. Rahmane, M. Althamthami, Enhancing sunlight-driven photocatalysis: High transparency and hydrophilic advancements in Ba-doped ZnO thin films, Journal of Materials Engineering and Performance, 2024, doi: https://doi.org/10.1007/s11665-024-10126-0.

[12] K. Yousra, E. Guettaf Temam, R. Saâd, H. Barkat, Effect of film thickness on the electrical and the photocatalytic properties of ZnO nanorods grown by SILAR technique, Physica Scripta, vol. 12, 2023, doi: https://doi.org/10.1088/1402-4896/ad0ae7.

[13] I. Khan, K. Saeed, I. Zekker, B. Zhang, A.H. Hendi, A. Ahmad, S. Ahmad, N. Zada, H. Ahmad, L.A. Shah, T. Shah, I. Khan, Review on Methylene Blue: Its Properties, Uses, Toxicity and Photodegradation, Water, vol. 14, no. 242, 2022, doi: https://doi.org/10.3390/w14020242.

[14] N. El Messaoudi, M. El Khomri, A. El Mouden, A. Bouich, A. Jada, A. Lacherai, H.M.N. Iqbal, S.I. Mulla, V. Kumar, J.H.P. Américo-pinheiro, Regeneration and reusability of non conventional low cost adsorbents to remove dyes from wastewaters in multiple consecutive adsorption – desorption cycles : a review, Biomass Conversion and Biorefinery, vol. 14, pp. 11739–11756, 2024, doi: https://doi.org/10.1007/s13399-022-03604-9.

[15] N. Joseph, T. Sebastian, J.C. John, A. Paul, J. Cyriac, S. Augustine, Exploring the

photocatalytic potential of copper iodide thin films deposited via multiple spray technique, Applied Surface Science Advances, vol. 19 ,2024, doi: https://doi.org/10.1016/j.apsadv.2023.100570.

[16] J. Kaur, S. Singhal, Facile synthesis of ZnO and transition metal doped ZnO nanoparticles for the photocatalytic degradation of Methyl Orange, Ceramics International. vol. 40, pp. 7417–7424, 2014, , doi: https://doi.org/10.1016/j.ceramint.2013.12.088.

[17] R. Gegova-Dzhurkova, D. Nesheva, I. Stambolova, K. Zaharieva, V. Dzhurkov, I. Miloushev, Enhanced photocatalytic performance under ultraviolet and visible light illumination of ZnO thin films prepared by modified Sol-Gel method, Molecules, vol.29, no. 4005, 2024, doi: https://doi.org/10.3390/ molecules29174005.

Chapter III.

SILAR-Processed ZnO Thin Films: Influence of Ba Doping Concentrations on Photocatalytic Degradation and Wettability

III.1. Introduction

This chapter delves into the influence of Ba doping on ZnO thin films synthesized via the SILAR technique, focusing on its impact on photocatalytic degradation of methylene blue (MB) and wettability. By systematically analyzing the doping concentrations (1 wt.%, 3 wt.%, 5 wt.%, 7 wt.%), the study investigates how Ba incorporation alters film thickness, crystallinity, surface morphology, and photocatalytic efficiency. These modifications are critical in optimizing the films for applications such as pollutant degradation and self-cleaning surfaces.

The results presented in this chapter contribute to a deeper understanding of the structure-property-performance relationship in doped ZnO thin films. This knowledge is pivotal for advancing the design of materials tailored for sustainable and efficient technological solutions.

Furthermore, the main objectives of this chapter are:

- Identification of the optimal dopant concentration that enhances the photocatalytic degradation of MB dye, while preserving the stability and uniformity of prepared thin films.
- Represent structural, morphological, topographical, and optical properties of undoped and barium-doped zinc oxide thin films at different concentration and their photocatalytic degradation of methylene blue dye, as patterns, figures, and tables.
- Interpretation and discussion of the obtained results.

III.2. Results and Discussion

III.2.1. Measurement of film Thickness

Figure III.1(a) illustrates the influence of Ba doping varying concentration on the surface thickness of ZnO films. In Comparison to undoped ZnO films, the thickness values reduced from 116.97 nm to 101.5 nm at a Ba doping level of 1 wt.% due to the initiation of restructuring mechanisms within the films. Noting that, whereas the doping concentration is equal to 1 wt. %, the intensity of the (002) peak and the film thickness decrease. This variation suggests that the observed changes result by structural modifications induced by Ba doping [1]. Barium atoms can generate a new energy levels below the conduction band, causing a shift in the band gap energy. This modification enhances the optoelectronic properties of the material, enabling it to absorb

visible light [2]. Notably, with Ba doping concentration increasing to 7 wt.%, the film thickness increased to 319.05 nm, as seen in **Table.III.1**.

Table III.1. *Values of thickness and roughness profile (Ra) of Ba-doped ZnO thin films*

Samples	Thickness (nm)	Roughness (nm)
Undoped ZnO	116.97	87.1
Ba-doped ZnO (1 Wt.%)	101.5	164
Ba-doped ZnO (3 Wt.%)	210.5	86.1
Ba-doped ZnO (5 Wt.%)	239.17	252
Ba-doped ZnO (7 Wt.%)	319.05	91.1

Figure III.1(b) presents the scanning electron microscopy (SEM) cross-sectional image of 7 wt.% Ba doped ZnO films. The thickness measurement of the film determined via this method confirms the result obtained by the AFM analysis. The average thickness, calculated from 50 measurements, is 374.6 ± 6.5 nm, which closely matches the AFM measurement of 319.05 nm. These findings highlight the considerable effect of Ba doping on the thickness of ZnO films, which in turn affects the films' optical, structural, self-cleaning, and photocatalytic characteristics.

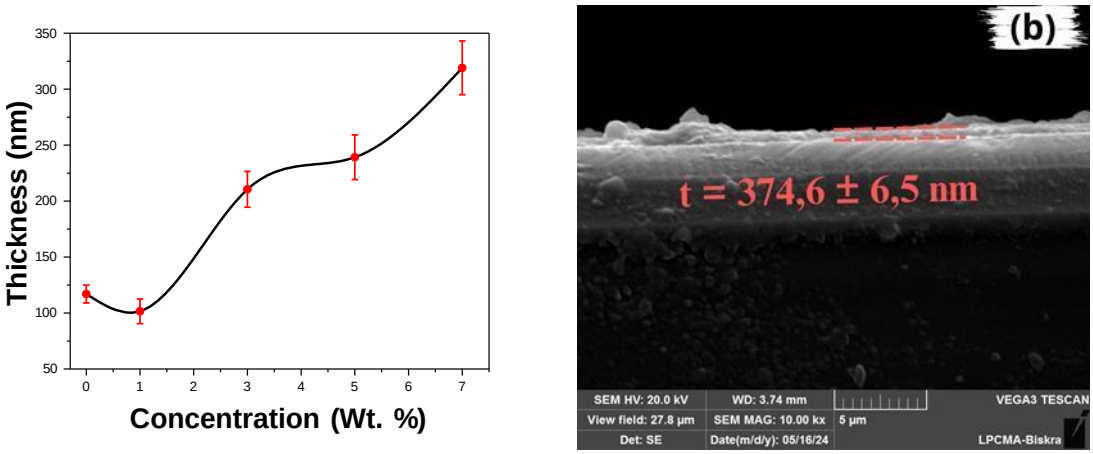

Figure III. 1 (a). Impact of Ba doping concentration on the film thickness variation, and **(b)** SEM cross-sectional image for 7 wt.% Ba-doped ZnO film

III.2.2. Structural properties

The X-ray diffraction technique is a suitable method for studying the crystallographic analysis of thin films. In this study, the XRD patterns of the undoped and barium-doped ZnO films at different dopant concentrations (1 wt.%, 3 wt.%, 5 wt.%, and 7 wt.%) were investigated, and several diffraction peaks are shown in **Figure III.2(a)**. It displayed the polycrystalline nature of all films obtained with a hexagonal wurtzite structure according to the JCPDS card (**75-0576**). The major diffraction peaks observed with the most intense peak are corresponding to 2θ= 31.8 °, 34.47 °, and 36.31 ° along to (100), (002) and (101) planes, respectively. Other peaks were also observed, such as (102), (110), (103), and (112). The XRD patterns of undoped and 1 wt. %, 3 wt. %, 5 wt. %, and 7 wt. % Ba doping shows no evidence of any impurity peak, confirming the proper doping of prepared films.

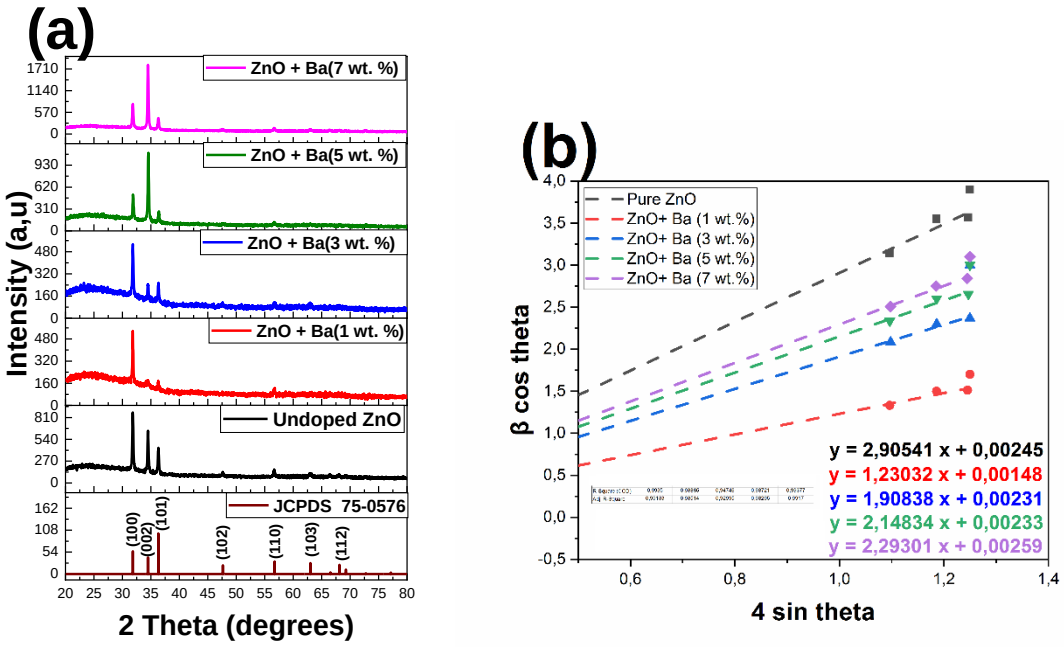

Figure.III.2 (a) XRD patterns of un-doped ZnO and Ba-doped ZnO thin films, **(b)** Williamson–Hall plots of βcos(θ) versus 4sin(θ)

The XRD diffractograms show that undoped and ZnO films doped with 1 and 3 wt.% of Ba grow preferentially along the (100) direction due to experimental conditions of SILAR process [3]. Based on the literature, the incorporation of barium into ZnO at higher concentrations alters the surface energy, which promotes a change in the preferred growth orientations of nanostructures [4]. It is clear that in the samples of 5 and 7 wt.% Ba-doping, the (002) plane is the predominant orientation. This shift is may be due to the low free surface energy compared to the (100) direction [5][6][7]. The Williamson–Hall method was used to calculate the structural characteristics based on the major intense peaks for each sample as expressed in **Eq II.6**. This model was employed to plots of β cosθ as a function of 4sinθ as illustrated in **Figure III.2(b)**. The intercept of the linear fit drawn has been taken to find the value of D and slope leads to ε value.

Table III.2 demonstrates that incorporating Ba leads to a reduction in the crystallite size from 98.2 nm for undoped ZnO to 34.6 nm for ZnO doped with 7 wt.% Ba. This decrease is attributed to the significantly larger Ba ion radius (1.33 A˚) than the Zn ion radius (0.74 A˚)[5]. In another case, due to the greater value of lattice strain as shown in **Table III.2**, the sample of 5 wt.% of Ba doping presented the largest crystallite size (113.6 nm). D. Kumar et al [9] reveals that the lattice strain increases linearly as the crystallite size increases. This is because crystallites contain more defects

and dislocations, which can lead to strain in the crystal lattice [10]. The influence of strain on the kinetics of crystal growth based on the diffusion of Ba ions within the ZnO potentially enhances the rate of crystal growth, resulting in larger crystallites [11]. Furthermore, in the photocatalytic process, materials that have larger crystallites can absorb lighter due to their large volume. Such behavior can to generate of more electron–hole pairs, which are necessary for the occurrence of photocatalytic reactions [12].

Table III.2. *Structural parameters of undoped ZnO and Ba-doped ZnO thin films.*

Samples	**2θ (°)**	**D (nm)**	**FWHM**	**d-spacing (A°)**	**$\varepsilon * 10^{-3}$**	**$\delta * 10^{4}$ (nm^{-2})**	**$N * 10^{4}$**
Undoped ZnO	31.80	98.2	0.19	2.81341	1.61	1.03699	1.235
Ba/ZnO (1 wt.%)	31.81	86.6	0.1181	2.81254	1.17	1.33341	1.562
Ba/ZnO (3 wt.%)	31.81	44.7	0.1574	2.59923	0.147	5.00477	23.56
Ba/ZnO (5 wt.%)	31.86	113.6	0.1771	2.81260	1.86	0.77489	1.631
Ba/ZnO (7 wt.%)	31.85	34.6	0.1968	2.60193	-0.427	8.35310	77.02

The d-spacing values, calculated using (**Eq II.7-8**), decrease with the increase of Ba doping concentration. This reduction is attributed to substituting Zn atoms with Ba atoms, leading to a reduction in the interplanar distance.

The dislocation density has an inverse relationship with crystallite size and it was increased with higher Ba doping concentration due to the created defects in the crystal structure, as shown in **Table III.2**. A rise in dislocation density enhanced the hardness of a material, with smaller crystallite-sized materials exhibiting higher dislocation densities and greater hardness [13]. These dislocations can function as recombination sites for electron–hole pairs generated during the photocatalytic process. A lower dislocation density indicates fewer recombination sites, allowing more electron–hole pairs to contribute to photocatalytic reactions, thereby enhancing their efficiency [14].

Table III.2 reveals a change in the number of crystallites (N) as the Ba doping concentration increases. A larger crystallite size of 113.6 nm corresponds to a reduction in the crystallite number ($1.631 * 10^{4}$). This behavior can be due to the introduction of additional energy levels within the

ZnO band gap by Ba doping. These introduced energy levels serve as traps for charge carriers like electrons and holes, which can extend their lifetimes, thereby improving the film's photocatalytic efficiency[15].

III.2.3 3D surface topography analysis

The profilometer has been proven to be an effective method for analyzing the surface topography of a film. The 3D images of Ba-doped ZnO are reported in **Figure III.3**, which provides detailed insights into the surface properties influenced by varying Ba concentrations. The surface roughness parameters, including average roughness (Ra) was evaluated using the Apex analysis software.

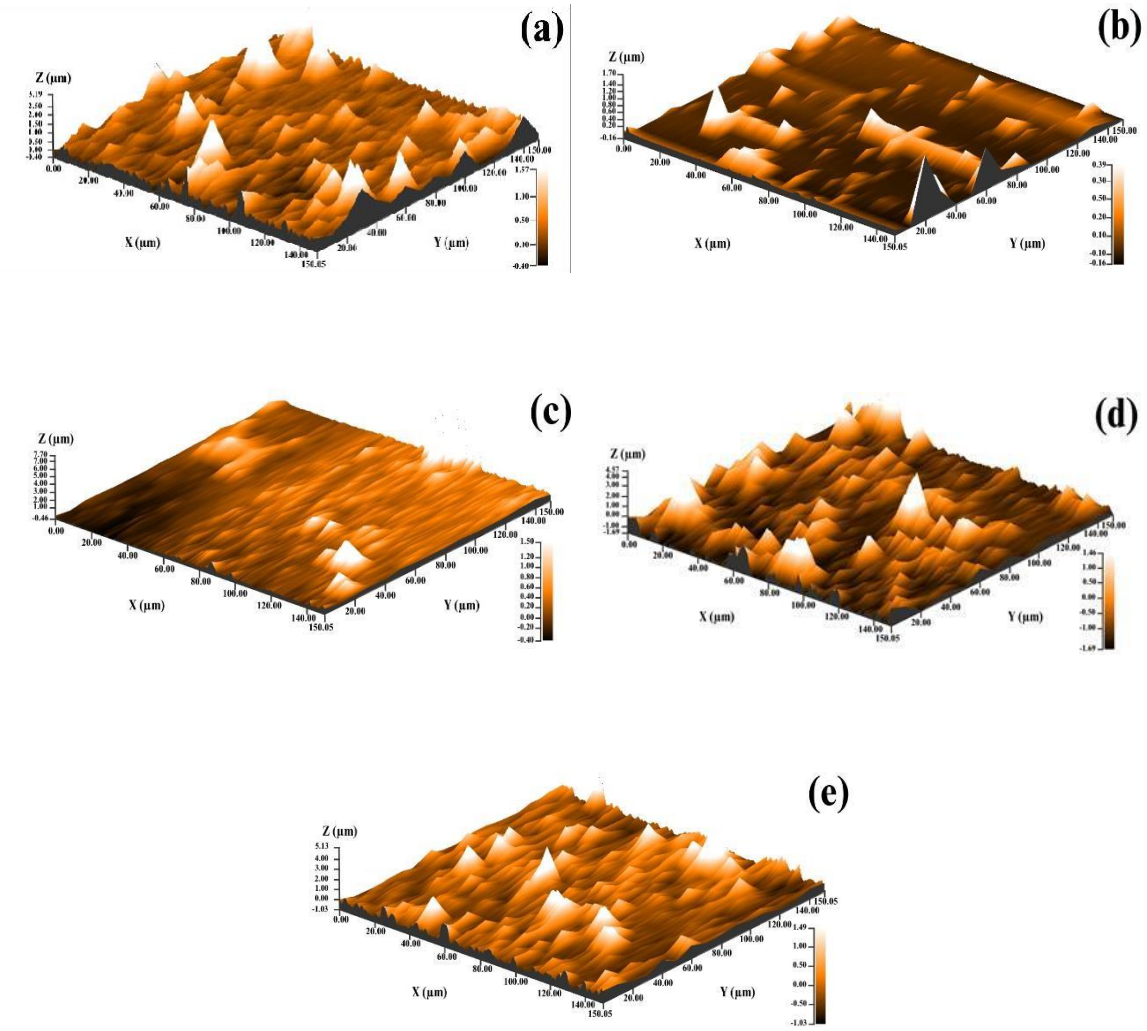

Figure III.3. 3D surface topography of Ba-doped ZnO thin films: **(a)** undoped ZnO, **(b)** 1 wt.% Ba-doped ZnO, **(c)** 3 wt.% Ba-doped ZnO, **(d)** 5 wt.% Ba-doped ZnO, **(e)** 7 wt.% Ba-doped ZnO.

As can be seen in **Table III.1**, the values of Rq range from 86.1 nm to 252 nm. The 5 wt.% Ba-doped ZnO film exhibited the greatest surface roughness, suggesting a direct relationship between surface heterogeneity and increasing Ba concentrations. These surface irregularities considerably influence the optical characteristics of the films, impacting aspects including, transmittance and band gap energy. Higher surface heterogeneities result in increased light scattering, which leads to decrease light transmittance. Moreover, the surface roughness enhances the effective surface area, accordingly the photocatalytic efficiency enhanced by providing more active sites for dye degradation [16].

III.2.4. Surface morphology and elemental analysis

Surface morphology is an important method for obtaining detailed information about the microstructure of thin films [17]. The morphology of varying Ba doping concentrations in ZnO thin films fabricated via the SILAR process is analyzed by observing SEM images as shown in **Figure III.4.** All the films were deposited under the optimized conditions and were uniformly covering the substrate with good adherence. This SEM images depicted that the surface morphology changes accordingly with the doping concentration.

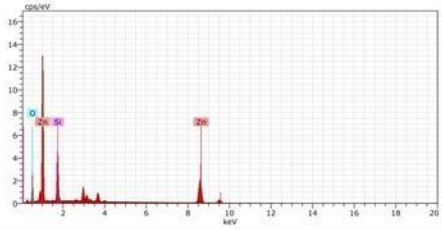

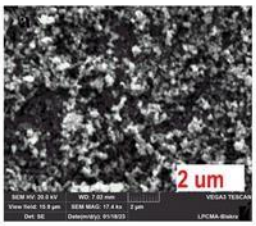

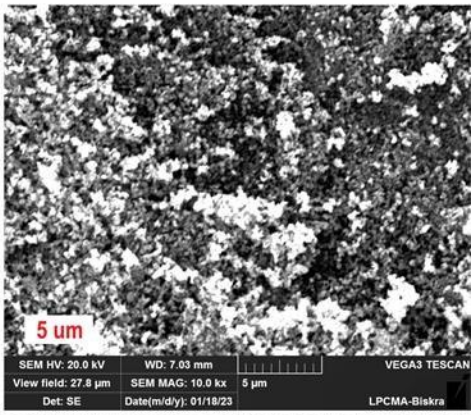

a

El	AN	Series	unn. C [wt.%]	norm. C [wt.%]	Atom. C [at.%]	Error (1 Sigma) [wt.%]
Zn	30	K-series	35.78	62.25	33.07	1.03
O	8	K-series	12.44	21.65	47.01	1.78
Si	14	K-series	9.25	16.10	19.92	0.43
Total:			57.48	100.00	100.00	

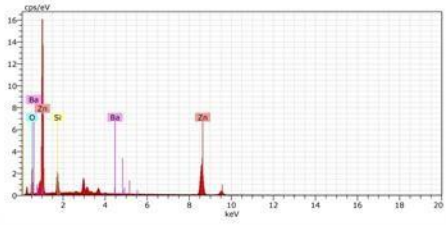

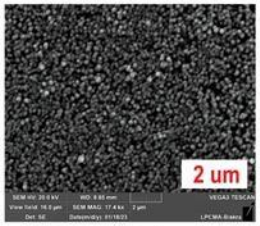

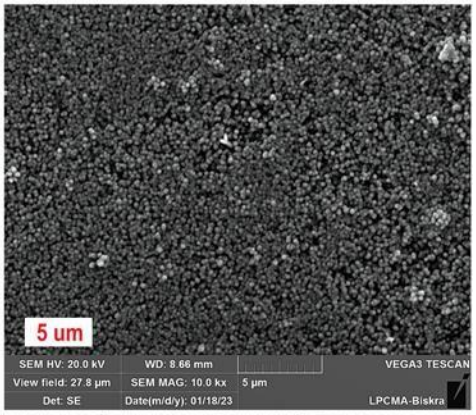

b

El	AN	Series	unn. C [wt.%]	norm. C [wt.%]	Atom. C [at.%]	Error (1 Sigma) [wt.%]
Zn	30	K-series	47.62	75.11	45.58	1.35
O	8	K-series	11.44	18.05	44.76	1.67
Si	14	K-series	4.33	6.84	9.66	0.22
Ba	56	L-series	0.00	0.01	0.00	0.03
Total:			63.40	100.00	100.00	

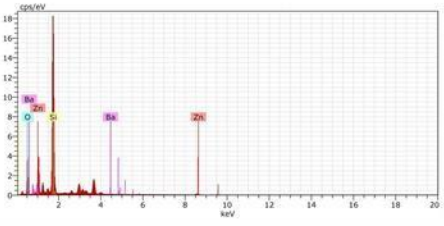

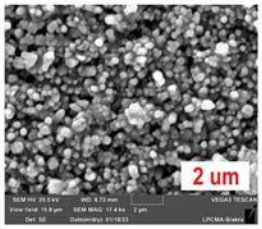

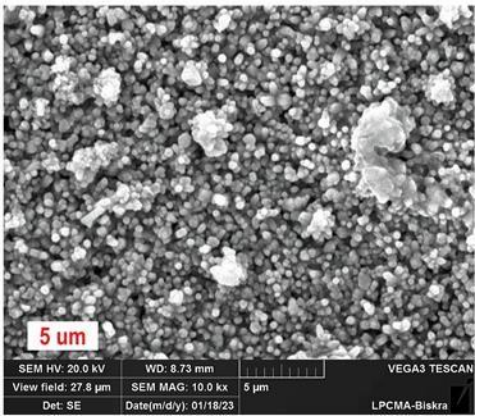

c

El	AN	Series	unn. C [wt.%]	norm. C [wt.%]	Atom. C [at.%]	Error (1 Sigma) [wt.%]
Si	14	K-series	18.39	54.30	42.25	0.81
O	8	K-series	13.95	41.21	56.28	1.89
Zn	30	K-series	1.48	4.36	1.46	0.09
Ba	56	L-series	0.04	0.13	0.02	0.03
Total:			33.87	100.00	100.00	

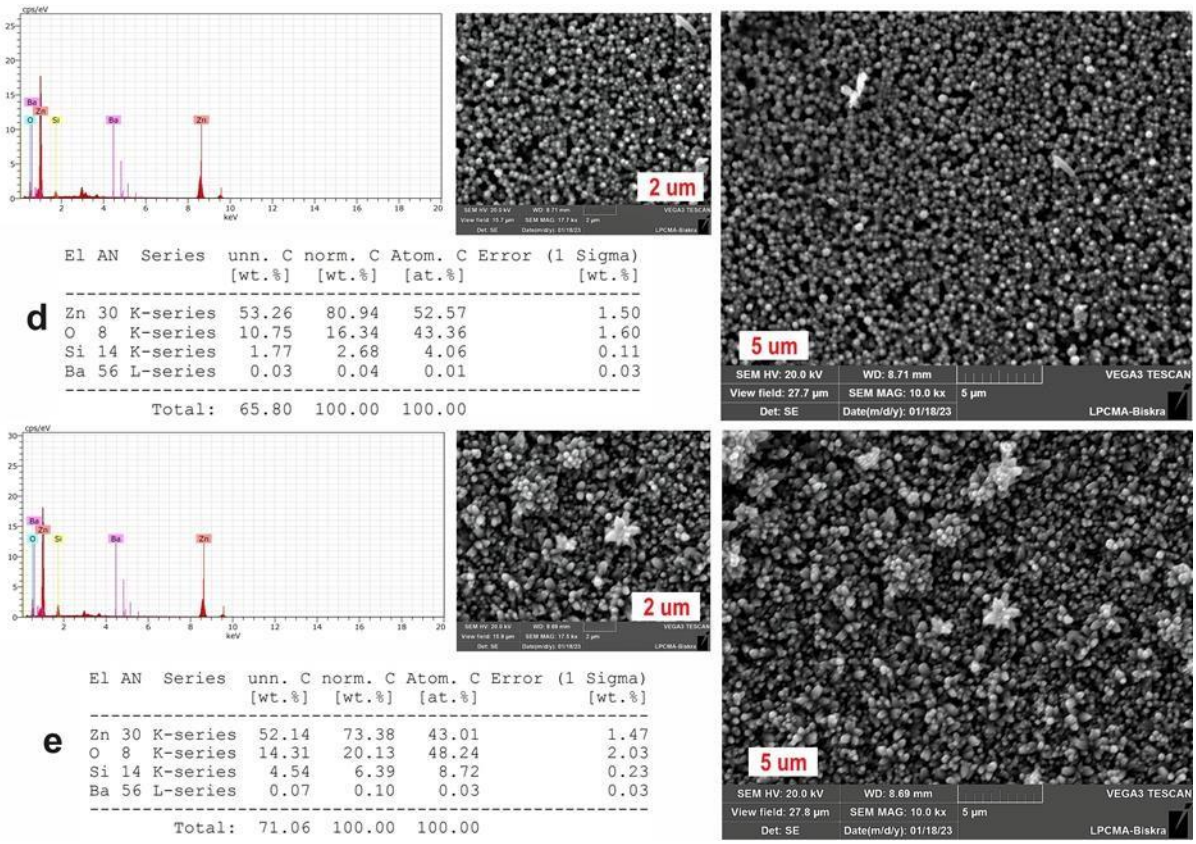

Figure III.4. SEM images and EDX pattern analysis of Ba-doped ZnO thin films: (a) undoped ZnO, (b) 1 wt.% Ba-doped ZnO, (c) 3 wt.% Ba-doped ZnO, (d) 5 wt.% Ba-doped ZnO, (e) 7 wt.% Ba-doped ZnO

In more detail, the undoped ZnO films have a uniform and smooth surface compared with the other substrates. However, the introduction of 1 wt.% Ba doping results in a granular surface, which indicates the formation of Ba-doped ZnO films. Then, the surface becomes more granular when the concentration of Ba increases to 3 wt.%, and with larger agglomerates and a rougher texture at 5 wt.% Ba. Furthermore, at 7 wt.% Ba, the film's surfaces become highly irregular and porous, indicating the possibility of saturation or phase separation.

To identify the elemental composition of synthesized undoped ZnO and Ba-doped ZnO thin films, the Energy Dispersive X-Ray Spectroscopy (EDX) compositional analysis was employed and the result is illustrated in **Figure III.4**. This spectrum confirms the presence of Zn, O, and Si elements in the deposited films. Trace amounts of Si are also detected in the film from the glass substrate [1]. The high intensity of the Zn and O peaks suggests that the samples mainly contain ZnO. The principal purpose of using this technique (EDX) is to confirm the presence of

barium. All the spectra display the presence of this element, coming from the doping and we notice an increase in the percentage of Ba with doping rate increment, supporting the successful incorporation of Ba into the ZnO matrix.

III.2.5. Optical Properties

Study of the optical properties of the undoped ZnO and Ba-doped ZnO thin films with increasing concentration from 1 wt.% to 7 wt.% were based on the results obtained from UV–Vis spectroscopy, as shown in **Figure III.5 (a).**

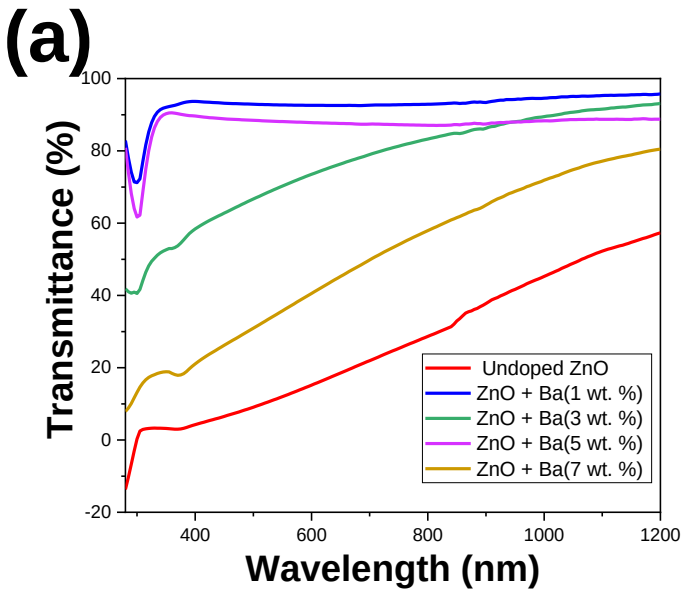

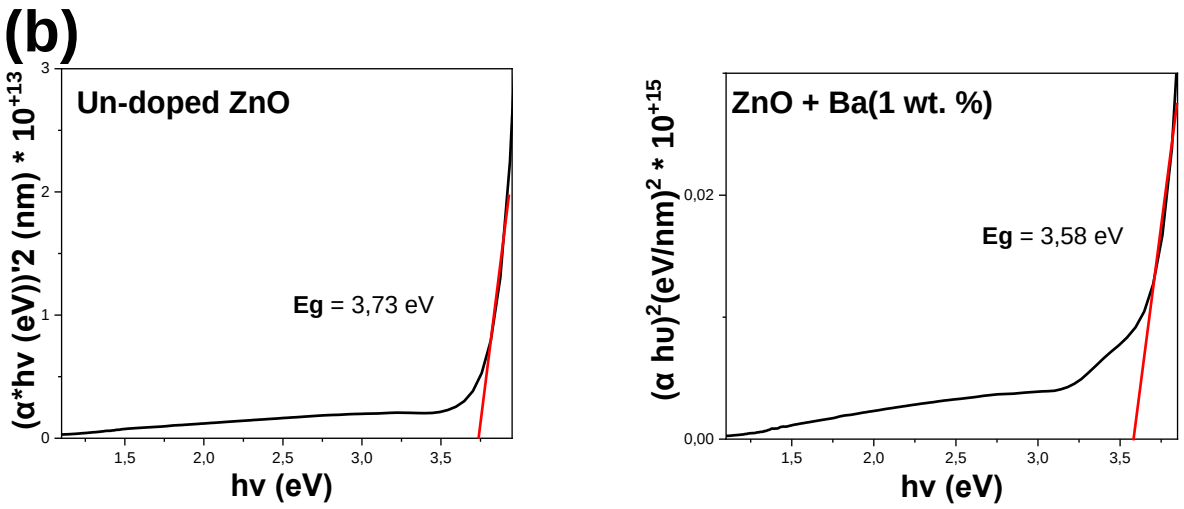

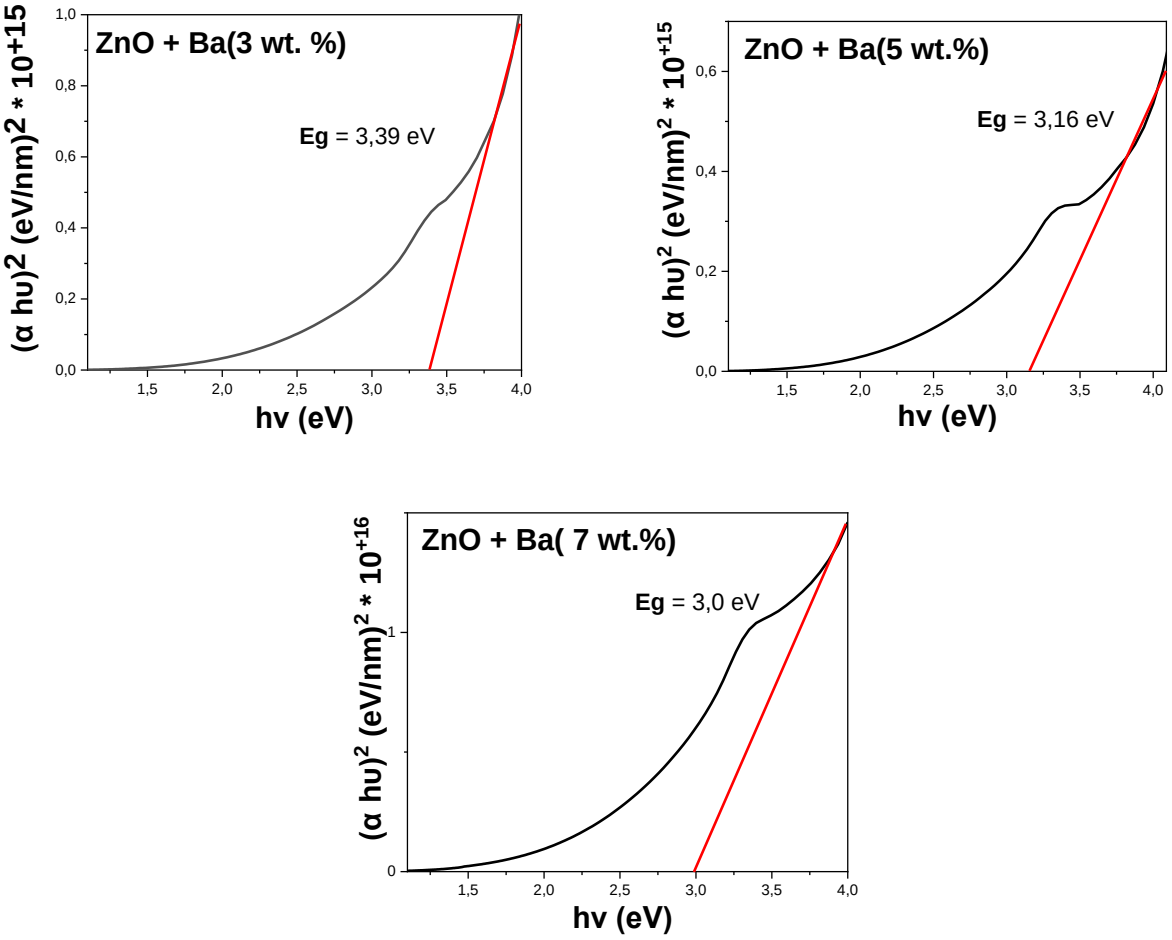

Figure III.5. (a) UV–Vis optical of un-doped and Ba-doped ZnO thin films, and **(b)** determination of the optical band gap

Optical transmission spectrum shows that Ba-doped ZnO films exhibited higher transparency in the visible spectrum compared to undoped ZnO, with the 1 wt.% Ba-doped sample showing the highest transparency, likely due to a reduced film thickness (101.5 nm). However, as the Ba doping concentration increased to 3, 5, and 7 wt.%, a significant reduction in transmittance was observed. This decline is attributed to the incorporation of additional Ba atoms into interstitial positions within the ZnO lattice, which induces light scattering, aligning with previous research [18]. These results emphasize the complex relationship between dopant concentration and the optical properties of Ba-doped ZnO materials.

The optical band gap (Eg) was obtained by extrapolating the linear portion of the plot $(Ahv)^2$

versus photon energy (hv). **Figure III.5. (b)** shows the Tauc plots for the undoped ZnO and barium-doped ZnO thin films deposited at different concentrations. The obtained values of optical band gaps are 3.73 eV, 3.58 eV, 3.39 eV, 3.16 eV and 3.00 eV for un-doped and doped ZnO films at 1 wt.%, 3 wt.%, 5 wt.%, and 7 wt.% barium-doping concentrations, respectively. As shown in **Table III.3**, the bandgap of ZnO films decreases with increasing of doping concentration from 1 wt.% to 7 wt.%. This decreasing trend is attributed to Ba atoms inducing lattice distortions and defect states, narrowing the band gap. Additionally, variations in strain contribute to the reduction in bandgap values, as strain alters the interatomic spacing in semiconductors, thereby impacting the energy gap. The reduction in Eg may also be linked to the increase in film thickness [19]. This variation in the band gap has a substantial effect on light absorption and enhances photocatalytic performance.

Table III.3 Calculated optical band gap energy of undoped and Ba-doped ZnO thin films.

Ba-doping rate (wt %)	**Eg (eV)**
0	3.73
1	3.58
3	3.39
5	3.16
7	3.00

III.2.6. Water Droplet Contact Angle (WCA) Measurements

Surface free energy, topography, microstructure, and chemical composition affect a film's wettability behavior. The water contact angle (WCA), illustrated in **Figure III.6**, gives an insight into the hydrophilicity of Ba-doped ZnO films.

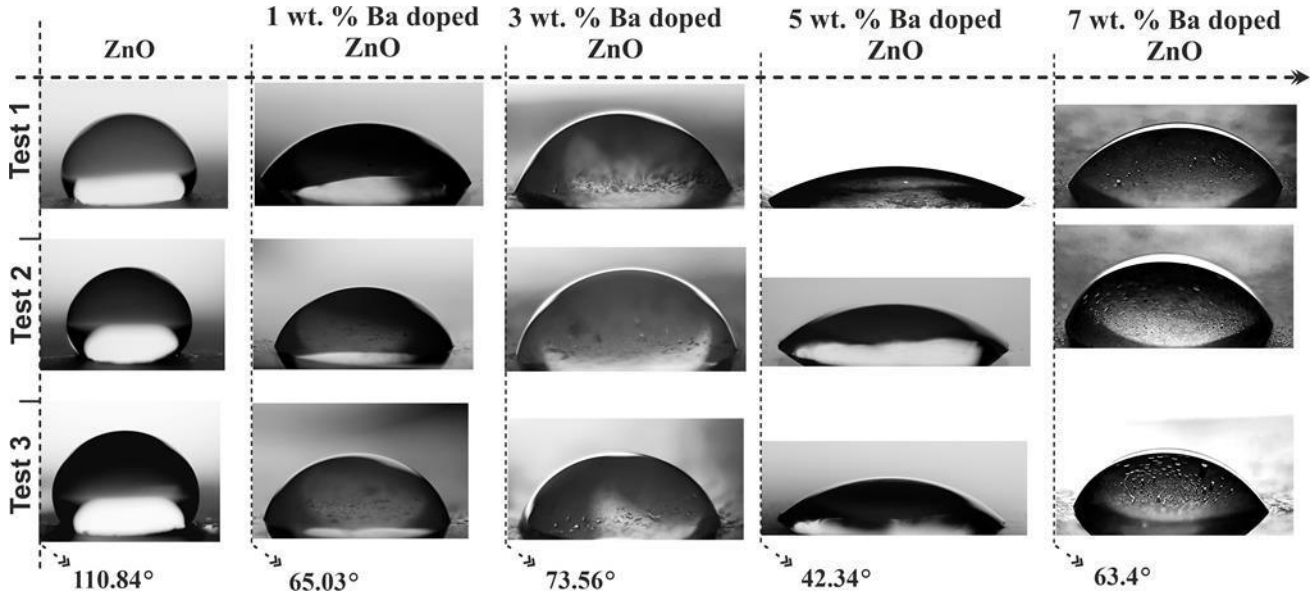

Figure III.6. Contact angle measurement of water droplets for un-doped and Ba-doped ZnO thin film

As seen in **Figure III.6**, the sample of undoped ZnO thin film exhibits distinct hydrophobic properties, with a contact angle approximately of 110.84°. Furthermore, it is noteworthy that doping concentration is crucial to influencing surface properties and contact angles. Increasing Ba-doping improves the surface wettability of films. Additionally, increased in surface roughness enhances the specific surface area and wettability, thereby improving the adsorption of organic dyes and boosting photocatalytic efficiency[20]. In other words, the WCA reduces as Ba doping increased, which can be attributed to the larger crystallites and rougher surfaces of the doped films.

These results highlight the important role of the hydrophilic properties of Ba-doped ZnO films and its relationship with the specific surface area. The observed hydrophilicity, independent of doping concentration, demonstrates the stable and beneficial attributes of Ba/ZnO films, making them promising candidates for applications in catalysis, sensing, and energy conversion.

III.2.7. Photocatalytic Tests

The photocatalytic efficiency of undoped and Ba-doped ZnO thin films under sunlight irradiation was evaluated through the degradation of methylene blue (MB) dye in a water solution with a concentration of 4 ppm. **Figures III.7 (a)** present the photocatalytic efficiency of undoped ZnO and Ba-doped ZnO thin films at various concentrations across wavelengths of 400–800 nm over

time from 0 hour in a dark environment to 5 hours under sunlight irradiation and meteorological conditions in Biskra, Algeria, on January 11, 2023, which presented in **Table III.4.**

(a)

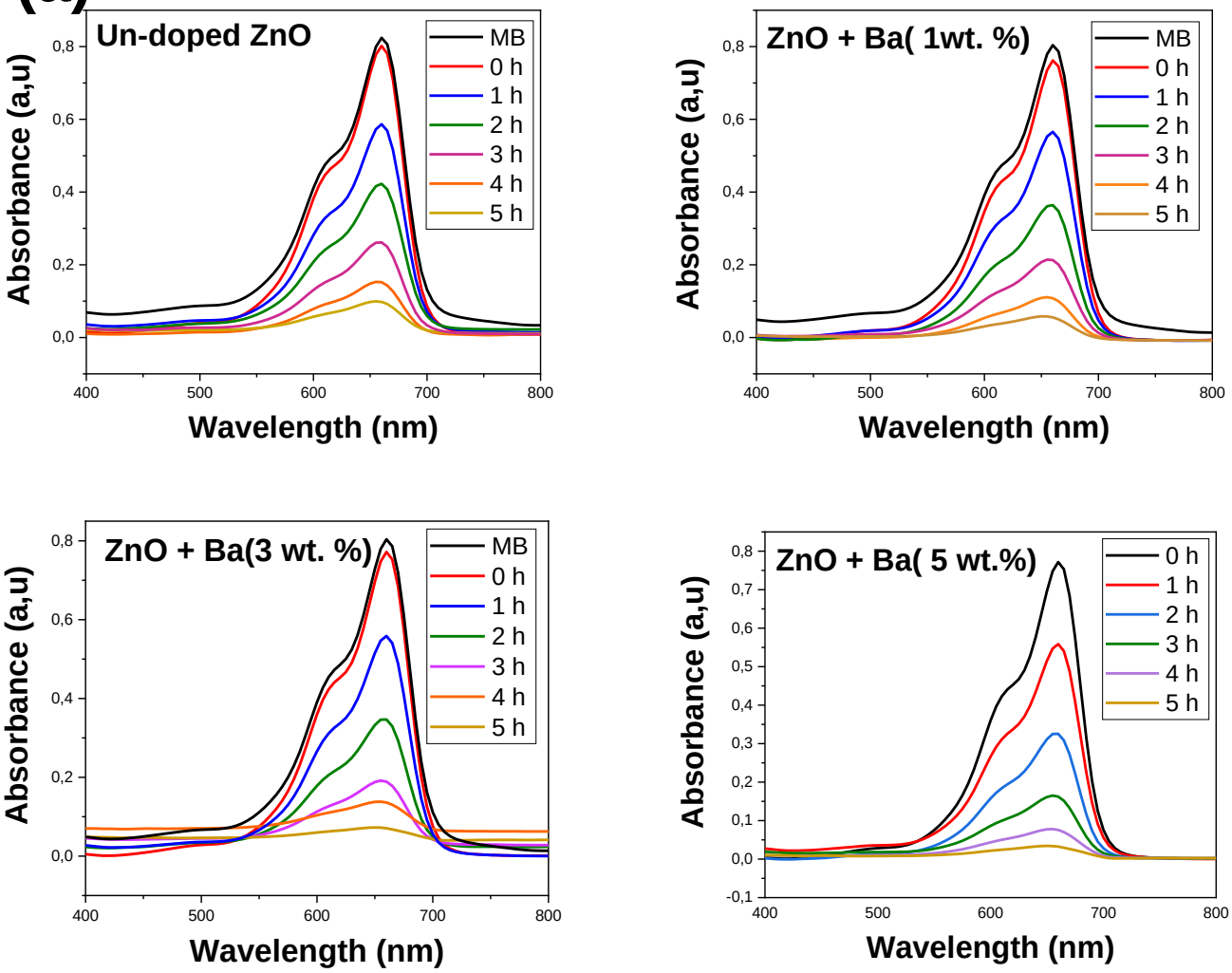

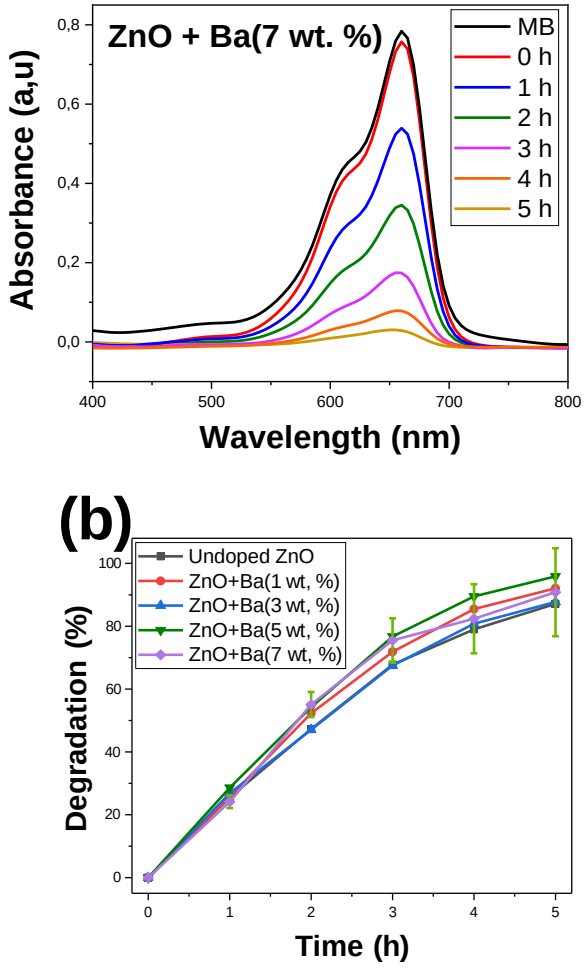

Figure III.7. (a) Variation of UV–Vis spectra of MB during photodegradation over undoped ZnO and Ba-doped ZnO films at 1 wt.%, 3 wt.%, 5 wt.%, 7 wt.% concentrations, and **(b)** Plot of photocatalytic efficiency rate as a function of irradiation time

Table III.4 Parameters and results of photocatalytic tests.

Samples	*Undoped ZnO*	*Ba/ZnO:1 wt.%*	*Ba/ZnO:3 wt.%*	*Ba/ZnO:5 wt.%*	*Ba/ZnO:7 wt.%*
Removal (%)	86.59	92.59	87.22	95.78	90.54
K (h^{-1})	0.4113	0.5258	0.4225	0.6386	0.4782
The date	*11/01/2023*				
The Temperature (°C)	*11*				
Wind speed (km/h)	*10*				
Humidity(%)	*46*				
irradiation intensity (mW/cm^2)	*0.1357*				

The photodegradation of MB under sunlight irradiation was studied to assess the stability of the MB dye. The dye's stability during the photocatalysis process was confirmed by the constant MB concentration after five hours of sunlight exposure in the absence of the photocatalyst. However, photodegradation of the MB dye began when photocatalysts were present. The degradation efficiency of MB dye for various irradiation times is summarized in **Figure III.7(b)** and **Table III.4**. The decrease in the intensity of the absorbance peak of MB cast over undoped and Ba-doped films after the irradiation suggested the photodegradation of MB. It is observed from **Figure III.7(b)** that the photocatalytic efficiency of ZnO was enhanced with increasing at different percentages of Ba films for 1 wt. %, 3 wt. %, 5 wt. %, and 7 wt. % for the degradation of MB. Furthermore, at 1 wt.% Ba, the removal efficiency increased to 92.59% compared to the undoped ZnO sample, attributed to improved light absorption and charge separation. At 3 wt.% Ba, the removal efficiency slightly decreased to 87.22%, probably due to grain boundaries acting as recombination centers [16]. In another hand, the best performance was 95.78% at 5 wt.%, attributed to enhanced light absorption and active sites for reactions, and the increase of free charge carriers introduced by Ba^{2+} ions [21]. The doping of Ba^{2+} ions generates electron-accepting centers near the conduction band, where electrons are captured in these new levels. This results in the

enhancement of photoinduced electron-hole separation, which improves the generation of HO• and $O2^{\bullet-}$ and increases the photocatalytic process [22]. Nevertheless, it noted that at 7 wt.% Ba concentration the removal efficiency was reduced to 90.54%, possibly due to an excessive Ba incorporation leading to defect states and light scattering [16].

The linear relationship between ln(C_o/Ct) and irradiation time is illustrated in **Figure III.8** and the rate constants obtained from the graph slope, are presented in **Table III.4**. These results are suggesting that the photocatalytic degradation MB pollutant follows the pseudo-first-order reaction kinetic model using both undoped ZnO and Ba-doped ZnO thin films. The first-order rate constant (K) for the undoped ZnO films was determined to be 0.4113 h^{-1}. It was observed that K increased with higher doping concentrations, reaching its maximum value of 0.6386 h^{-1} at a doping level of 5 wt.%, indicating optimal degradation efficiency of the MB dye for this sample.

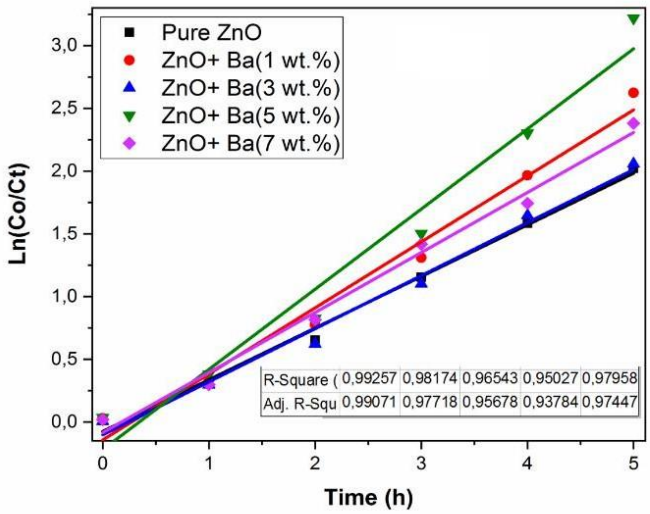

Figure III.8. pseudo-first-order kinetics plot of undoped and Ba-doped ZnO for MB degradation

III.2.8. The surface morphology after photo-degradation process

The SEM micrographs of the 5 wt.% Ba-doped ZnO films after photocatalytic degradation, as presented in **Figure III. 9**, reveal notable changes in surface morphology due to repeated use. The surface displays signs of nanostructure aggregation and coarsening, indicative of structural degradation over time. The surface roughness might be increased, likely resulting from prolonged solar exposure and repeated cycling. Furthermore, the formation of microcracks and pores in

certain regions highlights areas of structural weakness that develop during the degradation process. These morphological changes, including nanostructure coarsening and crack formation on the surface of Ba-doped ZnO, contribute to a reduction in the active surface area, which can reduce the photocatalytic efficiency of the material [23] [24]. The structural degradation including, the formation of pores with an increased in surface roughness, and emerging defects compromise the integrity of the films, raising concerns about their long-term durability and performance reliability in practical applications [24][25].

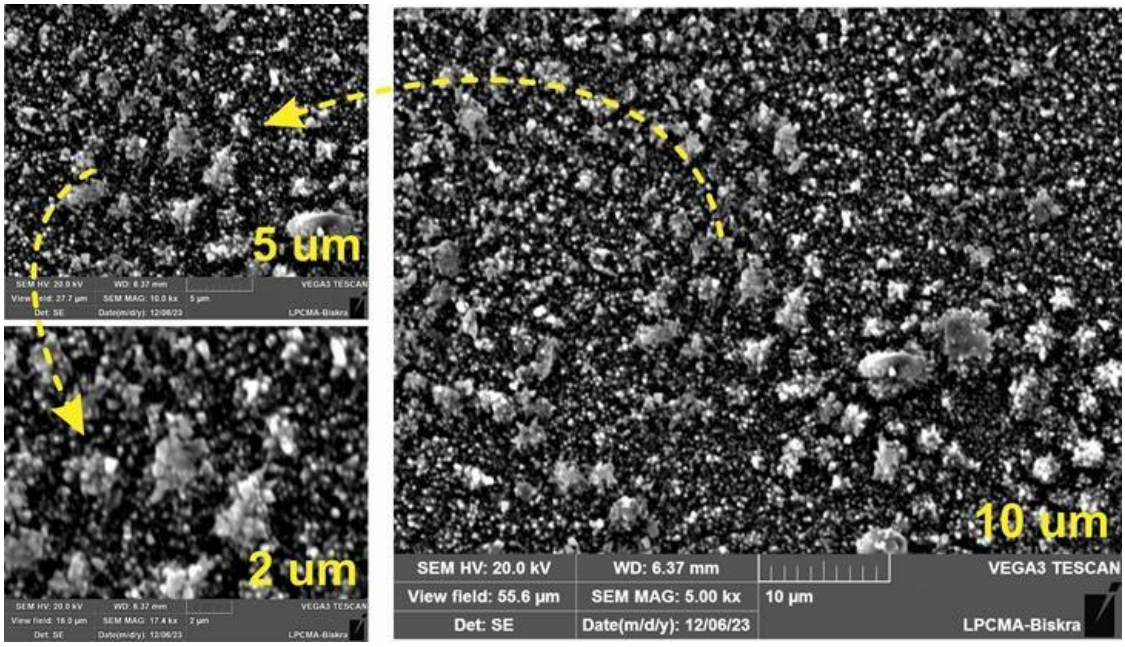

Figure III.9. SEM images of the surface morphology of the 5 wt.% Ba-doped ZnO sample after Photocatalytic activity

III.2.9. The reusability of 5 wt.% Ba-doped ZnO Photocatalyst

For practical applications, the reusability of the photocatalyst is an important key characteristic. To evaluate the viability of the photocatalysts, a sample containing 5 wt.% barium was tested in fifth successive cycles, as shown in **Figure III.10**, during a 5 h under normal conditions, as detailed in **Table III.5**. The photocatalytic degradation efficiency decreased from 85.99% in the first cycle to 68% in the fifth cycle.

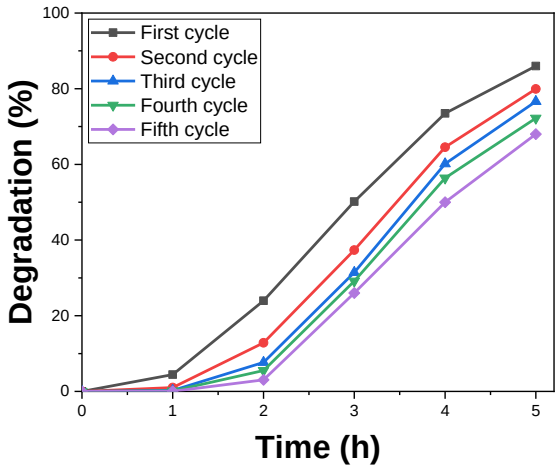

Figure III.10. Plot showing the photocatalytic performance of the 5 wt.% sample over five cycles

These findings demonstrated that the sample of 5 wt.% Ba-doped ZnO thin film was exceptionally well active, stable, and reusable material for dye removal applications.

Table III.5 The conditions and results of five recycling photocatalytic tests.

Cycle	The date	Temperature C°	Wind speed km/h	Humidity %	Irradiation intensity mW/cm^2	Removal in 5 h %
0	11/01/2023	11	10	46	0.1357	95.78
1	31/01/2023	11	10	46	0.1357	85.99
2	01/02/2023	8	10	45	0.1355	79.94
3	27/11/2023	37	5	40	0.1241	76.63
4	28/11/2023	38	5	40	0.1219	72.20
5	29/11/2023	37	5	44	0.1214	68.00

III.3. Conclusion

In summary, a low cost, effective, and simple SILAR method was successfully employed to prepare a homogeneous un-doped and Ba-doped ZnO thin films on glass substrate. This study examined the impacts of varying barium doping concentrations (1 wt.%, 3 wt.%, 5 wt.%, and 7 wt.%) on the self-cleaning properties, photocatalytic efficiency, and reusability of ZnO thin films in the degradation of MB dye. The varying of doping concentrations affected the structural, topographical, morphological, and optical properties. The results revealed the polycrystalline nature of all films and confirmed the successful doping of Ba into the ZnO lattice, showing well-defined peaks corresponding to the hexagonal wurtzite structure of ZnO with slight shifts indicating Ba doping with the preferred planes along (100) and (002). At the 5 wt.% Ba doping level, the surface roughness significantly increased to 252 nm, accompanied by larger agglomerates and a rougher texture. This increase can be attributed to the larger crystallite size (113.6 nm) and the higher lattice strain (1.86×10^{-3}). The transmittance of the films increased with Ba doping, indicating improved optical transparency. Additionally, the optical band gap of Ba-doped ZnO showed a slight reduction compared to un-doped ZnO, decreasing from 3.73 eV to 3.0 eV at higher doping concentrations. The evaluation of WCA revealed a significant enhancement in surface hydrophilicity for the 5 wt.% Ba-doped ZnO sample, as the WCA decreased notably from 110.84° for undoped ZnO films to 42.34°. The 5 wt.% Ba-doped ZnO films exhibited the highest photocatalytic efficiency, achieving 95.78% degradation of MB under sunlight irradiation within 5 hours. This sample was demonstrated remarkable stability, reusability, and maintained their performance across five cycles. From the above results, it can be concluded that Ba-doped ZnO thin films hold significant promise for photocatalytic applications, particularly in degrading organic dyes present in wastewater. Moreover, their superior wettability makes them highly suitable for developing self-cleaning surfaces and anti-fogging coatings, offering practical solutions for future environmental and industrial challenges. The next chapter will focus on optimizing the SILAR deposition cycles parameter to further enhance film performance.

References

[1] B. Fouad, Deposition and analysis of Zinc Oxide thin films elaborated using spray pyrolysis for photovoltaic applications, Doctoral thesis, University Mohamed Khider of Biskra, Algeria, 2019, http://thesis.univ-biskra.dz/id/eprint/4533.

[2] A. Mudhoo, S. Paliya, P. Goswami, M. Singh, G. Lofrano, M. Carotenuto, F. Carraturo, G. Libralato, M. Guida, M. Usman, S. Kumar, Fabrication, functionalization and performance of doped photocatalysts for dye degradation and mineralization: a review, Springer International Publishing, vol. 18, pp.1825–1903, 2020, doi: https://doi.org/10.1007/s10311-020-01045-2.

[3] K. Yousra, E. Guettaf Temam, S. Rahmane, H. Barkat, Effect of film thickness on the electrical and the photocatalytic properties of ZnO nanorods grown by SILAR technique, Physica Scripta, vol.98, no.12, pp.1–40, 2023, doi: https://doi.org/10.1088/1402-4896/ad0ae7.

[4] Y. Gu, J. Qi, Y. Zhang, Surface Energy of Indium Doped ZnO Studied by PAW + U Method, vol. 561-565, pp.1861–1864, 2007, doi: https://doi.org/10.4028/www.scientific.net/MSF.561-565.1861.

[5] V. Gopala Krishnan, P. Elango, M. Ragavendar, P. Sathish, G. Gowrisankar, Effect of doping on the surface modification of nebulizer sprayed $Ba_xZn_{1-x}O$ nanocrystalline thin films, Materials Research Express. vol. 4, no. 3, 2017, doi: https://doi.org/10.1088/2053-1591/aa6077.

[6] J. Ghatak, J.H, Huang, C.P. Liu, Derivation of surface free energy of ZnO and GaN using in-situ electron beam hole drilling, Nanoscale, vol. 8, pp. 634-640, 2015, doi: https://doi.org/10.1039/C5NR06198A.

[7] M. Zhou, S. Guo, J. Li, X. Luo, Z. Liu, T. Zhang, X. Cao, M. Long, B. Lu, A. Pan, G. Fang, J. Zhou, S. Liang, Surface-Preferred Crystal Plane for a Stable and Reversible Zinc Anode, Advanced materials, vol. 33, no. 21, pp. 1–9, 2021, doi: https://doi.org/10.1002/adma.202100187.

[8] A. Modwi, K.K. Taha, L. Khezami, A.S. Al-Ayed, O.K. Al-Duaij, M. Khairy, M.

Bououdina, Structural and Electrical Characterization of Ba/ZnO Nanoparticles Fabricated by Co-precipitation, Journal of Inorganic and Organometallic Polymers and Materials, vol. 30, pp. 2633–2644, 2020, doi: https://doi.org/10.1007/s10904-019-01425-4.

[9] D. Kumar, M. Singh, A.K. Singh, Crystallite Size Effect on Lattice Strain and Crystal Structure of $Ba_{1/4}Sr_{3/4}MnO_3$ Layered Perovskite Manganite, vol. 1953, no. 1, pp. 2–7, 2018, doi: https://doi.org/10.1063/1.5032520.

[10] H. Gencer, M. Gunes, A. Goktas, Y. Babur, H.I. Mutlu, S. Atalay, LaBaMnO films produced by dip-coating on a quartz substrate, Journal of Alloys and Compounds, vol. 465, no. 1-2, pp. 20–23, 2008, doi: https://doi.org/10.1016/j.jallcom.2007.10.110.

[11] D. Sahu, A. Palai, N.R. Panda, Electrical conduction mechanism in nanocrystalline ZnO induced by donor/acceptor doping, Journal of Materials Science: Materials in Electronics, vol. 33, pp. 8504–8518, 2022, doi: https://doi.org/10.1007/s10854-021-06401-8.

[12] S. Pigeot-Rémy, D. Gregori, R. Hazime, A. Hérissan, C. Guillard, C. Ferronato, S. Cassaignon, C. Colbeau-Justin, O. Durupthy, Size and shape effect on the photocatalytic efficiency of TiO_2 brookite, Journal of Materials Science, vol. 54, pp. 1213–1225, 2019, doi: https://doi.org/10.1007/s10853-018-2924-x.

[13] Z.N. Kayani, I. Sheri, S. Waseem, S. Riaz, S. Naseem, Effect of Alkaline Dopant Ba^{2+}on TiO_2 thin films: Insights of Synthesis and Properties, Materials Research Bulletin, vol. 169, no. 0025-5408, 2024, doi: https://doi.org/10.1016/j.materresbull.2023.112513.

[14] F. Xu, B. Weng, Photocatalytic hydrogen production: an overview of new advances in structural tuning strategies, Journal of Materials Chemistry A, vol. 11, pp. 4473–4486, 2023, doi: https://doi.org/10.1039/d2ta09614e.

[15] A. Khlyustova, N. Sirotkin, T. Kusova, A. Kraev, V. Titov, A. Agafonov, Doped TiO_2: The effect of doping elements on photocatalytic activity, Materials Advances, vol. 1, pp. 1193–1201, 2020, doi: https://doi.org/10.1039/d0ma00171f.

[16] H. Barkat, E. Guettaf Temam, H. Ben Temam, N. Mokrani, S. Rahmane, and M. Althamthami, Enhancing sunlight-driven Photocatalysis: High transparency and hydrophilic advancements in Ba-doped ZnO thin films, Journal of materials engineering and performance, 2024, doi: https://doi.org/10.1007/s11665-024-10126-0.

[17] E. Şennik, S. Kerli, Ü. Alver, Z.Z. Öztürk, Effect of fluorine doping on the NO_2^- sensing properties of ZnO thin films, Sensors and Actuators B: Chemical, vol. 216 pp. 49–56, 2015, doi: https://doi.org/10.1016/j.snb.2015.04.023.

[18] S. Wongrerkdee, S. Krobthong, Synthesis, Characterization, and Photocatalytic property of Ba-doped ZnO nanoparticles synthesized using facile precipitation, integrated ferroelectrics, vol. 224, pp. 192–204, 2022, doi: https://doi.org/10.1080/10584587.2022.2035609.

[19] V.J. Shukla, Synthesis and characterization of pure and doped ZnO thin films by colloidal solution route, Doctoral thesis, Gujarat technological University,2022.

[20] A. Hamrouni, M. Moussa, N. Fessi, L. Palmisano, R. Ceccato, A. Rayes, F. Parrino, Solar Photocatalytic Activity of Ba-Doped ZnO Nanoparticles : The Role of Surface Hydrophilicity, Nanomaterials, vol.13, no. 20, 2023 doi: https://doi.org/10.3390/nano13202742.

[21] I. Aadnan, O. Zegaoui, A. El Mragui, I. Daou, H. Moussout, J.C.G. Esteves, Structural , optical and photocatalytic properties of Mn doped ZnO nanoparticles used as Photocatalysts for Azo-dye degradation under visible light, Catalysts, vol. 12, no. 11, 2022, doi: https://doi.org/10.3390/catal12111382.

[22] I. Jellal, O. Daoudi, K. Nouneh, M. Boutamart, S. Briche, M. Fahoume, J. Naja, Comparative study on the properties of Al- and Ni-doped ZnO nanostructured thin films grown by SILAR technique: application to solar photocatalysis, Optical and Quantum Electronics, vol. 55, no. 620, 2023, doi: https://doi.org/10.1007/s11082-023-04798-6.

[23] R.K. Hariharalakshmanan, F. Watanabe, T. Karabacak, In Situ Growth and UV Photocatalytic Effect of ZnO Nanostructures on a Zn Plate Immersed in Methylene

Blue, Crystals, vol. 12, no. 12, pp.1–12, 2022, doi: https://doi.org/10.3390/catal12121657

[24] M. Govindhasamy, M.R. Kumar, H. Garalleh, S. Arabia, M. Garaleh, Decoration of ZnO surface with tiny sulfide-based nanoparticles for improve photocatalytic degradation efficiency, Environmental Research, vol.220, no. 0013-9351, 2023, doi: https://doi.org/10.1016/j.envres.2022.115171.

[25] B. El Filali, T. Torchynska, G. Polupan, E. Velázquez, Surface Morphology and Structure in ZnO films doped with Ga and In impurities Surface Morphology and Structure in ZnO films doped with Ga and In impurities, Journal of Physics: Conference Series, vol. 2307, 2022, doi: https://doi.org/10.1088/1742-6596/2307/1/012029.

Chapter IV.

Influence of SILAR Deposition Cycles on Ba-Doped ZnO Thin Films and their Photocatalytic Application

IV.1. Introduction

Following the findings from Chapter Three, where the 5 wt.% Ba-doped ZnO thin films demonstrated the highest photocatalytic efficiency, this chapter focuses on optimizing the properties of these films by varying the number of SILAR deposition cycles. The number of deposition cycles plays a crucial role in influencing key film characteristics, including surface thickness, crystallinity, surface morphology, and optical properties, all of which directly affect photocatalytic performance.

In this study, Ba-doped ZnO thin films were synthesized via SILAR with different deposition cycles (3, 6, 9, 12, and 15 cycles). Their photocatalytic activity for the degradation of methylene blue (MB) and amoxicillin (AMX) was evaluated, alongside their wettability properties. This investigation provides valuable insights into optimizing Ba-doped ZnO thin films for a wide range of environmental and industrial applications.

Through these details, the main objectives of this chapter are:

- To determine the optimal number of SILAR deposition cycles that maximize the photocatalytic activity of MB and AMX dyes, while maintaining film stability, uniformity, and reusability.
- To present the structural, morphological, and optical properties of Ba-doped ZnO thin films at various deposition cycles, using patterns, figures, and tables for clear representation.
- To analyze and discuss the obtained results.

IV.2. Results and Discussion

IV.2.1. Measurement of film Thickness

Figure IV.1 (a) illustrates the variation in the number of deposition SILAR cycles as a function of the thickness of Ba-doped ZnO thin films. As the number of cycles increased from 3 to 15 cycles, the thickness of prepared films grew from 69.28 nm to 1153.28 nm, a value calculated using the gravimetric method.

To confirm these results, the cross-sectional scanning electron microscopy (SEM) image of Ba-doped ZnO films with 5 wt.% Ba after 15 cycles was displayed in **Figure IV.1 (b).** The results of

film thickness measured are similar in both methods. Furthermore, the average thickness, determined from 50 measurements, is 1.16 ± 0.6 µm, which closely matches the gravimetric value of 1.1532 µm. These results emphasize the considerable influence of SILAR deposition cycles on the Ba-doped ZnO films, impacting their structural, optical, self-cleaning, and photocatalytic characteristics.

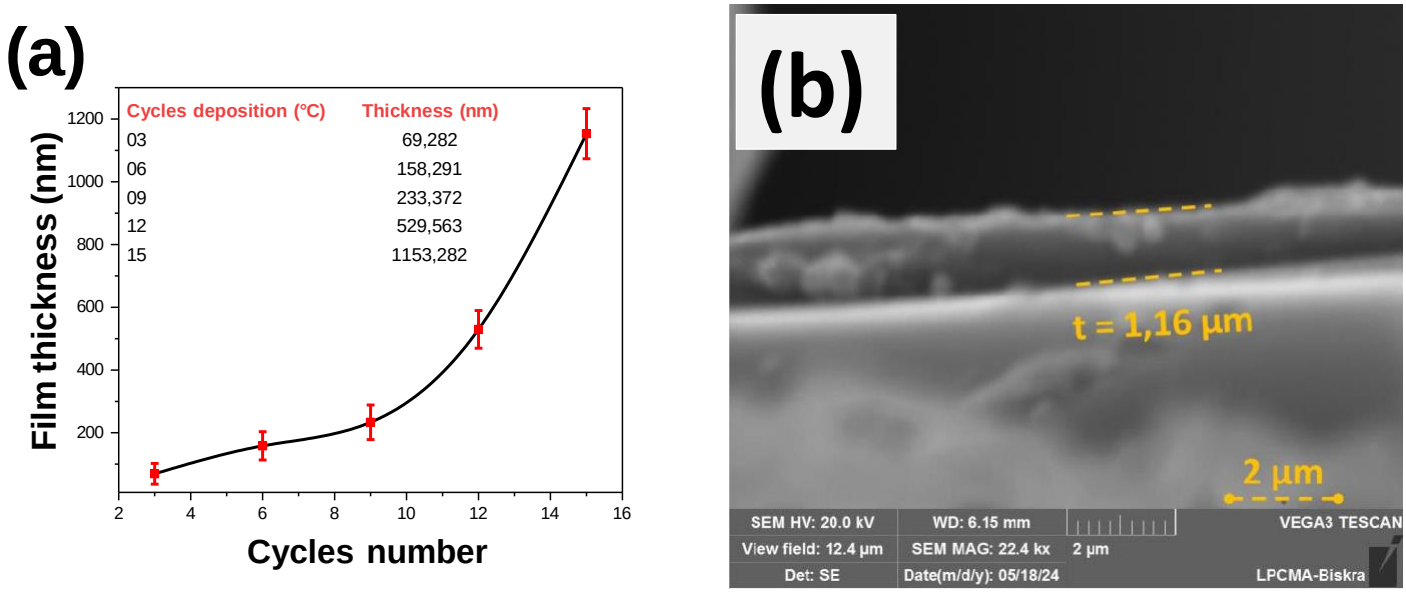

Figure IV.1. (a) Plot of film thickness of Ba-doped ZnO thin film as a function of cycles number, **(b)** SEM cross-sectional image of 5 wt.% Ba-doped ZnO film at 15 cycles

IV.2.2. Structural study

X-ray diffraction patterns have been used to confirm the crystalline nature and phases of the deposited films produced by SILAR process on glass substrates. XRD pattern recorded for Ba-doped ZnO thin films obtained at different SILAR deposition cycles (3, 6, 9, 12, and 15) are shown in **Figure. IV.2 (a)**. It is noticed that the preferred diffraction peaks at 2θ = 31.81 °, 34.54 °, and 36.42 ° corresponding to the lattice planes (100), (002), and (101), respectively. This indicated that all films have a polycrystalline nature with a hexagonal wurtzite structure consisted with JCPDS card no. 75-0576. The major diffraction peak was changed at the (100) plane to (002) at 3 to 15 cycles, respectively probably due to its low surface free energy and to technical conditions of SILAR method [1]. When the number of SILAR dipping cycles increased, the intensity of the main peaks increased. The structural parameters were determined from the three main intense peaks using the Williamson–Hall method.

This model was applied to plots of β cosθ as a function of 4 sinθ as illustrated in **Figure. IV.2 (b)**. The values of D and ε were determined by the intercept of the drawn linear fit.

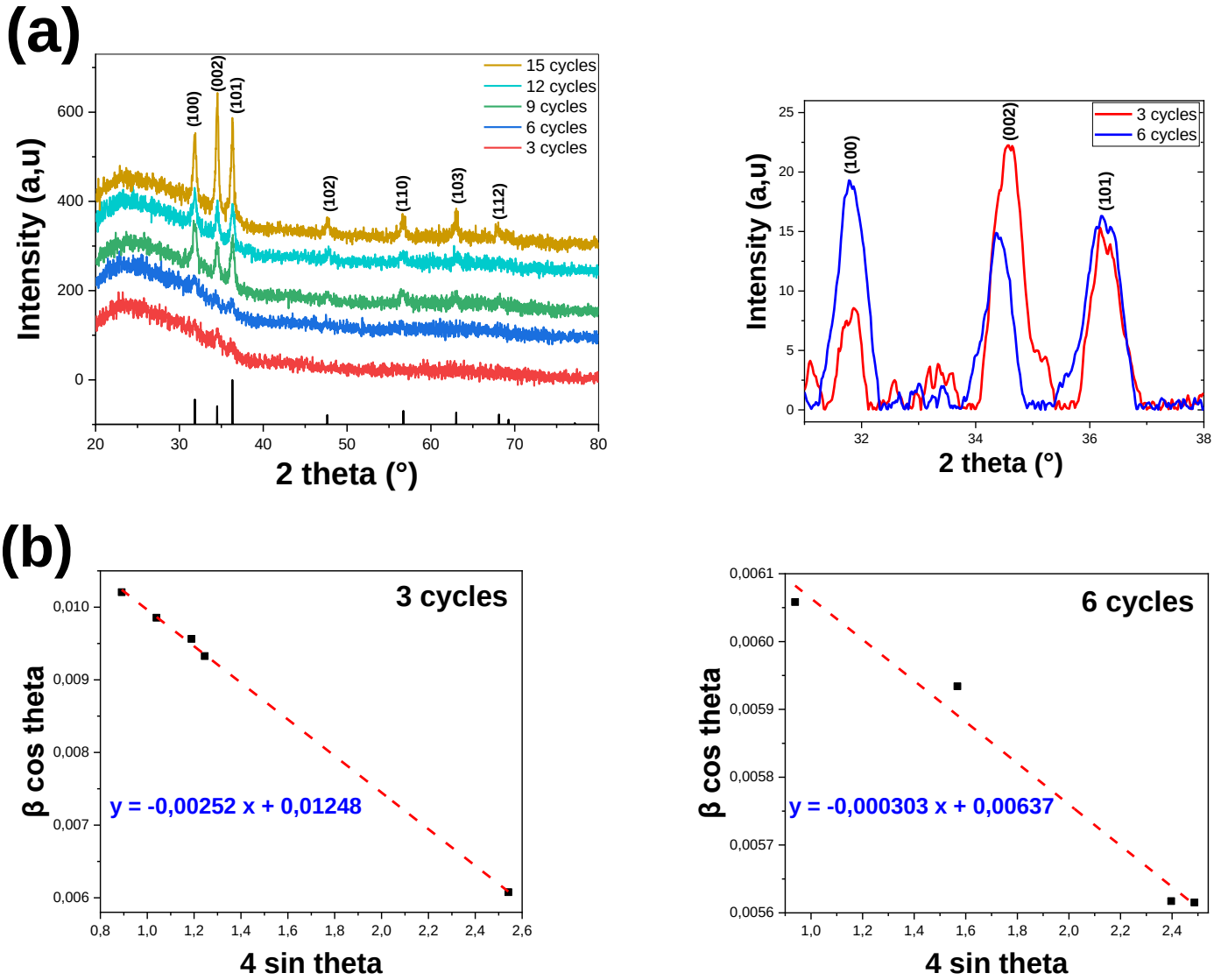

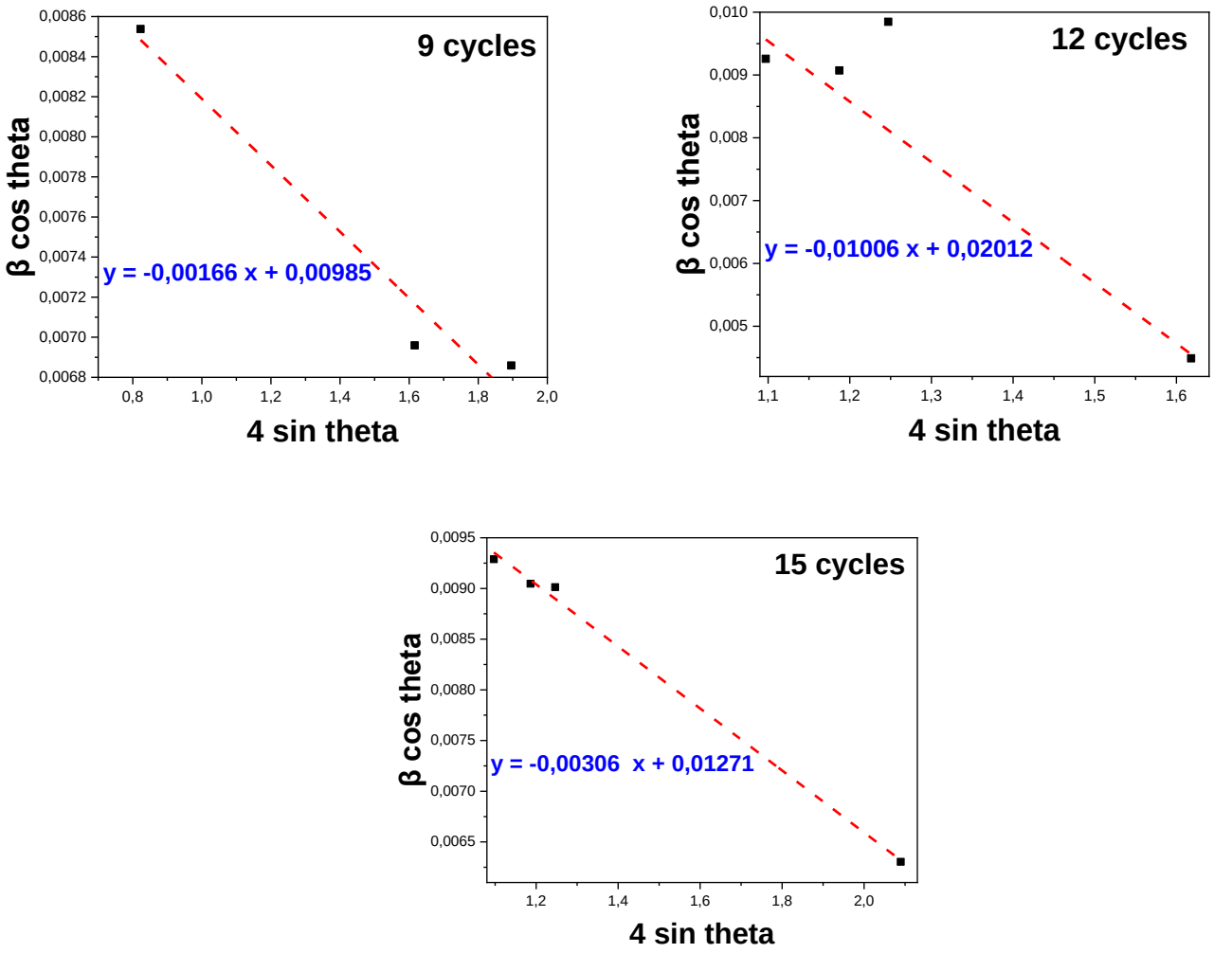

Figure. IV.2 (a) XRD patterns of Ba-doped ZnO thin films for various deposition cycles, **(b)** Williamson–Hall plots for the prepared samples

Table IV.1 presents the corresponding values for D and ε for all films. As the number of cycles increases, the lattice strain in Ba-doped ZnO films rises linearly with crystallite size. This behavior is due to the increased presence of defects and dislocations in the crystallites, which contribute to higher strain in the crystal lattice[2]. Furthermore, the strain can influence crystal growth by affecting the diffusion of Ba ions within the ZnO matrix, potentially increasing the growth rate and resulting in larger crystallites [3]. The decrease in crystallite size observed at 12 cycles can be attributed to lattice distortions induced by excessive deposition and the incorporation of Ba ions with a larger ionic radius, which inhibits growth and causes crystallite fragmentation [3][4][5].

Table IV.1. Value of estimated structural parameters of 5 wt.% Ba-doped ZnO thin films at different deposition SILAR cycle numbers

Cycle numbers	**2θ (°)**	**FWHM**	**D (nm)**	**ε**	**δ*10^{-3} (nm^{-2})**	**N**
03	34.53	0.2	11.105	−0.0025	8.108	0.05
06	34.41	0.28	21.75	−0.0003	2.113	0.01
09	34.45	0.36	14.07	−0.0016	5.051	0.08
12	34.51	0.29	6.88	−0.0096	21.1	1.62
15	34.55	0.33	10.904	−0.0030	8.41	0.88

As the results of **Table IV.1**, the dislocation density (δ) reached its superior value of 21.1*10^{-3} nm^{-2} at 12 cycles, indicating a decrease in the crystallization of Ba-doped ZnO films. The increase in dislocation density influences the movement of atoms on the surface, which decelerates crystallite growth. Therefore, the grains become minimal, reducing the quality of the film's crystalline structure. Similar results have been mentioned by Ashour et al.[6]. Furthemore, as the SILAR dipping cycle increases from 3 to 15 cycles, the crystallite number (N) increases from 0.05 to 0.88.

IV.2.3. Morphological study

Figure. IV.3 depicted the SEM micrographs and EDX analyses of Ba-doped ZnO thin films deposited via the SILAR approach at various deposition cycles (3, 6, 9, 12, and 15). The change in the surface morphology observed in these SEM images may be due to the increasing dipping cycles. Moreover, a smaller grain size was observed at 3 and 6 cycles, compared to other sample cycles, with a non-uniform and non-homogeneous distribution on the surface of thin films. It was also shown that all the film images exhibited voids between the grains, except the sample deposited at 15 cycles, which displayed a highly compact morphology with uniform grains. As the number of SILAR growth cycles grew from 3 to 15 cycles, the grain size diameter increased from 29.71 nm to 44.79 nm, which confirms our XRD results.

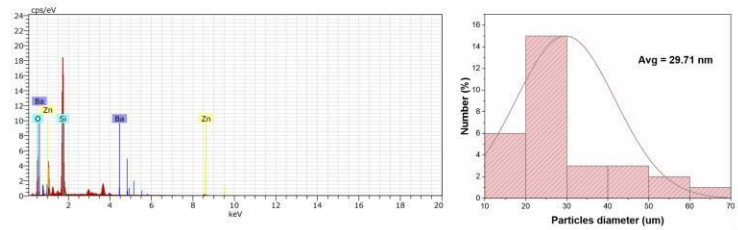

El	AN	Series	unn. C [wt.%]	norm. C [wt.%]	Atom. C [at.%]	Error (1 Sigma) [wt.%]
Si	14	K-series	21.82	44.82	35.09	0.96
O	8	K-series	21.73	44.64	61.36	2.81
Zn	30	K-series	5.13	10.54	3.54	0.20
Ba	56	L-series	0.01	0.01	0.00	0.03
		Total:	48.68	100.00	100.00	

(a)

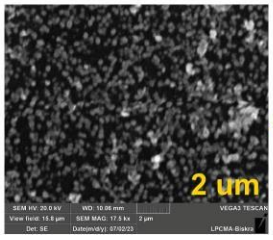

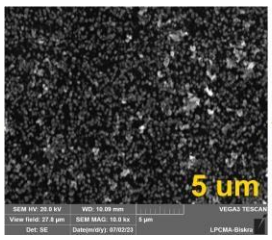

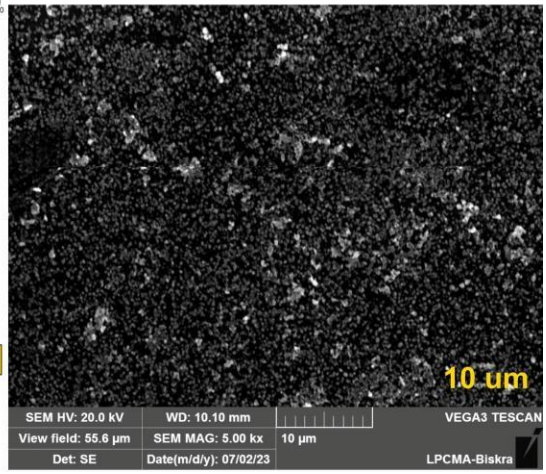

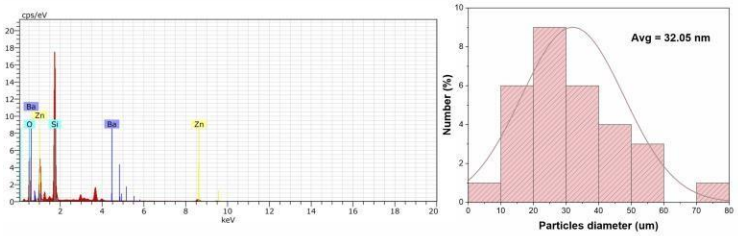

El	AN	Series	unn. C [wt.%]	norm. C [wt.%]	Atom. C [at.%]	Error (1 Sigma) [wt.%]
Si	14	K-series	17.99	48.95	40.38	0.80
O	8	K-series	13.96	37.98	55.00	1.91
Zn	30	K-series	4.77	12.98	4.60	0.19
Ba	56	L-series	0.03	0.09	0.02	0.03
		Total:	36.76	100.00	100.00	

(b)

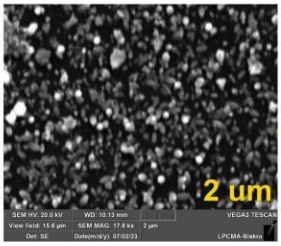

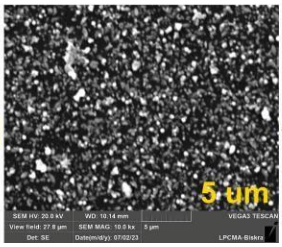

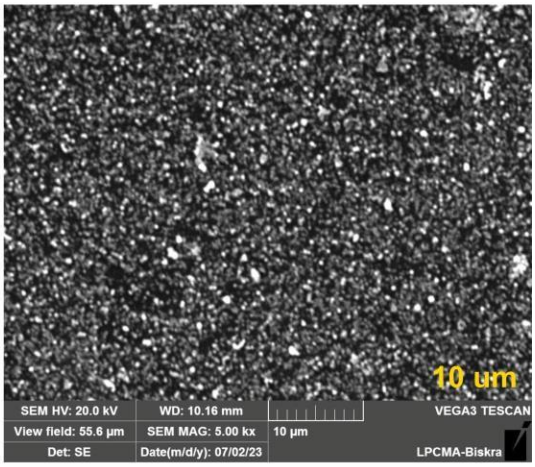

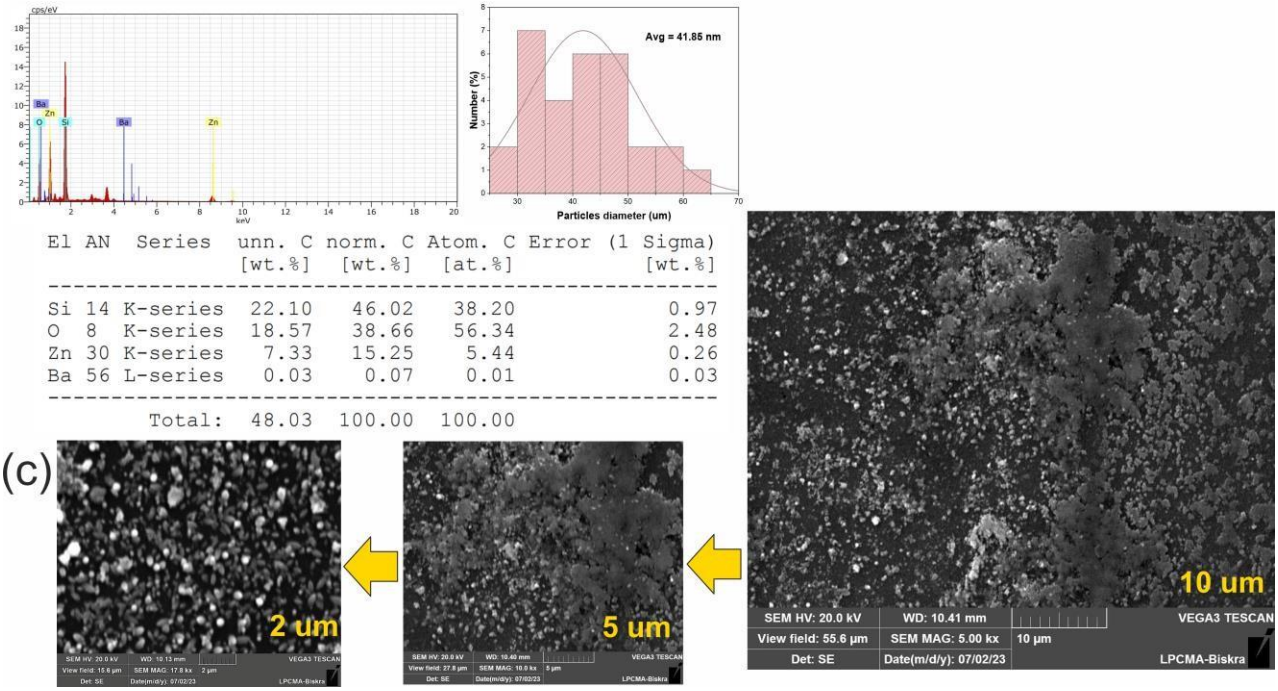

El	AN	Series	unn. C [wt.%]	norm. C [wt.%]	Atom. C [at.%]	Error (1 Sigma) [wt.%]
Si	14	K-series	22.10	46.02	38.20	0.97
O	8	K-series	18.57	38.66	56.34	2.48
Zn	30	K-series	7.33	15.25	5.44	0.26
Ba	56	L-series	0.03	0.07	0.01	0.03
		Total:	48.03	100.00	100.00	

(c)

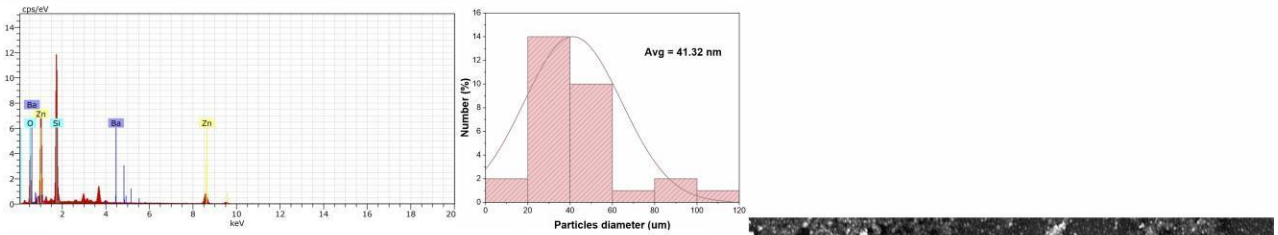

El	AN	Series	unn. C [wt.%]	norm. C [wt.%]	Atom. C [at.%]	Error (1 Sigma) [wt.%]
Si	14	K-series	18.03	39.32	35.61	0.80
O	8	K-series	15.58	33.98	54.02	2.11
Zn	30	K-series	12.22	26.65	10.37	0.39
Ba	56	L-series	0.02	0.05	0.01	0.03
		Total:	45.86	100.00	100.00	

(d)

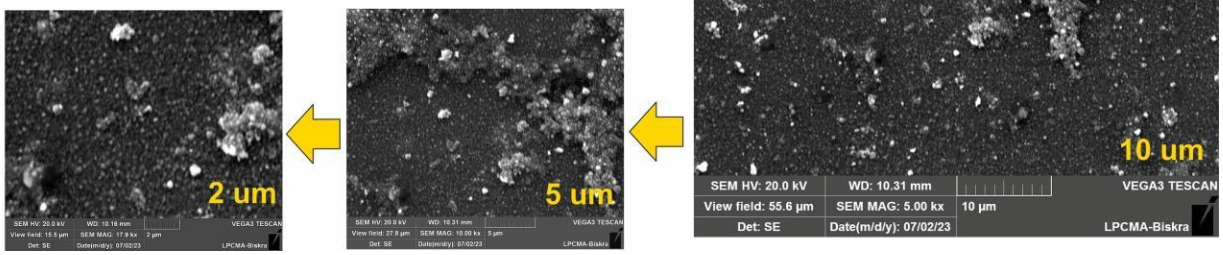

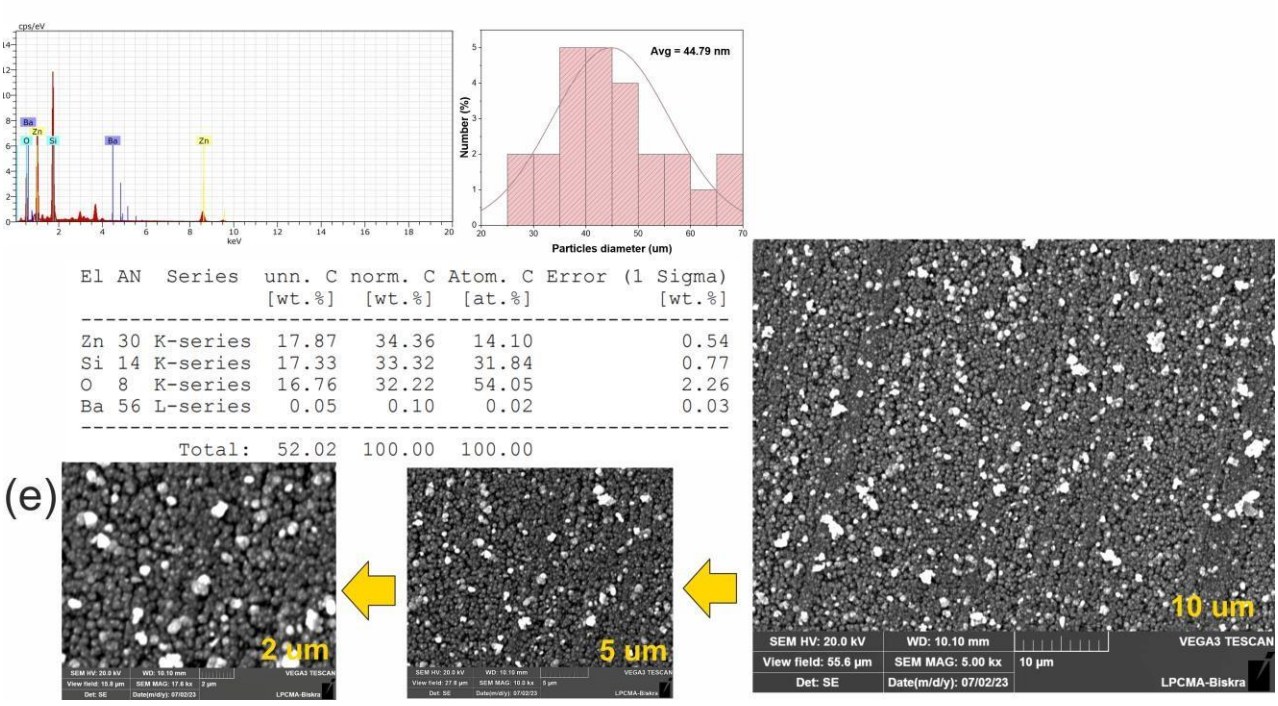

Figure. IV.3 SEM images, EDX analysis, and particles diameter measurements of prepared films before photocatalytic degradation at: (a) 3 cycles, (b) 6 cycles, (c) 9 cycles, (d) 12 cycles, and (e) 15 cycles

To determine the chemical elemental compositions of prepared films at different SILAR dipping cycles, EDX analyses was performed. It was recorded the presence of Zn, O, Ba, and Si elements. The change in the EDX absorption spectra indicating the interaction between barium and zinc oxide.

IV.2.4. Optical study

Figure. IV.4 shows the transmittance spectra of 5 wt.% Ba-doped ZnO synthesized by SILAR process deposited with different SILAR dipping cycles (3, 6, 9, 12, and 15) in the wavelength range from 380 nm to 1200 nm with glasses as the reference. These spectra showed that deposited films had good transparency in the visible spectrum. From this figure, we noticed that the transmittance of samples increased with the increase of the wavelength. Furthermore, the transmittance was decreased with increasing of cycle numbers. Thus, the highest average transmittance was 78.42 % at 550 nm, which was observed in the thinnest sample at 3 cycles. This result is consistent with previous studies, which have shown that an increase in film thickness

enhances light scattering, reducing transmittance [7]. This change in the transmittance edge results in a change alteration in the energy of the band gap [8].

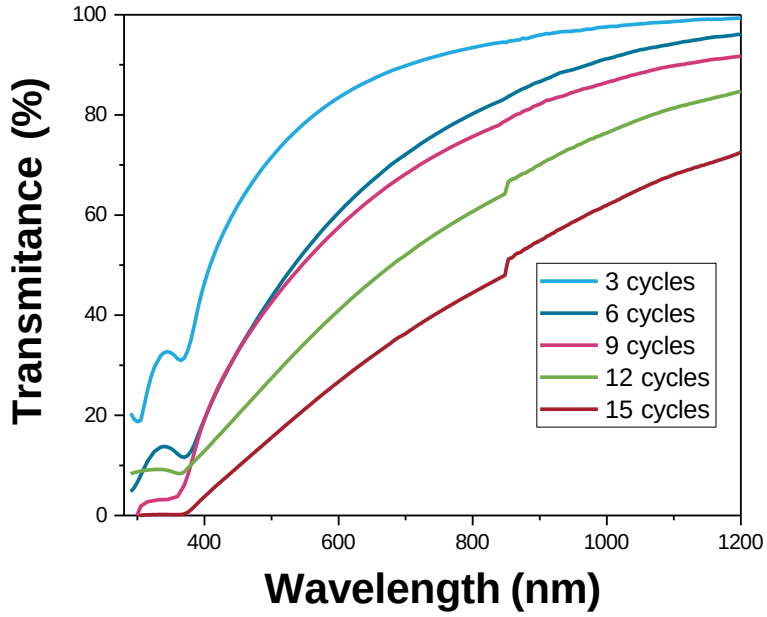

Figure. IV.4 UV–Vis spectra of Ba-doped ZnO films using various deposition cycles

To determine the band gap values of Ba-doped ZnO films, the linear portion of the graph should be extended until it intersects the photon energy (hυ) axis, as illustrated in **Figure. IV.5**. The direct band gap of all fabricated films with varying deposition SILAR cycles is presented in **Figure. IV.6**. It is noticed that an increase in thickness of Ba-doped ZnO films produced from 69.282 to 1153.282 nm yields a decrease in optical band gap from 3.68 to 3.25 eV, respectively. The literature explains several factors that cause the band gap to decrease as the film thickness increases. First, the addition of Ba ions, which are larger than Zn ions, introduces strain and defects in the ZnO lattice. These distortions affect the material's electronic structure, forming localized states near the conduction and valence bands, thereby reducing the band gap. Morphological changes in the films can also affect the band structure, lowering the band gap further. Lastly, as the film thickness increases, the localized states may merge with the band edges, leading to a further reduction in the band gap [9].

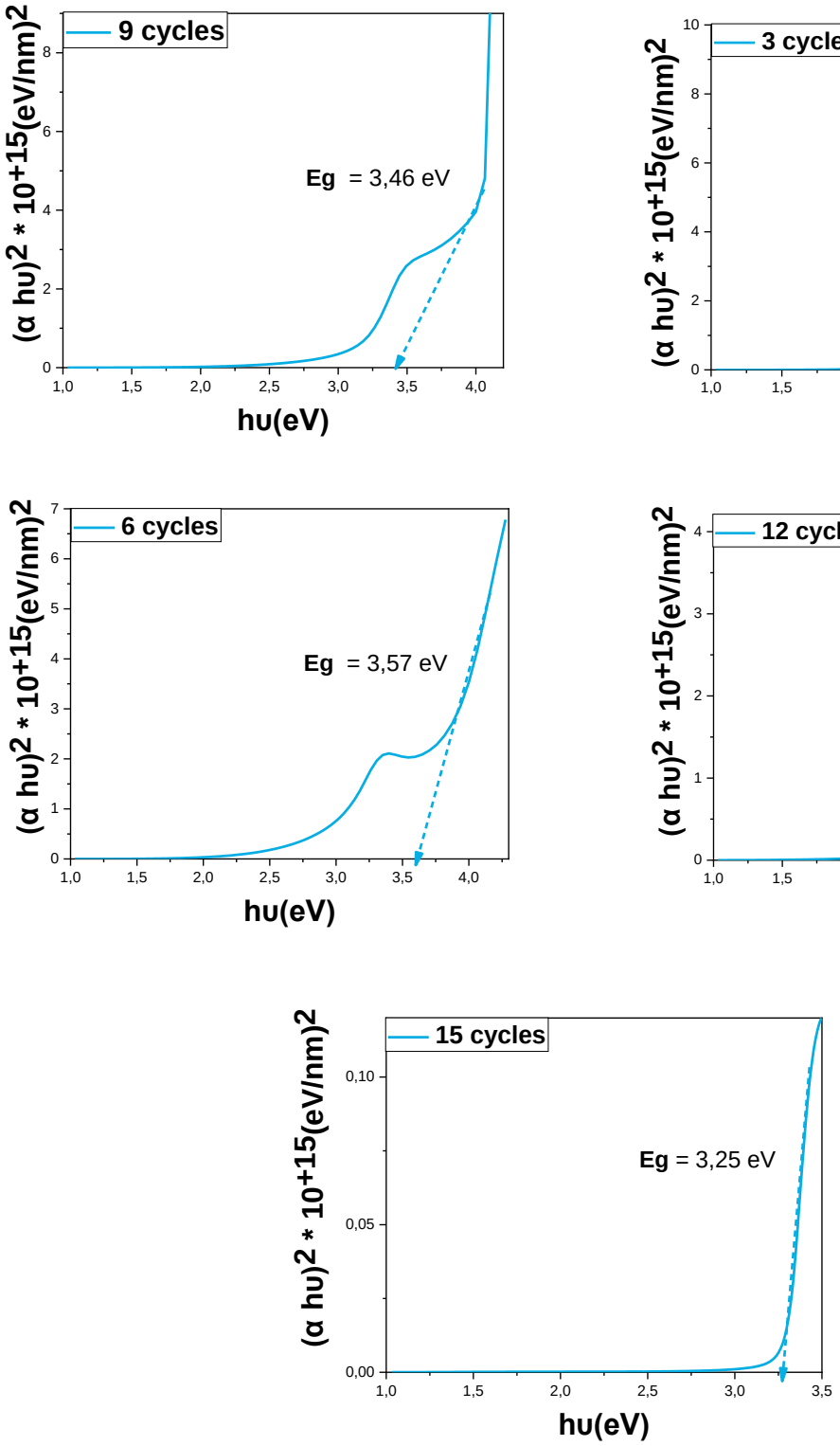

Figure. IV.5 Plots of (hν) versus $(\alpha h\nu)^2$ for Ba-doped ZnO films at different cycles number

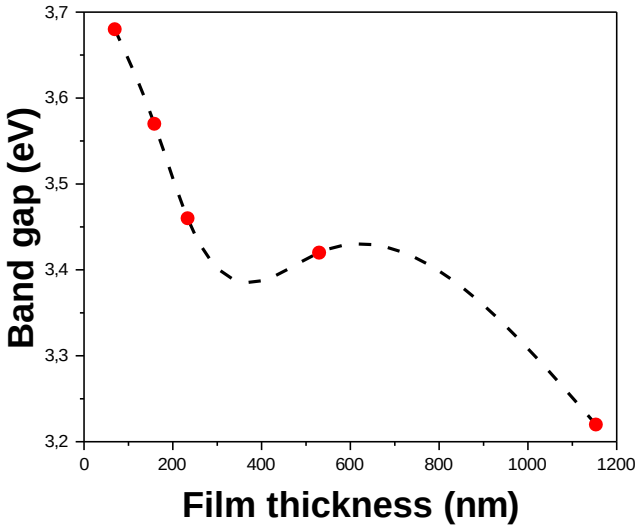

Figure. IV.6 Plot of band gap energy as a function of film thickness

IV.2.5. Wettability study

The contact angle measurements of water droplets on Ba-doped ZnO thin films for 3, 6, 9, 12, and 15 cycles were 21.23°, 38.37°, 43.21°, 46.87°, and 56.55°, respectively, indicating that all the film surfaces are hydrophilic (contact angles < 90°). As shown in **Figure. IV.7**, the increase in the number of deposition cycles and film thickness is associated with a rise in the average water droplet contact angle due to morphological changes. Previous studies have shown that the surface characteristics of Ba-doped ZnO films influence their physicochemical properties and the behavior of water droplets on their surface. The sample of 3 cycles Ba-doped ZnO exhibits better wettability, likely due to defect chemistry, particularly oxygen vacancies in the valence band, which affect the adsorption of hydroxyl groups [10][11].

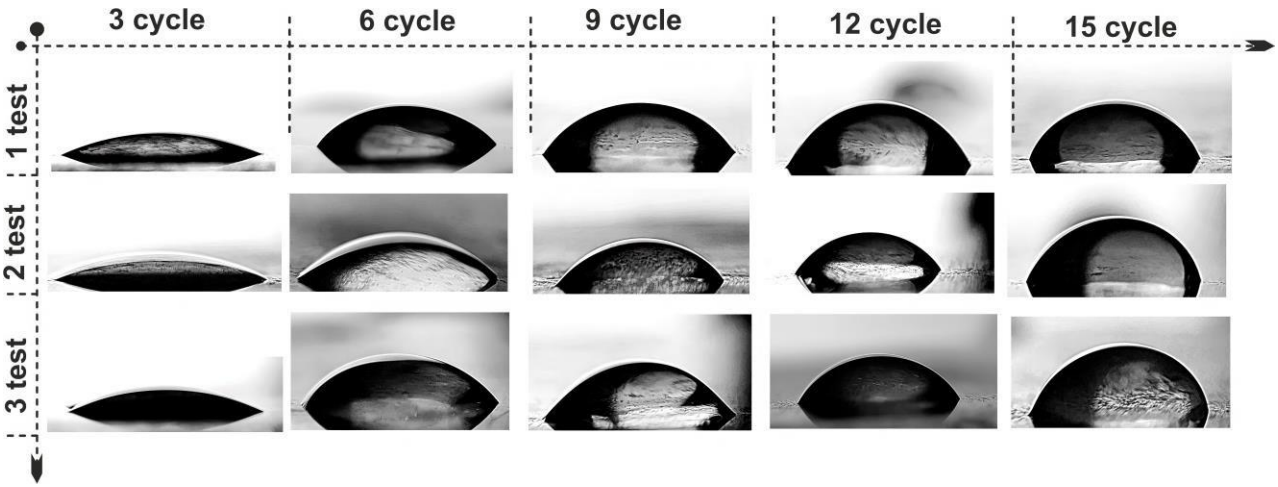

Figure. IV.7 The droplet contact angle on the surfaces of Ba-doped ZnO films at different dipping cycles

IV.2. 6. Photocatalytic activity

The photocatalytic activity and reusability of Ba-doped ZnO thin films, synthesized through different SILAR deposition cycles (3, 6, 9, 12, and 15), were investigated under sunlight irradiation using methylene blue (MB) and amoxicillin (AMX) dyes as model pollutants. The weather conditions on June 26th, 2023, in Biskra, Algeria, are presented in **Table IV.2**. Moreover, this study reports the surface thickness, morphological, and optical characterizations of the prepared samples before and after the photocatalytic process.

Table IV.2 Meteorological conditions of photocatalytic experiment of MB and AMX dyes.

The date	*Temperature (°C)*	*Wind speed (km/h)*	*Humidity (%)*
26/06/2023	44° ± 5	08 ± 1	16% ± 2

IV.2. *6. 1. Photo-degradation analysis of MB*

The photocatalytic degradation of the synthesized Ba-doped ZnO films was performed by degrading an aqueous MB solution with an initial concentration of 4 mg/L under sunlight irradiation for 5 hours.

The absorption spectra of MB as a function of wavelength, ranging from 350 to 800 nm, for irradiation times of Ba-doped ZnO films were depicted in **Figure. IV.8 (a).** The MB degradation

by the prepared thin films at varying cycle numbers: 3, 6, 9, 12, and 15 was recorded as 92.66%, 92.71%, 92.80%, 93.17%, and 93.51%, respectively. These results suggested the impact of dipping SILAR cycles on the photocatalytic efficiency of the MB pollutant. As shown in **Figure. IV.8 (b),** the highest photodegradation was found at 15 cycles after 5 h of reaction, corresponding to the thicker films (1153.282 nm). This observation can be attributed to photocatalytic surface reactions taking place more effectively on the photocatalyst's surface at a greater film thickness compared to other samples [12].

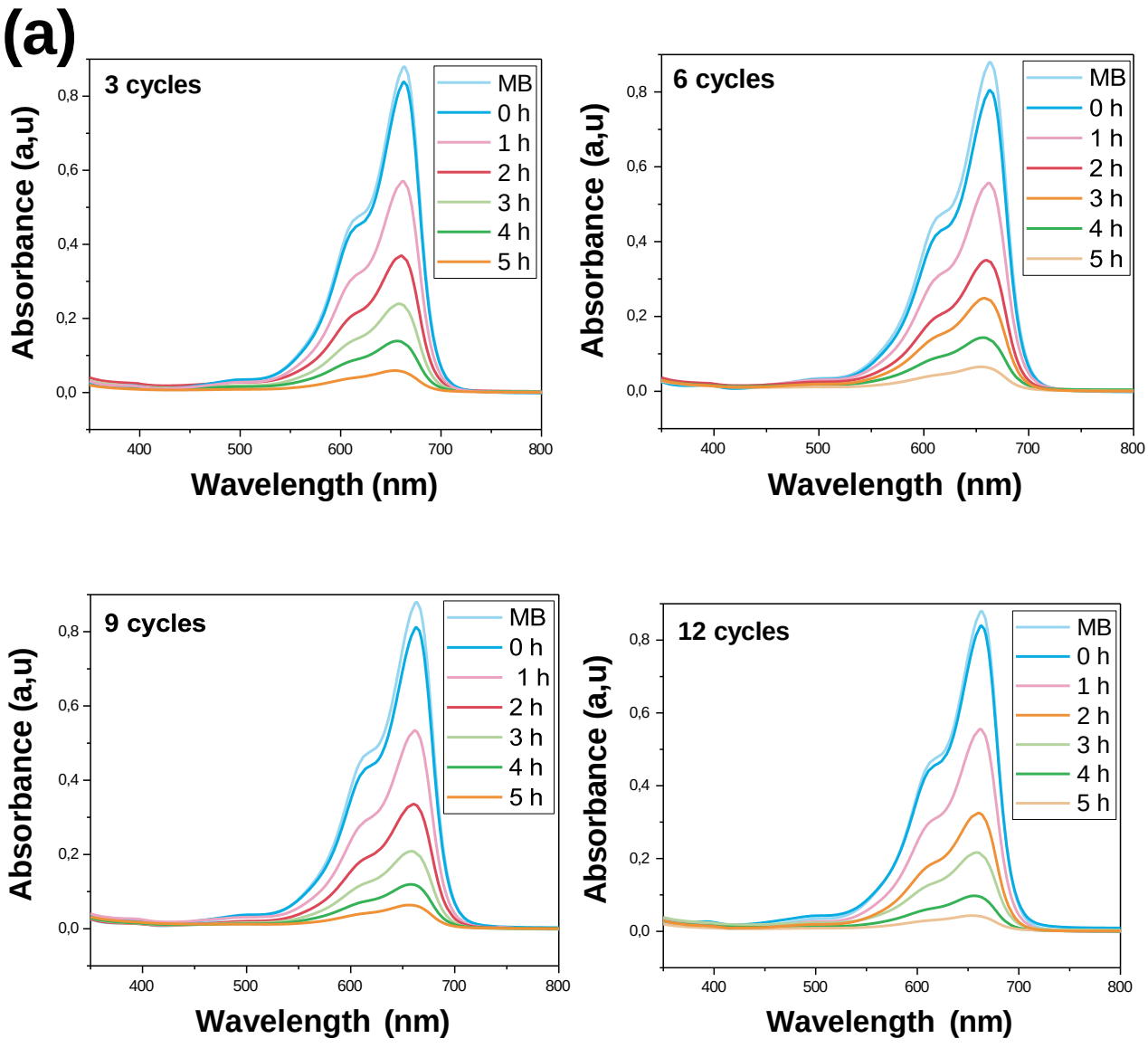

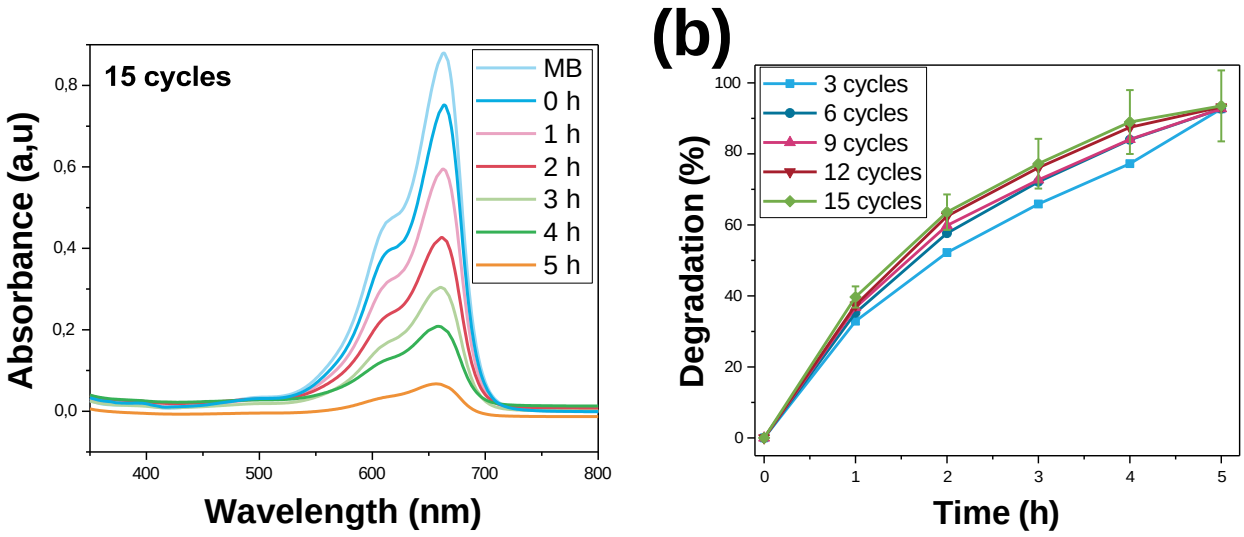

Figure. IV.8 (a) Absorption spectra of MB versus irradiation time of Ba-doped ZnO thin films at different cycle deposition, and **(b)** Plot of % degradation of MB as a function of time at various cycles number

The kinetics reaction were determined by plotting the logarithm of the concentration ratios of MB versus the time of irradiation, as presented in **Figure. IV.9.** The straight lines indicate that the reactions follow pseudo-first-order kinetics with R^2 value near unity ($R^2 \sim 0.98$) and rate constants were extracted from the slope of the graph, with the corresponding values listed in **Table IV.3.** It can be noticed that the rate constant value K increased from 0.4692 h^{-1} to 0.5273 h^{-1} as the number of cycles increased from 3 to 15, respectively, which confirms the faster degradation of MB in water compared to low cycles. This variation may be attributed to changes in crystallinity and bandgap energies [13].

Table IV.3 k and R^2 values of Ba-doped ZnO films at different dipping cycles for MB dye

Cycles	**3**	**6**	**9**	**12**	**15**
K	0,4692	0,4977	0,4944	0,5218	0,5273
R^2	0.9075	0.97453	0.97445	0.99048	0.98697
Removal (%)	92.66	92.71	92.80	93.17	93.51

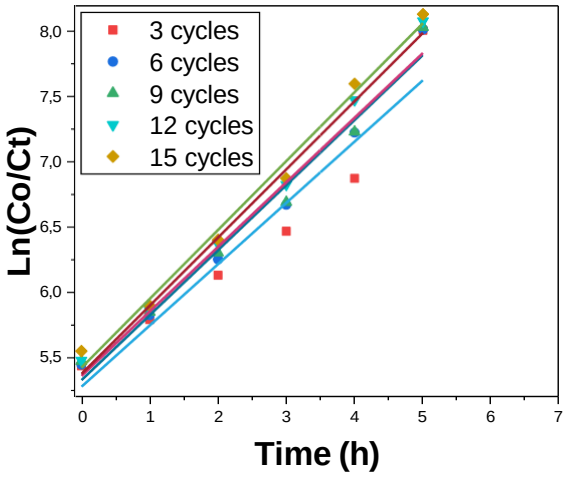

Figure. IV.9 Ln (C_0/C) versus irradiation time curves of Ba-doped ZnO films at different cycles for MB degradation

IV.2. 6. 2. Photo-degradation analysis of AMX

Amoxicillin, a penicillin antibiotic, is widely used to treat various bacterial infections, including those affecting the dental, chest, ear, throat, and sinus infections [14]. The effectiveness of photocatalysis was assessed by performing the photodegradation of AMX, using Ba-doped ZnO thin films as the catalyst. **Figure. IV.10 (a-e)** displays the UV–Vis spectra of AMX removal at different deposition cycles. The results show a decrease in the absorption intensity of AMX at λ_{max} = 283 nm with increasing exposure time. These figures show that photocatalytic activity improved with the increase in cycle numbers. The degradation of amoxicillin under sunlight irradiation for 2 hours was 43.14%, 44.16%, 45.68%, 46.71%, and 54.31% at 3, 6, 9, 12, and 15 cycles, respectively, as shown in **Table IV. 4** and **Figure. IV. 10 (f)**. The higher photocatalytic activity observed at 15 cycles was corresponding to the lower band gap energy.

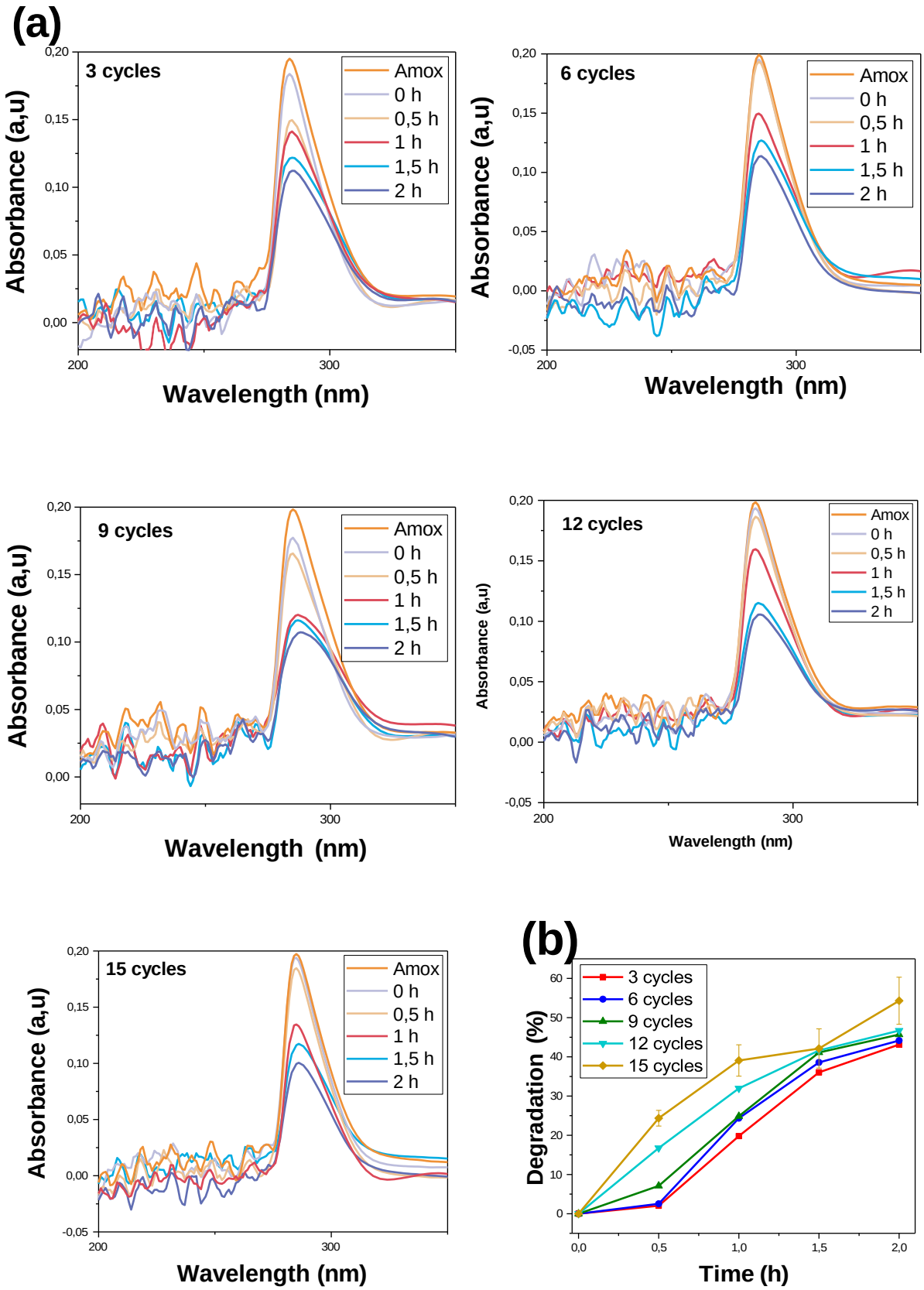
(a)
3 cycles
6 cycles
9 cycles
12 cycles
15 cycles
Amox
0 h
0,5 h
1 h
1,5 h
2 h
Absorbance (a,u)
Wavelength (nm)
(b)
Degradation (%)
Time (h)

Figure. IV.10 (a) Absorption spectra of AMX versus irradiation time of Ba-doped ZnO thin films at different cycle deposition, and **(b)** Plot of % degradation of AMX as a function of time at various cycles number

The reaction kinetics were evaluated by graphing the logarithm of the AMX concentration ratios against irradiation time, as shown in **Figure IV.11.** The resulting straight lines suggest that the reactions adhere to pseudo-first-order kinetics, with an R^2 value near to 1 (approximately 0.98). The rate constants were derived from the graph's slope, and their values are detailed in **Table IV.4**. Notably, the rate constant (K) rose from 0,3050 h^{-1} to 0,3218 h^{-1} as the number of cycles increased from 3 to 15, indicating that AMX degrades more rapidly in water at higher cycle counts compared to lower ones.

Table IV.4 k and R^2 values of Ba-doped ZnO films at different dipping cycles for AMX dye

Cycles	**3**	**6**	**9**	**12**	**15**
K	0,3050	0,3118	0,3250	0,2932	0,3218
R^2	0.9256	0.95496	0.94461	0.98073	0.96769
Removal (%)	43.14	44.16	45.68	46.71	54.31

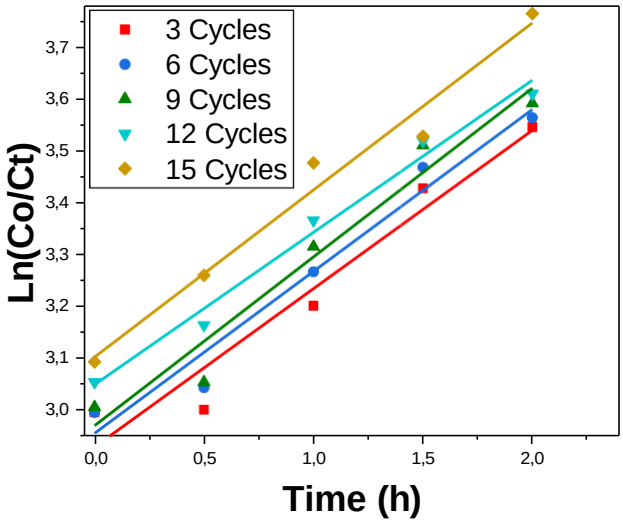

Figure. IV.11 Ln (C_0/C) versus irradiation time curves of Ba-doped ZnO films at different cycles for AMX degradation

IV.2. 7. The surface morphology and film thickness after photo-degradation process

The surface morphology and EDX analysis of Ba-doped ZnO thin films after the photodegradation process were illustrated in **Figure IV.12**. For 5 hours of irradiation, all surface films stayed uniform. On the other hand, there was a void between the grain sizes because the films were less compact than they were before to the photocatalytic degradation. Ampattu R. J. et al.[15] also remarkable that the surface morphology changed after photodegradation. Additionally, the presence of Zn, O, Si, and Ba elements was confirmed by EDX analysis, and the quantity of these chemical elements in the films varied, reflecting their involvement in the reaction during photocatalysis. This led to a decrease in the thickness of the thin films across all deposition SILAR cycles (3, 6, 9, 12, and 15), as shown in **Table IV.5**. This reduction in thickness can be attributed to the erosion of the photocatalytic material, which effectively reduces its thickness. This effect is particularly noticeable in thin films, where the degradation of organic pollutants can physically remove material from the surface, as reported by Yasun Y. et al. [16].

(a)

El	AN	Series	unn. C [wt.%]	norm. C [wt.%]	Atom. C [at.%]	Error (1 Sigma) [wt.%]
Si	14	K-series	18.85	55.51	42.23	0.83
O	8	K-series	14.56	42.89	57.27	1.96
Zn	30	K-series	0.50	1.47	0.48	0.06
Ba	56	L-series	0.04	0.13	0.02	0.03
		Total:	33.95	100.00	100.00	

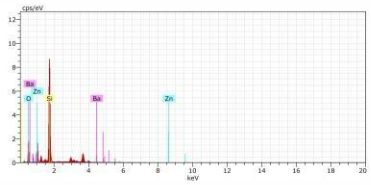

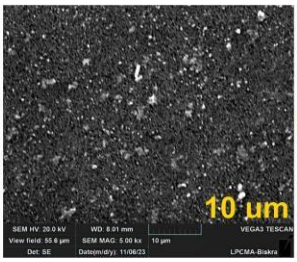

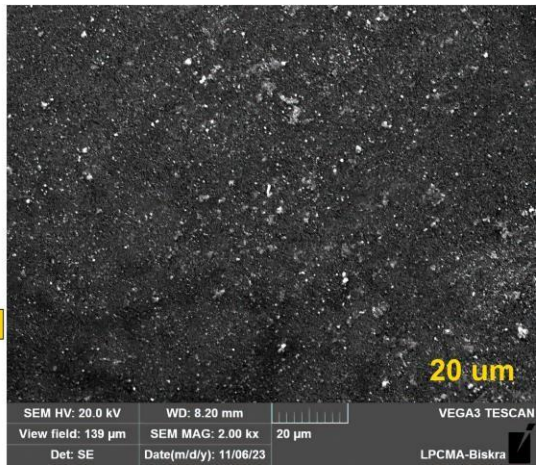

(b)

El	AN	Series	unn. C [wt.%]	norm. C [wt.%]	Atom. C [at.%]	Error (1 Sigma) [wt.%]
Si	14	K-series	20.98	53.37	40.81	0.92
O	8	K-series	17.02	43.29	58.11	2.27
Zn	30	K-series	1.28	3.27	1.07	0.08
Ba	56	L-series	0.03	0.08	0.01	0.03
		Total:	39.31	100.00	100.00	

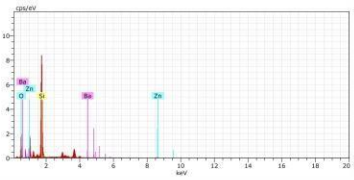

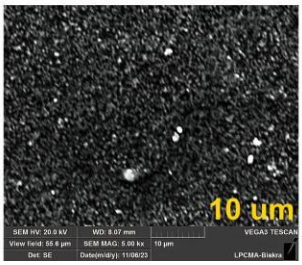

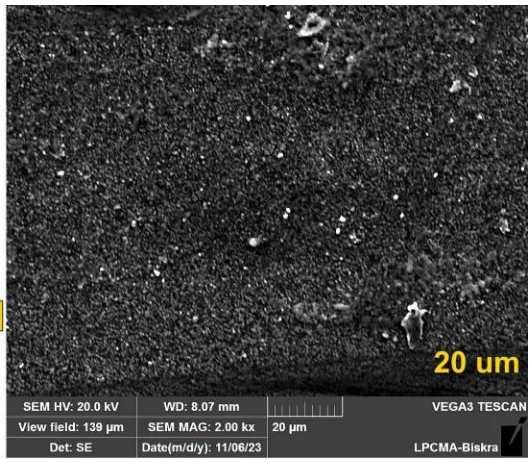

(c)

El	AN	Series	unn. C [wt.%]	norm. C [wt.%]	Atom. C [at.%]	Error (1 Sigma) [wt.%]
Si	14	K-series	19.29	48.09	36.65	0.85
O	8	K-series	18.41	45.89	61.39	2.40
Zn	30	K-series	2.38	5.94	1.94	0.12
Ba	56	L-series	0.03	0.07	0.01	0.03
		Total:	40.11	100.00	100.00	

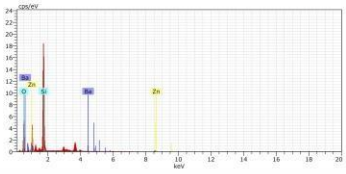

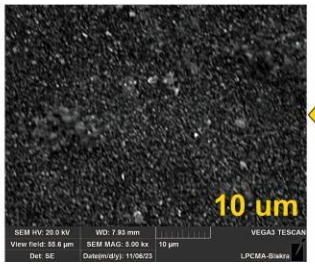

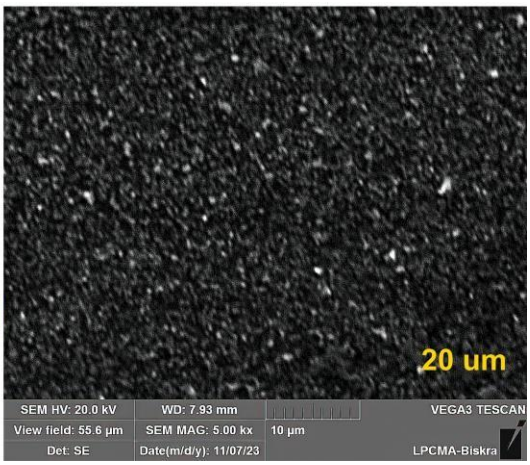

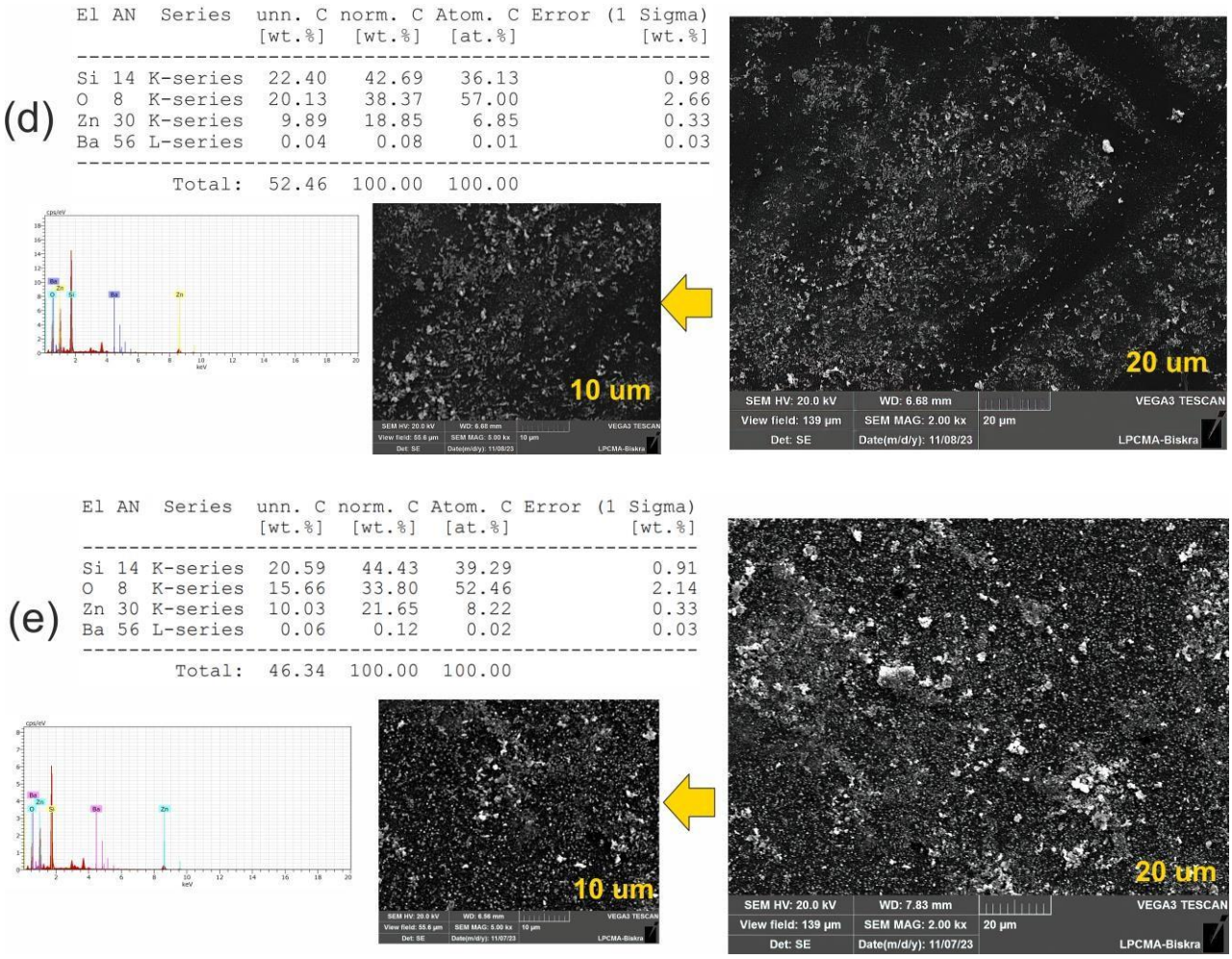

Figure. IV.12 SEM images and EDX analysis of Ba-doped ZnO thin films after photocatalytic degradation at: **(a)** 3 cycles, **(b)** 6 cycles, **(c)** 9 cycles, **(d)** 12 cycles, and **(e)** 15 cycles

Table IV.5 The thickness values before and after the photocatalytic activity of Ba-doped ZnO thin films

Cycles	**3**	**6**	**9**	**12**	**15**
Before photocatalytic activity	69.28	158.29	233.37	529.56	1153.2
After photocatalytic activity	68.96	157.9	233.0	529.3	1152.9

IV.2. 8. The optical properties of films after photo-degradation process

Figure IV.12 (a) displays the UV-Vis absorption spectra of Ba-doped ZnO thin films after the photocatalytic activity across different SILAR deposition from 3 to 15 cycles. The photocatalytic process significantly impacts the optical properties of the thin films, with alterations in the band gap that affect their light absorption and scattering characteristics, ultimately resulting in reduced transmittance [17]. As presented in **Table IV.6**, the average transmittance of all films decreased after the photocatalytic activity, compared to the values before this process. This decrease can be attributed to changes in the surface morphology induced by the photocatalytic activity, which increases light scattering and decreases transmittance. Furthermore, the accumulation of carbonyl groups during the degradation process suggests chemical modifications that further influence the films' light transmission properties [18][19]. Kekeli N. et al. similarly explored the UV-Vis absorption spectra of Ba-doped ZnO thin films after photocatalytic degradation of MB dye. Their results demonstrated that incorporating BaO enhances the photocatalytic efficiency of ZnO, achieving high degradation rates within short periods under UV irradiation [20].

Figure IV.12 (b) illustrated the band gap energy of Ba-doped ZnO thin films varying cycle numbers after photocatalytic activity. The observed reduction in band gap values following photocatalytic degradation is primarily due to the interaction between residual organic compounds from the dyes and the photocatalyst surface [21]. Additionally, the degradation process likely generates new active sites on the photocatalyst surface, contributing to the further reduction in the band gap [9].

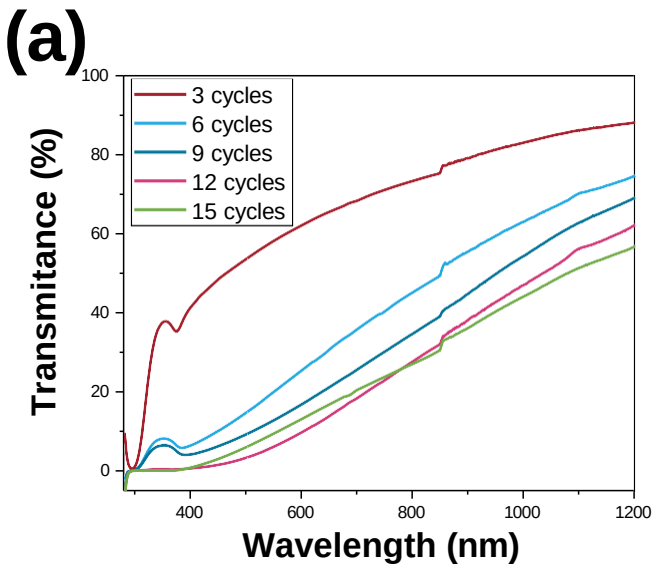

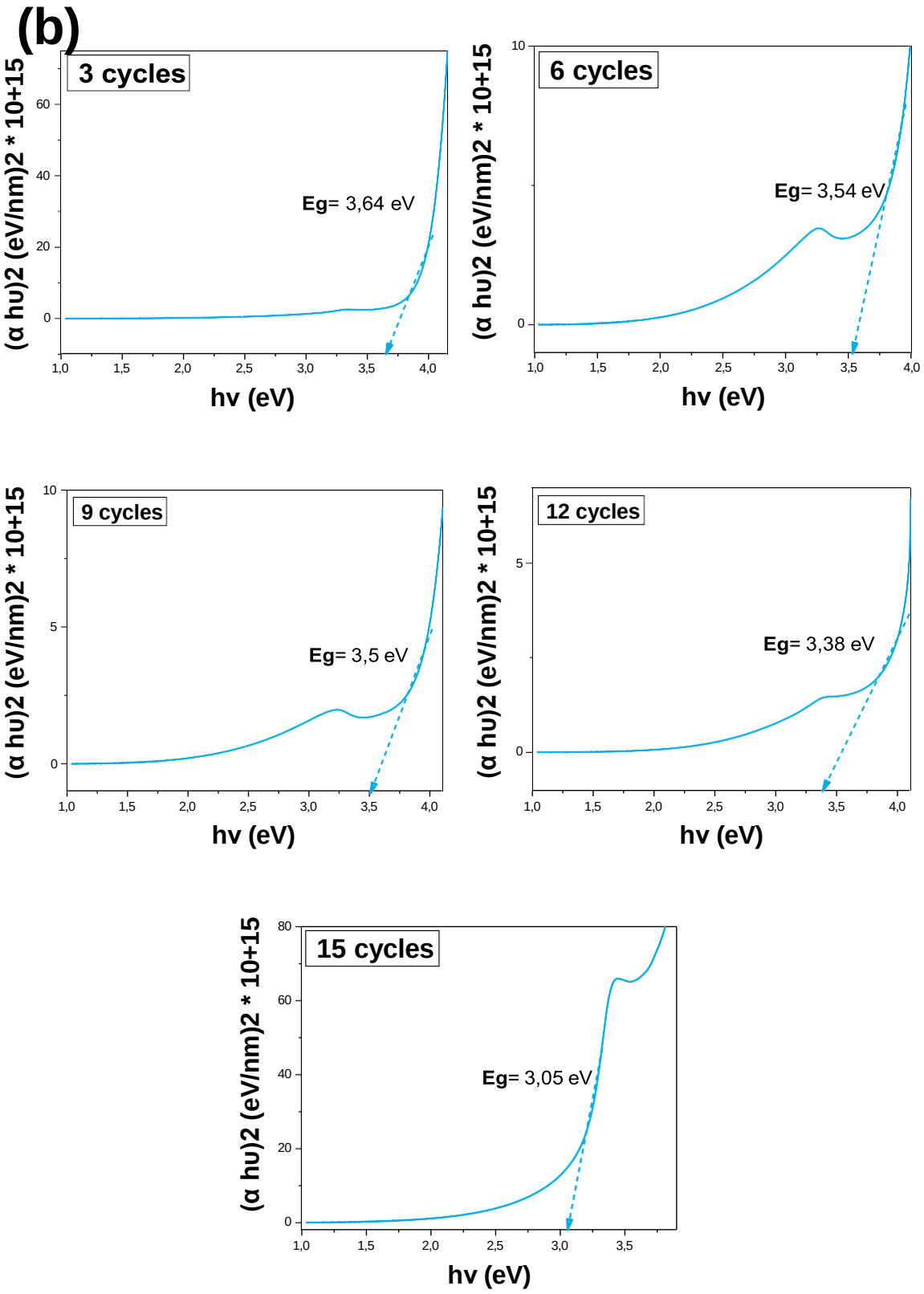
(b)
3 cycles
Eg= 3,64 eV
6 cycles
Eg= 3,54 eV
9 cycles
Eg= 3,5 eV
12 cycles
Eg= 3,38 eV
15 cycles
Eg= 3,05 eV
(α hu)2 (eV/nm)2 * 10+15
hv (eV)

Figure IV.12 (a) UV–Vis spectra of Ba-doped ZnO thin films after photocatalytic degradation at varying deposition, **(b)** Band gap energy of Ba-doped ZnO thin films at different cycle numbers

Table IV.6 The average of transmittance, and band gap energy before and after the photo degradation process

	3		***6***		***9***		***12***		***15***	
	T (%)	**Eg (eV)**	**T (%)**	**Eg (eV)**	**T (%)**	**Eg (eV)**	**T (%)**	**Eg (eV)**	**T(%)**	**Eg (eV)**
Before	78.42	3.68	52.81	3.57	50.66	3.46	34.45	3.37	21.27	3.25
After	58.08	3.64	19.99	3.54	12.77	3.5	6.1	3.38	9.42	3.05

IV.2. 9. Recyclability of the Ba-doped ZnO Photocatalyst

The recycling experiment assessed the performance of the Ba-doped ZnO thin film deposited with 15 cycles, demonstrating significant degradation efficiency over a five hours photocatalytic process under standard conditions recorded on December 03rd, 04th, and 5th,2023, in Biskra, Algeria. During these experiments, the air temperature was 22 °C, humidity was 29%, wind speed was 05 km/h, and the sunlight index was 0.1341 W/m^2. The photocatalytic efficiency for MB decreased from 90.71% in the first cycle to 82.63% in the third cycle, while for AMX, it decreased from 51.09% to 44.76%, as depicted in **Figure IV.13 (a) and (b),** respectively. Notably, the Ba-doped ZnO thin film with 15 deposition cycles exhibited excellent photocatalytic activity, stability, and reusability, highlighting its strong potential for dye degradation applications. **Table IV.7** summarized the removal of pollutant dyes.

Table IV.7 The results of third recycling photocatalytic experiment of MB and AMX dyes.

Recycles	**Photocatalytic degradation (%)**	
	MB	***AMX***
First	90.71	51.09
Second	85.89	47.79
Third	82.63	44.76

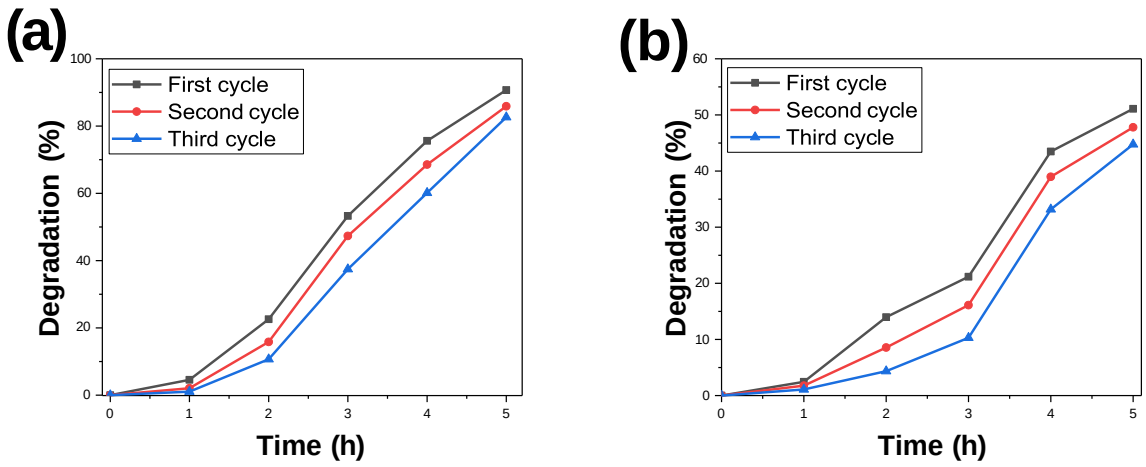

Figure IV.13 Recyclability of Ba-doped ZnO photocatalyst deposited at 15 cycles: **(a)**: for MB and **(b):** for AMX dyes over third cycles

IV.3. Conclusion

In summary, Ba-doped ZnO thin films were successfully synthesized using the SILAR method with different deposition cycles (3, 6, 9, 12, and 15). The number of cycles significantly affected the structural, morphological, and optical properties. XRD confirmed a polycrystalline hexagonal wurtzite structure, with improved crystallinity at higher cycles. SEM analysis showed a compact and uniform surface morphology at 15 cycles, where grain size increased from 29.71 nm to 44.79 nm. EDX confirmed the presence of Zn, O, and Ba elements. Furthermore, transmittance decreased with increasing cycles, while bandgap energy reduced from 3.68 eV to 3.25 eV at 03 and 15 cycles, respectively. Wettability tests confirmed the films' hydrophilic nature, with the highest wettability at 3 cycles related to the lower thickness depicted. The Photocatalytic efficiency improved with increasing cycles, achieving 93.51% ($k = 0.5273\ h^{-1}$) and 54.31% ($k = 0.3218\ h^{-1}$) degradation of methylene blue and amoxicillin, respectively, under sunlight for 5 hours. Moreover, examination of the films after the photocatalytic process showed that the films underwent changes in optical properties, but they still retained their structural property and demonstrated good performance, which is typical in photocatalytic applications. The reusability test over three cycles demonstrated the high stability and recyclability of the prepared films. These findings highlight the potential of Ba-doped ZnO thin films for wastewater treatment. The following chapter will focus on optimizing the annealing temperature of Ba-doped ZnO films to further improve their performance.

References

[1] K. Yousra, E. Guettaf Temam, R. Saâd, H. Barkat, Effect of film thickness on the electrical and the photocatalytic properties of ZnO nanorods grown by SILAR technique, Physica Scripta, vol.12, 2023, doi: https://doi.org/10.1088/1402-4896/ad0ae7.

[2] K.A. Musiliyu, E.D. Ogunmola, A.A. Ajayi, O.W. Abodunrin, Effect of concentration on the properties of nitrogen-doped zinc oxide thin films grown by electrodeposition, Materials for Renewable and Sustainable Energy, vol.12, pp. 23–29, 2023, doi: https://doi.org/10.1007/s40243-022-00225-0.

[3] A.S. Ibrahim, K. V. Alex, M.B. Latha, K. Kamakshi, S. Sathish, J.P.B. Silva, K.C. Sekhar, Effect of the thickness on the photocatalytic and the photocurrent properties of ZnO films deposited by spray pyrolysis, Discover Materials, vol. 2, 2022, doi:https://doi.org/10.1007/s43939-022-00031-5.

[4] S. Göktaş, Synergic Effects of pH, reaction temperature, and various light sources on the Photodegradation of methylene blue without Photocatalyst: A relatively high degradation efficiency, Chemistry Africa, vol. 7, pp. 4425–4437, 2024, doi: https://doi.org/10.1007/s42250-024-01036-8.

[5] M. Rabeel, S. Javed, R. Khan, M.A. Akram, S. Rehman, D.K. Kim, M.F. Khan, Controlling the Wettability of ZnO thin films by Spray pyrolysis for Photocatalytic applications,J. Materials. vol. 15, no. 9, 2022. doi: https://doi.org/10.3390/ma15093364.

[6] A.M. Ahmed, E.M. Abdalla, M. Shaban, Simple and Low-Cost Synthesis of Ba-Doped CuO thin films for highly efficient Solar generation of hydrogen, J. Physical Chemistry C. vol. 124, no. 41, pp. 22347–22356, (2020), doi: https://doi.org/10.1021/acs.jpcc.0c04760.

[7] E. Benrezgua, R. Bourdj, B. Arreiridj, A. Boukhari, R. Bourdj, B. Arreiridj, R. Amari, B.B. Arreiridj, S. Terchi, R. Bourdj, B. Arreiridj, Low thickness effect on the properties of Mn-doped ZnO thin films synthesized by sol-gel spin coating technique, J.Studies in engineering and exact sciences, vol. 5, no.2, pp. 1–16, 2024, doi: https://doi.org/10.54021/seesv5n2-443.

[8] E.H.M. Cavalcante, F.A.G. da Silva Junior, M.A.T. Pereira, P.J. Pereira, M.M. da Costa, H.P. de Oliveira, Antibacterial activity of chitosan and zinc oxide impregnated in PVA-based membranes, Research, Society and Development. vol.12, no. 3, 2023, doi: https://doi.org/10.33448/rsd-v12i3.40720.

[9] H. Barkat, E. Guettaf Temam, H. Ben Temam, N. Mokrani, S. Rahmane, Thickness‐dependent photocatalytic performance and wettability of barium‐doped ZnO thin films synthesized via SILAR technique, Transition Metal Chemistry. 2025. https://doi.org/10.1007/s11243-025-00631-z.

[10] V. Vinitha, M. Preeyanghaa, V. Vinesh, R. Dhanalakshmi, Two is better than one : catalytic , sensing and optical applications of doped zinc oxide nanostructures, Emergent Materials, vol.4, pp.1093–1124, 2021, doi: https://doi.org/10.1007/s42247-021-00262-x.

[11] Y. Yang, T. Shao, Y. Zhang, Y. Lu, M. Li, H. Liu, Q. Xu, Y. Xia, Anionic S-doping of a $ZnMn_2O_4$/CNTs cathode material enhances its Zn^{2+} storage performance in aqueous zinc-ion batteries, J. Power Sources. vol. 564, no. 232863, pp. 0378-7753, 2023, doi: https://doi.org/10.1016/j.jpowsour.2023.232863.

[12] M. Hajji, M. Ajili, N. Jebbari, A. Garcia, N. Turki, Photocatalytic performance and solar cell applications of coupled semiconductor CuO – ZnO sprayed thin films : Coupling effect between oxides, Optical Materials. vol. 140, no. 113798, pp. 0925-3467, 2023 doi: https://doi.org/10.1016/j.optmat.2023.113798.

[13] D. Ali, M.Z. Butt, B. Arif, A.A. Al-, F. Yakuphanoglu, The role of Al, Ba, and Cd dopant elements in tailoring the properties of c-axis oriented ZnO thin films, Physica B: Physics of Condensed Matter, vol.506, no. 0921-4526, pp.83-93, 2017, doi: https://doi.org/10.1016/j.physb.2016.11.003.

[14] X. Bai, W. Chen, B. Wang, T. Sun, B. Wu, Y. Wang, Photocatalytic Degradation of Some Typical Antibiotics: Recent Advances and Future Outlooks, International Journal of Molecular Sciences. vol. 23, no.15, 2022, doi: https://doi.org/10.3390/ijms23158130.

[15] A.R. Jayakrishnan, K. V. Alex, A.T. Tharakan, K. Kamakshi, J.P.B. Silva, M.S. Prasad,

K.C. Sekhar, M.J.M. Gomes, Barium-doped Zinc Oxide thin films as highly efficient and reusable Photocatalysts, Chemistry Select. vol. 5, pp. 2824–2834, 2020, doi: https://doi.org/10.1002/slct.201904943.

[16] Y.Y. Kannangara, R.W.R.M.G. Rajapakse, K.M.N. De Silva, Heterogeneous photocatalytic degradation of toluene in static environment employing thin lms of nitrogen-doped nano-titanium dioxide, International Nano Letters, vol. 8, pp. 31–39, 2018, doi: https://doi.org/10.1007/s40089-018-0230-x.

[17] A.G. Sultan Goktas, Ahmet Tumbul, Growth Technique–Induced Highly C-Axis-Oriented ZnO: Mn, ZnO: Fe and ZnO: Co Thin Films: A comparison of nanostructure, surface morphology, optical band gap, and room temperature ferromagnetism, Superconductivity and Novel Magnetism, vol. 36, pp. 1875–1892, 2023, doi: https://doi.org/10.1007/s10948-023-06630-4.

[18] C.C. Okorieimoh, U. Chime, A.C. Nkele, A.C. Nwanya, I.G. Madiba, A.K.H. Bashir, S. Botha, P.U. Asogwa, M. Maaza, F.I. Ezema, Room-temperature synthesis and optical properties of nanostructured Ba-Doped ZnO thin films, Superlattices and Microstructures, vol. 130, pp. 321–331, 2019,doi: https://doi.org/10.1016/j.spmi.2019.05.010.

[19] A. Modwi, L. Khezami, K.K. Taha, A.J. Bessadok, S. Mokraoui, Photo-degradation of a mixture of dyes using Barium doped ZnO nanoparticles, Materials Science: Materials in Electronics, vol. 30, pp. 14714–14725, 2019, https://doi.org/10.1007/s10854-019-01843-7.

[20] K. N'Konou, Y. Lare, M. Haris, M. Baneto, K. Amou, K. Napo, Influence of Barium Doping on Physical Properties of Zinc Oxide Thin Films Synthesized by SILAR Deposition Technique, Advances in Materials. vol. 3, no. 6, pp.63-67, 2014, doi: https://doi.org/10.11648/j.am.20140306.11.

[21] M. Ulfa, H. Al Afif, T. Endah Saraswati, H. Bahruji, Fast Removal of methylene blue via adsorption-Photodegradation on TiO_2/SBA-15 synthesized by slow calcination, J. Materials, vol. 15, no. 16, 2022, doi: https://doi.org/10.3390/ma15165471 .

Chapter V.

Influence of Annealing Temperature on Ba-Doped ZnO Thin Films and their Photocatalytic Application

V.1. Introduction

The annealing temperature is a critical parameter influencing thin films' structural, optical, morphological, and photocatalytic properties. In this chapter, we study the effect of annealing at different temperatures (300 °C, 350 °C, 400 °C, and 450 °C) on the Ba-doped ZnO thin films with optimized parameters (5 wt.% Ba doping and 15 SILAR cycles), which were identified as the most efficient for the degradation of methylene blue dye in the previous chapters.

The main objectives of this chapter are:

- Determination the optimal annealing temperature that maximizes the photodegradation of MB dyes, while maintaining film stability, uniformity, and reusability.
- Represent structural, morphological, topographical, and optical properties of barium-doped zinc oxide thin films at different annealing temperature and their photocatalytic degradation of methylene blue dye, as patterns, figures, and tables.
- Interpretation and discussion of the obtained results.

V.2. Results and discussion

V.2.1. Measurement of film Thickness

The variation of annealing temperature as a function of the thickness of the deposited Ba-doped ZnO thin films is presented in **Figure V.1**. The prepared films annealed at temperatures ranging from 300 °C to 450 °C depicted that the film thickness values increased from 85.234 nm to 244.107 nm, respectively. Based on these findings, the thickness of films increases when the annealing temperature increased. These results are well-matched with C.Elekalach’s study [1].

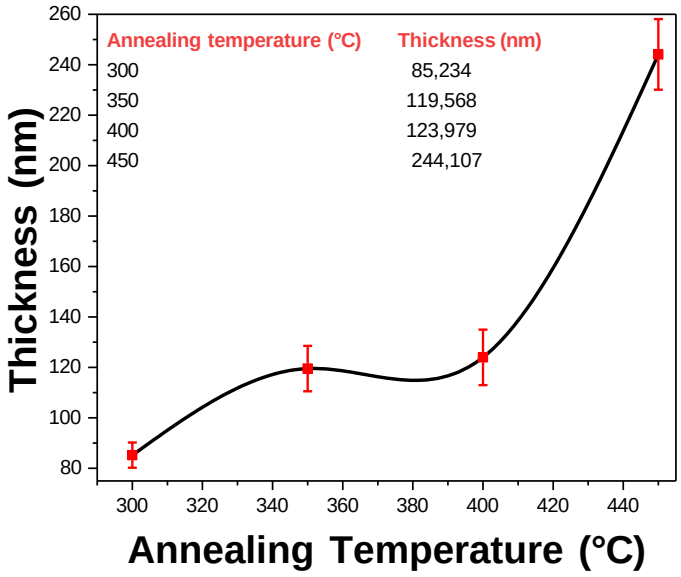

Figure V.1. Variation of film thickness with annealing temperature for Ba-doped ZnO thin films deposited via SILAR

V.2.2. Structural properties

The XRD patterns of Ba-doped ZnO thin films annealing at various temperature (300°, 350°, 400°, and 450°) were investigated, and different diffraction peaks presented in **Figure V.2(a)**. The major diffraction peaks observed at 31.85°, 34.53°, and 36.31° corresponding respectively to the lattice planes (100), (002), (101), indicating the polycrystalline nature of all films obtained with the hexagonal wurtzite structure according to the JCPDS card (**75-0576**). The strong intensity of the preferred peak at the (002) plane indicates the high crystalline quality of the films. Literature reports suggest that ZnO growth along this orientation is commonly observed in intrinsic ZnO films [2]. The diffractograms illustrated that the intensity of the peaks increases as the annealing temperature increased from 300° to 450°, suggesting enhanced crystallinity from 9.308 nm to 11.388 nm.

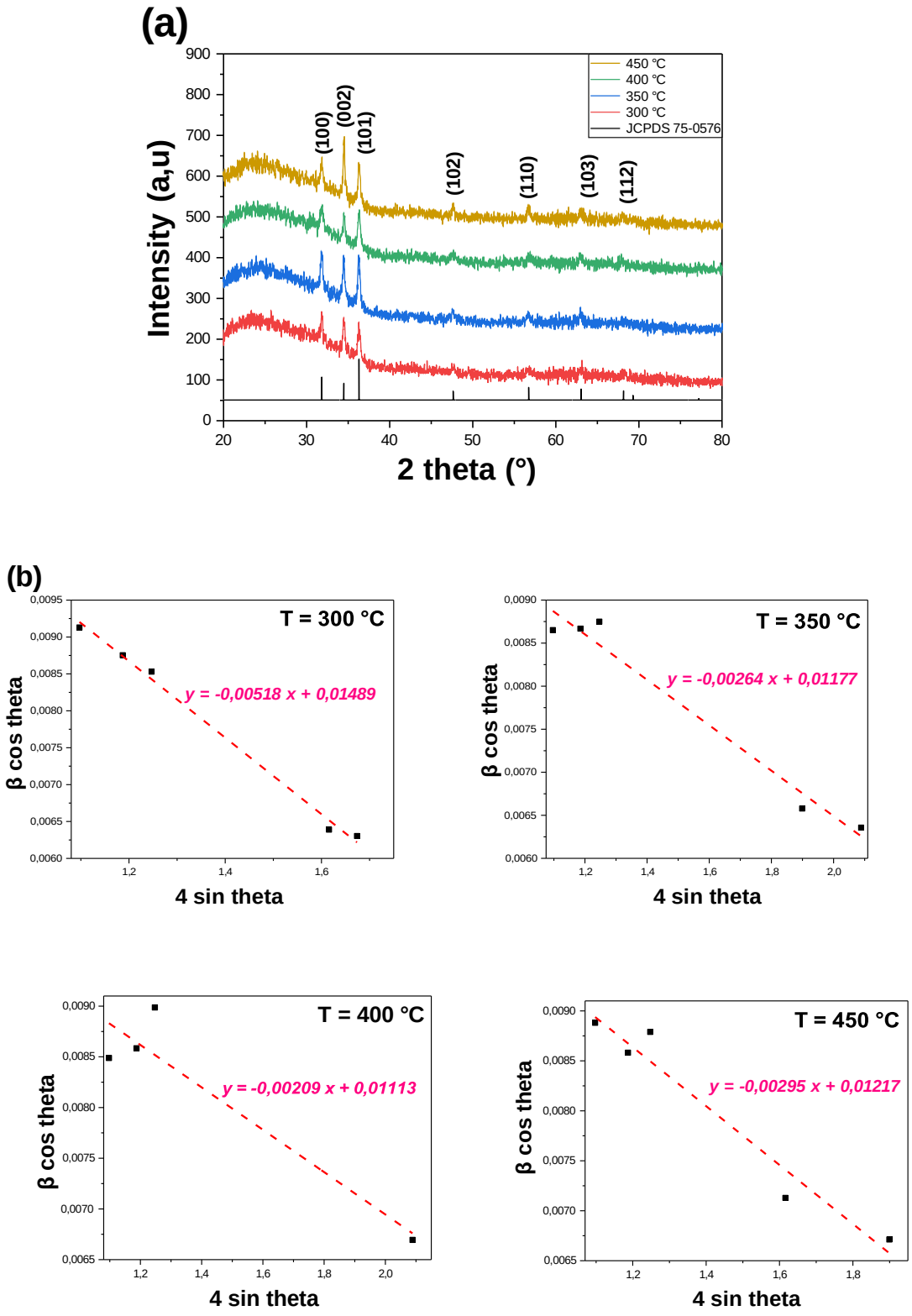

Figure V.2. (a) XRD Patterns of Ba-doped ZnO films grown at different temperatures, **(b)** Williamson–Hall plots of βcos(θ) versus 4sin(θ) of all samples

To determine the crystallite size (D) and lattice strain (ε) parameters of films, the Williamson–Hall method was applied based on the major intense peaks for each sample, the equation as presented in **Eq II.6** and the plots are shown in **Figure V.2(b).** The slope and y-intercept of the linear profile fit are identified as the values of ε and, D respectively. As presented in **Table V.1**, the crystallite size increases noticeably with rising annealing temperature due to coalescence and diffusion processes occurring during annealing from 300° to 400° [3]. This increasing in crystallites is attributed to the enhanced atomic mobility at elevated temperatures, allowing atoms to occupy more energetically favorable positions in the crystal lattice [1]. On the other hand, at 450°C, a decrease in crystallite size was observed, which may be attributed to thermal stress, leading to defect formation that hinders crystallite coalescence. The increase in strain (ε) and dislocation density (δ) at 450°C supports this, indicating the generation of structural imperfections [4]. This overall decrease in crystallite size results in an increase in the number of crystallites (N). **Figure V.2** bellow presented the inverse relationship between the crystallite size and the number of crystallites.

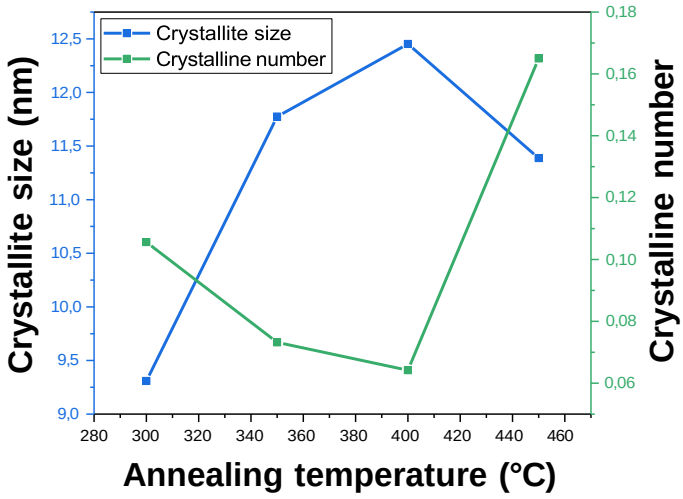

Figure V.3. Variation of crystallite size and lattice strain versus annealing temperatures graph of Ba-doped ZnO thin films

The density of dislocations (δ) value represents the percentage of deformities present in the fabricated Ba-doped ZnO thin films produced by internal strain and is presented in **Table V.1**.

Table.V.1. The structural parameters of Ba-doped ZnO thin films at varying temperatures

Annealing temperature (°)	**2θ (°)**	**FWHM**	**D (nm)**	**ε**	**δ (nm^{-2})**	**N**
300	34.52	0.2755	9.308	-0.0051	0.011	0.1056
350	34.49	0.1968	11.775	-0.0026	0.0072	0.0732
400	34.53	0.2362	12.452	-0.0020	0.0064	0.0642
450	34.53	0.1574	11.388	-0.0029	0.0077	0.165

V.2. 3. Surface morphology and elemental analysis

Figure V.4 presents SEM images illustrating the impacts of annealing temperatures at 300°C, 350°C, 400°C, and 450°C. At 300°C, the film exhibits dispersed, relatively small grains, indicative of the initial stages of nucleation, where grains are beginning to form but lack significant coalescence. At 350°C, the grains become more prominent and better defined compared to those at 300°C. Evidence of grain coalescence is observed, as neighboring grains begin to merge due to enhanced atomic mobility at this annealing temperature. The porosity decreases slightly, and the surface morphology becomes more uniform, indicating an improvement in the film's crystallinity. At 400°C, the surface morphology is notably more compact and uniform. The grain size increases significantly, reflecting substantial grain growth driven by enhanced atomic diffusion and coalescence. The reduced porosity at this stage corresponds with the observed improvements in crystallite size and crystalline quality as indicated by the XRD results. This temperature appears to be optimal for achieving a balance between grain growth and structural integrity, resulting in a dense and well-crystallized film. At 450°C, however, the morphology becomes less uniform compared to that at 400°C. The grains appear smaller and more fragmented, with noticeable defects or voids forming on the surface. This change suggests that thermal stress or structural defects dominate at this temperature, disrupting grain growth. The increased dislocation density and strain observed in the XRD data at 450°C further support this behavior, indicating the generation of structural imperfections that hinder coalescence and degrade the overall quality of the film. Furthermore, the increase in diameter of grain size from 648.75 to 733.47 nm with the increase of annealing temperature from 300°C to 450°C confirmed our XRD results.

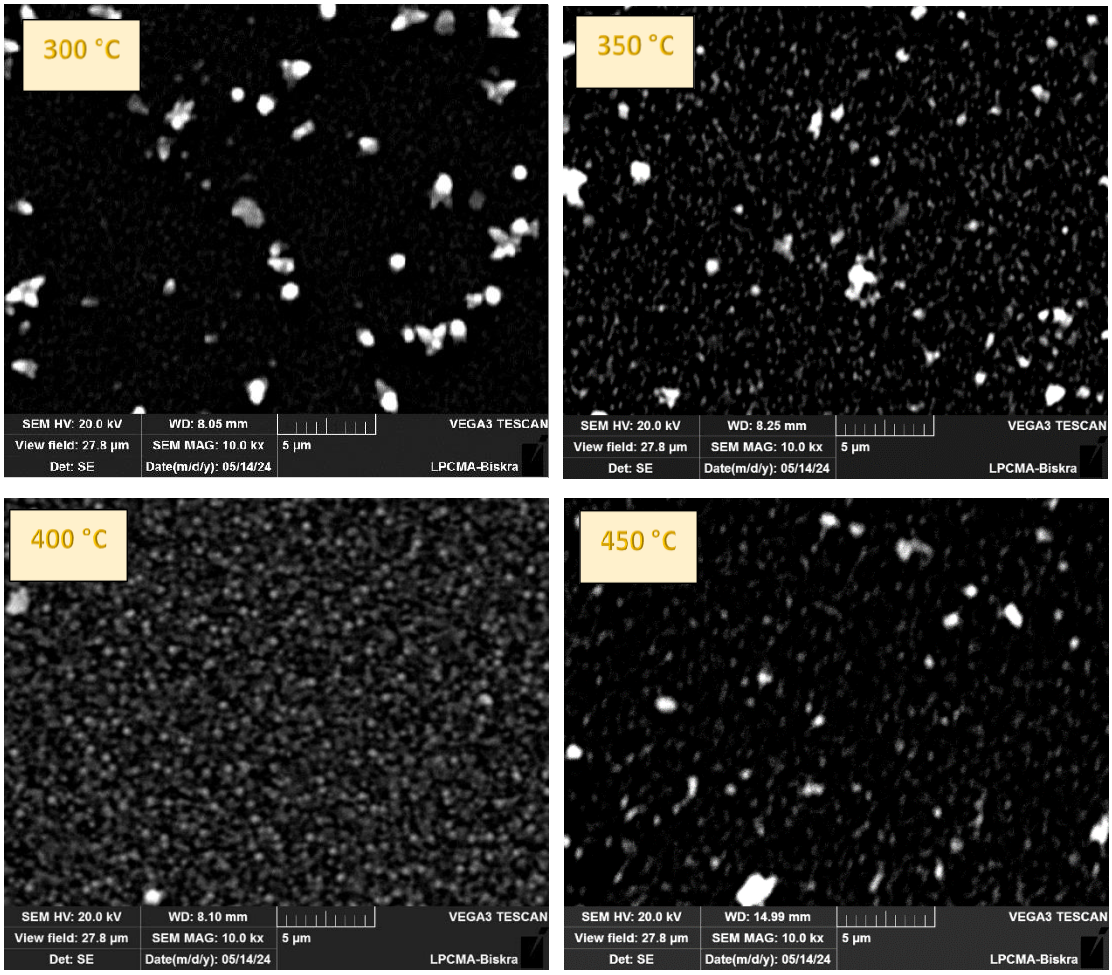

Figure V.4. SEM micrographs of Ba-doped ZnO thin films at different annealing temperatures (300, 350, 400, 450 °C)

As shown in **Figure V.5,** EDX was used to reveal the existence of the zinc, oxygen, barium, and silicone elements. The appearance of Ba in the EDX analysis confirms its incorporation into the ZnO structure.

300°C

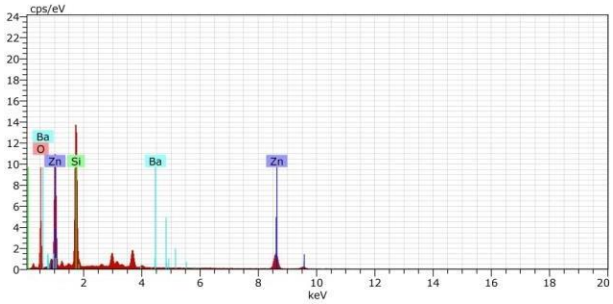

El	AN	Series	unn. C [wt.%]	norm. C [wt.%]	Atom. C [at.%]	Error (1 Sigma) [wt.%]
Zn	30	K-series	21.05	39.17	16.96	0.63
Si	14	K-series	17.31	32.20	32.47	0.77
O	8	K-series	15.35	28.56	50.55	2.11
Ba	56	L-series	0.04	0.07	0.01	0.03
		Total:	53.74	100.00	100.00	

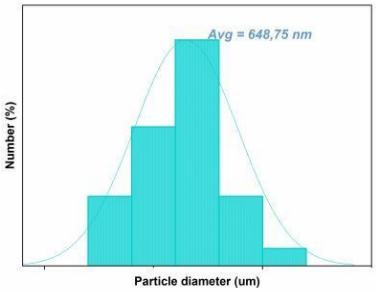

350°C

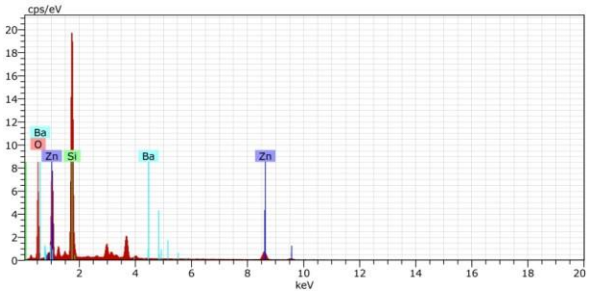

El	AN	Series	unn. C [wt.%]	norm. C [wt.%]	Atom. C [at.%]	Error (1 Sigma) [wt.%]
Si	14	K-series	19.63	41.89	35.79	0.87
O	8	K-series	17.74	37.86	56.78	2.36
Zn	30	K-series	9.48	20.23	7.42	0.32
Ba	56	L-series	0.01	0.02	0.00	0.03
		Total:	46.86	100.00	100.00	

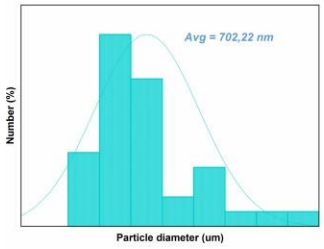

400°C

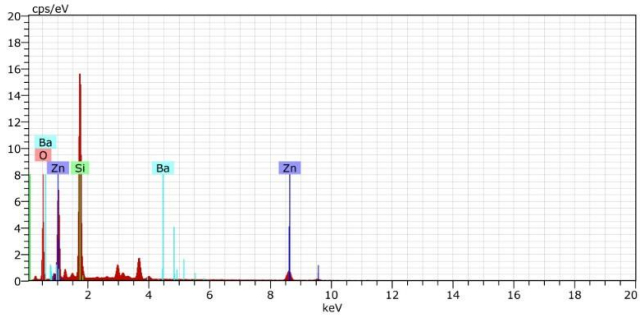

El	AN	Series	unn. C [wt.%]	norm. C [wt.%]	Atom. C [at.%]	Error (1 Sigma) [wt.%]
Si	14	K-series	18.69	42.25	37.27	0.83
O	8	K-series	15.45	34.94	54.09	2.08
Zn	30	K-series	10.09	22.81	8.64	0.33
Ba	56	L-series	0.00	0.00	0.00	0.00
		Total:	44.23	100.00	100.00	

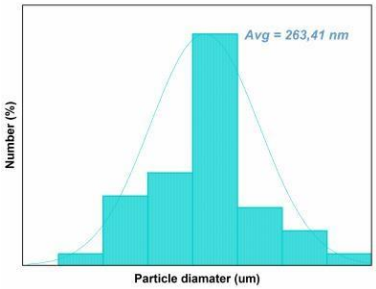

450°C

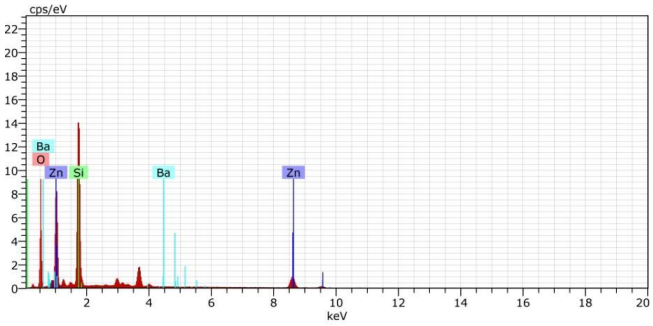

El	AN	Series	unn. C [wt.%]	norm. C [wt.%]	Atom. C [at.%]	Error (1 Sigma) [wt.%]
Si	14	K-series	20.34	36.95	33.62	0.90
O	8	K-series	19.06	34.62	55.29	2.54
Zn	30	K-series	15.61	28.35	11.08	0.48
Ba	56	L-series	0.04	0.08	0.02	0.03
		Total:	55.06	100.00	100.00	

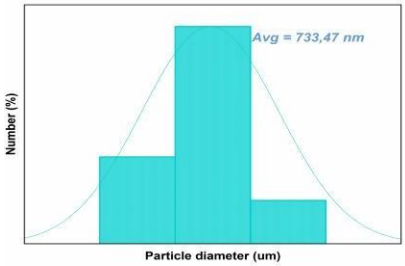

Figure V.5. EDX analysis and particles diameter measurement of Ba-doped ZnO thin films at various annealing temperatures

V.2. 4. Optical properties

Figure V.6 (a) shows the optical transmission spectra of Ba-doped ZnO thin films within the

wavelength range of 390 to 1200 nm for different annealing temperatures (300–450°C). The optical properties of transparent conductive films are known to be heavily influenced by the deposition methods and the preparation conditions employed during fabrication [5]. The results clearly demonstrate that annealing treatment significantly affects the films' optical behavior. Specifically, the transmittance decreases with increasing annealing temperature from 300°C to 450°C, which can be attributed to increased film thickness grown at higher annealing temperatures, and also can be due to high light scattering from voids or grains [6].

Furthermore, higher post-annealing temperatures caused the transmission spectra to shift towards longer wavelengths, indicating changes in the optical characteristics of films at elevated growth temperatures. This shift in transmission spectra is attributed to a reduction in the transition separation between levels, usually denoted as the bandgap energy (Eg), leading to a shift of the displacement of the absorption edge to longer wavelengths [6] [7].

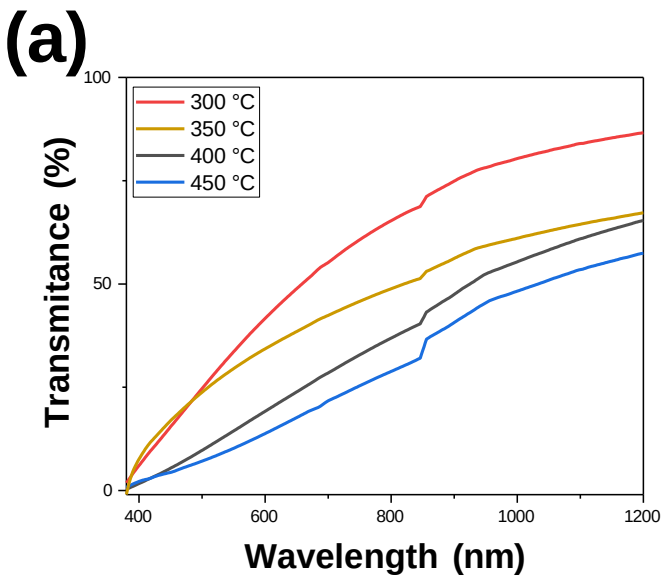

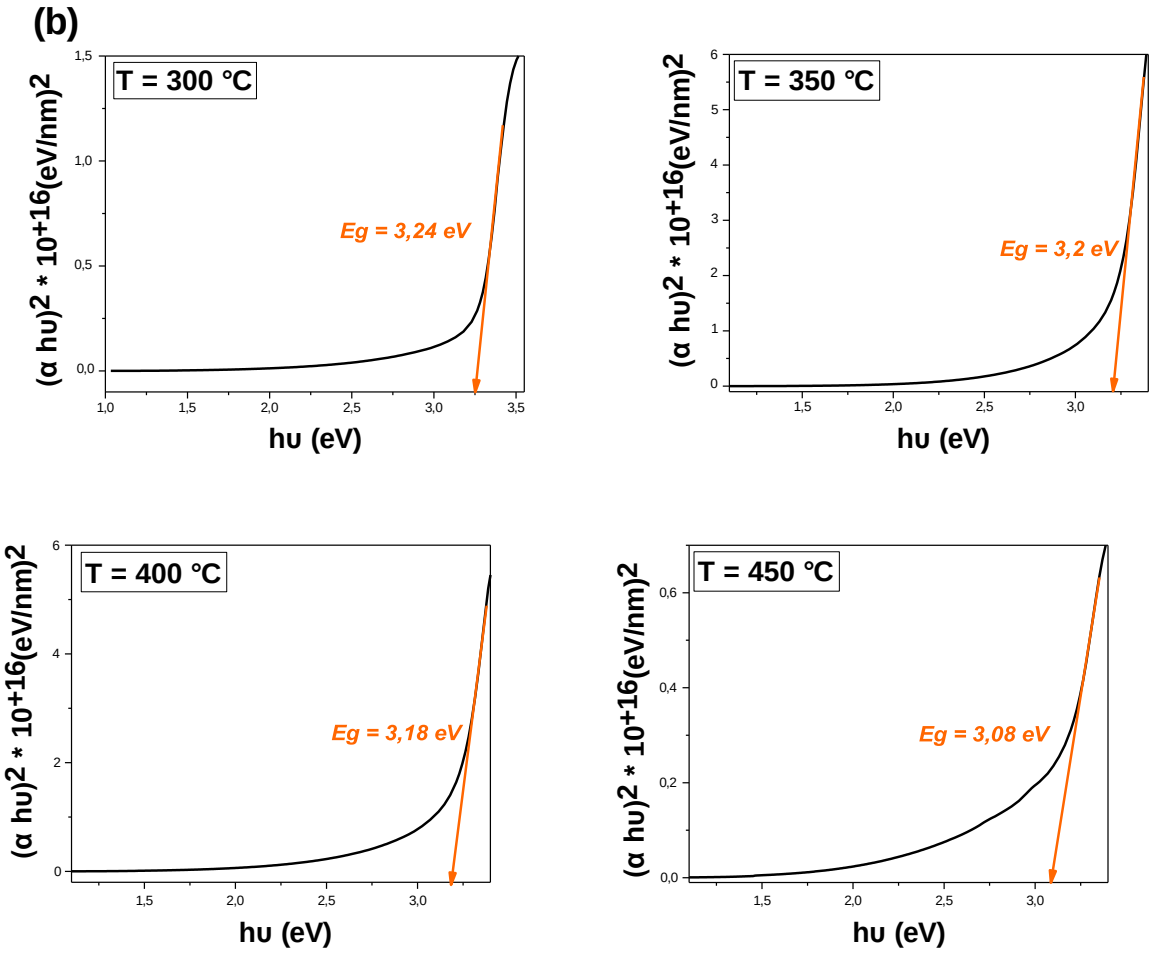

Figure V.6. (a) Transmittance spectra and **(b)** Tauc plot of Ba-doped ZnO thin films at different annealing temperature

To evaluate the optical band gap of prepared film samples, Tauc plots were created, as illustrated in **Figure.V.6 (b).** The plots reveal that the transition region occurs around 3.24 eV, corresponding to the direct bandgap transition between the valence band and conduction band, representing the optical bandgap energy (Eg) of ZnO.

The values of the band gap calculated are 3.24 eV, 3.2 eV, 3.18 eV, and 3.02 eV, corresponding to 300°C, 350°C ,400°C, and 450°C, respectively. These results of decreasing of Eg with increasing of annealing temperature can be attributed to improvements in crystal quality and larger crystal sizes at higher temperatures from 300 to 450°C [8]. This enhanced crystallinity and improved structural order lead to a reduction in the bandgap energy, facilitating the generation of electron-hole pairs and subsequently enhancing the material's photocatalytic and optical

performance [5].

V.2. 5. *Photocatalytic degradation of methylene blue*

Photocatalytic degradation of harmful organic contaminant in the environment using a photocatalyst has attracted significant attention in recent years. The degradation of methylene blue (MB), as a pollutant model, in the presence of Ba-doped ZnO thin films annealing at various temperatures, under sunlight irradiation is the subject of this experiment.

As shown in **Figure V.7 (a,b)**, photocatalytic activity increases with the increase in annealing temperature from 300°C to 450°C for methylene blue pollutant for 5 h under sunlight irradiation times and meteorological conditions in Biskra, Algeria, on May 26th, 2024, which presented in **Table V.2**. The degradation percentages were approximately 73.37%, 80.13%, 91.48%, and 96.17% for films annealed at 300°C, 350°C, 400°C, and 450°C, respectively, demonstrating enhanced photocatalytic efficiency with higher annealing temperatures. However, the low crystallinity obtained at low annealing temperature resulting the low photocatalytic performance of the film calcined at 300°C. Moreover, when the annealing temperature increasing from 350°C to 450°C, we noticed an enhancement in photocatalytic activity due to increased crystallinity at these temperatures.

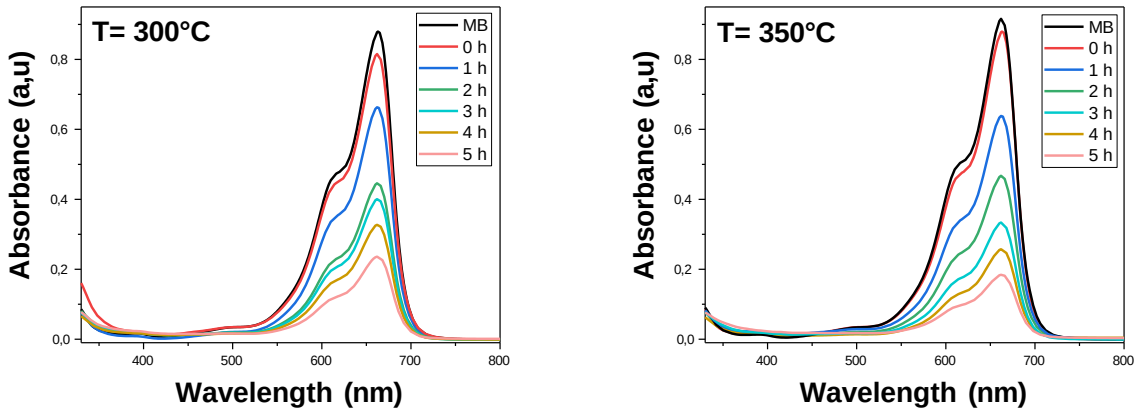

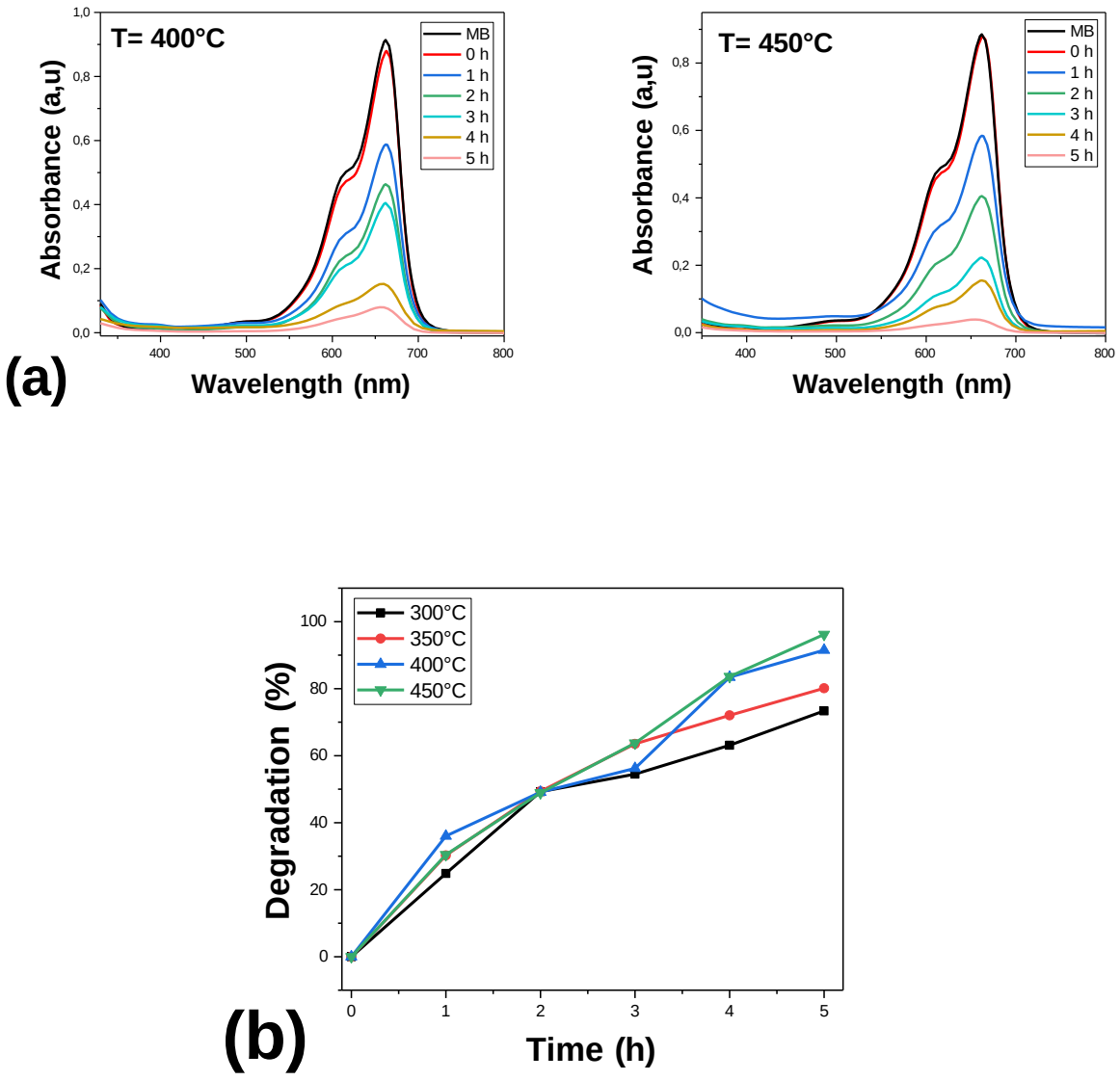

Figure V.7. Variation of UV–vis spectra of MB during photodegradation at various annealing temperature, **(b)** plot of % degradation of MB as a function of time

Table V.2 Parameters and results of photocatalytic tests.

Samples annealing at	***300°C***	***350°C***	***400°C***	***450°C***
Removal (%)	73.37	80.13	91.48	96.17
The date	*26/05/2024*			
The temperature (°C)	*39*			
Wind speed (km/h)	*09*			
Humidity (%)	*14*			
Irradiation intensity (mW/cm^2)	*0.1357*			

Numerous studies suggest that the reaction kinetics of various organic dyes' photodegradation in aqueous solutions can be effectively explained using the Langmuir–Hinshelwood model, described as the pseudo-first-order kinetic model [9]. The linear relationship between ln(Co/Ct) and irradiation time, which indicates that the degradation of MB essentially follows pseudo-first-order kinetics, is presented in **Figure V.8**, and the rate constants obtained from the graph slope are reported in the inset of this figure. The first-order rate constant (K) increased with higher annealing temperature from 0.312 h^{-1} to 0.353 h^{-1}, corresponding the optimal degradation efficiency of the MB dye for sample annealing at 450°C.

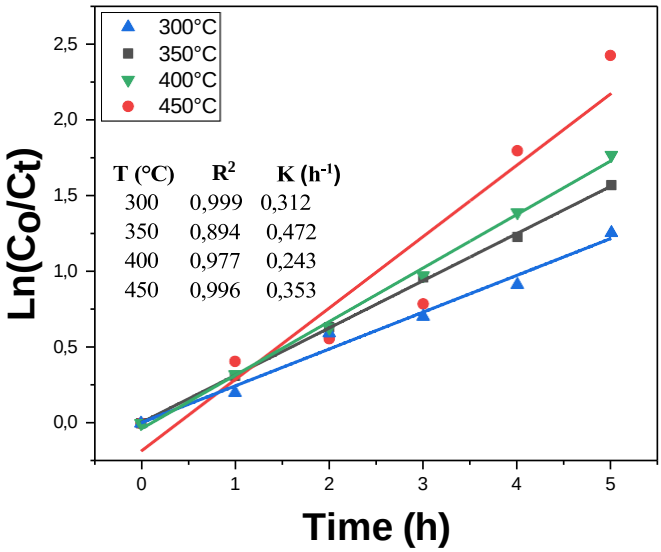

Figure V.8. Kinetics study of photocatalytic degradation MB under sunlight irradiation at different annealing temperatures

V.2. 6. Reusability of the Ba-doped ZnO Photocatalyst

Recyclability, or stability, is a crucial characteristic for the practical application of the Ba-doped ZnO catalyst, which demonstrated the best degradation efficiency at an annealing temperature of 450°C. **Figure V.9** illustrated the photocatalytic reusability of Ba-doped ZnO in the photodegradation of MB dye was exposed to 5 successive cycles of reusability within 5 h under sunlight irradiation at meteorology conditions presented in **Table V.3**. After the fifth recycling, the photodegradation performance gradually decreased from 95.97% to 94.89% for MB dye using a Ba-doped photocatalyst annealed at 450°C, indicating the stability and reusability of prepared films.

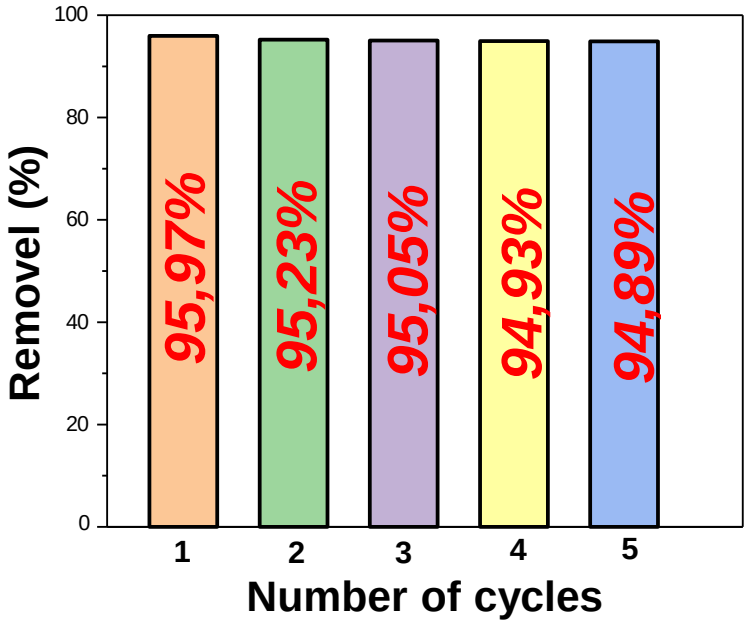

Figure V.9. The reusability and stability of Ba-doped ZnO photocatalyst annealed at 450°C for the degradation of MB over five cycles

Table V.3. The meteorology conditions of fifth recycling photocatalytic tests of MB dye

Cycles	The date	Temperature C°	Wind speed km/h	Humidity %
1	01/06/2024	40	07	16
2	02/06/2024	38	08	14
3	03/06/2024	40	07	16
4	04/06/2024	39	07	14
5	05/06/2024	39	07	14

V.3. Conclusion

As a conclusion for this chapter, 5wt.% Ba-doped ZnO thin films were produced via SILAR method at 15 cycles deposition and subjected to different annealing temperatures (300°C, 350°C, 400°C, and 450°C). The effect of annealing temperature on the structural, morphological, optical, and photocatalytic properties were investigated. It has been found that the crystallinity and thickness surfaces of films increased with annealing temperature. The SEM analysis revealed that annealing led to a more uniform and compact surface morphology. Also, it is found that the annealing temperature has a great effect on the transparency of the thin films in the visible range; it increases with the annealing temperature from 300 °C to 450°C. Furthermore, the resulting films exhibited remarkable photocatalytic activity of MB dye under sunlight irradiation for 5 hours and demonstrated promising reusability potential. Notably, the films annealed at 450°C achieved the highest degradation efficiency (96.17%) and slowly decreased to 94.89% after five cycles successively. These promising findings underscore the effectiveness, reusability, and stability of prepared thin films in photocatalytic processes and applications.

References

[1] C. I. Elekalachi, I. A. Ezenwa, N. A.Okereke, N. L. Okoli, A. N. Nwori, Thermal Annealing Impact on The Properties of CdSe/PbSe Superlattice Thin Films, OAJ Materials and devices , vol.8, 0211,2024, doi: https://doi.org/10.23647/ca.md2024021.

[2] A. Ouhaibi, N. Saoula, M. Ghamnia, M.A. Dahamni, L. Guerbous, Effect of Deposition Temperature on Morphological, Optical, and Photocatalytic Properties of ZnO Thin Films Synthesized by Ultrasonic Spray Pyrolysis Method, Crystal Research and Technology, vol. 57, 1–8, 2022, doi: https://doi.org/10.1002/crat.202100224.

[3] L. Fouaz, M. Ouchabane, S. Hassani, D. Driss, Structural, Optical, Electrical and Mechanical Properties of ZnO Co-doped Ag, Mg Thin Films: Annealing Temperature Effect, Proceedings of the 4th International Symposium on Materials and Sustainable Development, pp. 184–192, 2020, doi:https://doi.org/10.1007/978-3-030-43268-3_16.

[4] V. Prasad, S. Pendurti, Models for Stress and Dislocation Generation in Melt Based Compound Crystal Growth, Springer Handbook of Crystal Growth, pp 1335–1378, 2010, doi: https://doi.org/10.1007/978-3-540-74761-1_39.

[5] G.M. Wazzan, J.M. Alghamdi, N. Dalhat, T.S. Kayed, E. Cevik, Annealing Temperature Effects of Seeded ZnO Thin Films on Efficiency of Photocatalytic and Photoelectrocatalytic Degradation of Tetracycline Hydrochloride in Water, Catalysts, vol.15, pp. 15-71, 2025, doi: https://doi.org/10.3390/catal15010071.

[6] A. Fattah, S. Hussien, S. Mohammed, Influence of Annealing Temperature of Seed Layer on The Structural and Optical Properties of ZnO Nanorods Synthesized by SILAR and CBD Techniques, Materials Technology. vol. 40, no.1, pp. 1–16, 2025, doi: https://doi.org/10.1080/10667857.2024.2443205.

[7] M. T. Thuya, S.Y. Pung, A. Aziz, M. Itoh, Stacked ZnO Nanorods Synthesized by Solution Precipitation Method and their Photocatalytic Activity Study, J. Sol-Gel Sci Technolpp,vol. 74, pp. 260–271, 2015, doi: https://doi.org/10.1007/s10971-015-3646-z.

[8] Q. Humayun, M. Kashif, U. Hashim, Structural , Optical , Electrical , and Photoresponse Properties of Postannealed Sn-Doped ZnO Nanorods, J. Nanomaterials, pp. 1-8, 2013, doi:

http://dx.doi.org/10.1155/2013/792930.

[9] F. Mohamed, S. Hassaballa, M. Shaban, A. M. Ahmed, Highly Efficient Photocatalyst Fabricated from the Chemical Recycling of Iron Waste and Natural Zeolite for Super Dye Degradation, Nanomaterials, vol. 12, pp. 235, 2022, doi: https://doi.org/10.3390/nano12020235.

General Conclusions and Future Perspectives

General Conclusions and future perspectives

The original research presented in this thesis focused on producing high-performance undoped and Ba-doped ZnO thin films, which were successfully fabricated using the Successive Ionic Layer Adsorption and Reaction (SILAR) process and deposited on glass substrates. Several properties have been investigated, and different applications in the wastewater field has been explored.

To ensure an excellent-quality films for wettability tests and photocatalytic application, different deposition experimental parameters were adopted, including the concentration of barium dopant, cycles number, and annealing temperature. Our work studied the influence of these parameters on the structural, topographical, morphological, chemical composition, and optical (transmittance and gap energy) properties of barium doped zinc oxide films. Various techniques were employed to investigate the fabricated samples such as X-ray diffraction, scanning electron microscopy, profilometer, energy dispersive spectroscopy, and UV-vis spectrophotometry.

In the first part of our experimental work, we have prepared series of undoped and Ba-doped ZnO at different concentrations (1 wt.%, 3 wt.%, 5 wt.%, and 7 wt.%). X-ray diffraction analysis confirmed the successful doping of Ba into the ZnO lattice, revealing distinct peaks corresponding to the ZnO hexagonal wurtzite structure. Slight shifts in these peaks indicated the presence of Ba doping, with the preferred planes observed along (100) and (002). SEM images revealed that the films were well adherent and uniform. Surface topography studies depicted an increase in surface roughness (317 nm) with larger agglomerates and a rougher texture at 5 wt.% Ba, which was attributed to the larger crystallite size (113.6 nm) and higher lattice train ($1.86\ 9\ 10^{-3}$). The EDX patterns indicated the presence of Zn, O, and Ba signals as the main components of the synthesized thin films, confirming the high purity of the deposited film. The optical studies displayed that the transmittance of the films increased with increasing of Ba doping concentration, suggesting enhanced optical transparency. Furthermore, the optical band gap of Ba-doped ZnO exhibited a slight decrease compared to undoped ZnO, dropping from 3.37 eV to 3.0 eV at higher doping concentrations. The water contact angle analysis demonstrated a remarkable improvement in surface hydrophilicity for the 5 wt.% Ba-doped ZnO sample, with the WCA significantly decreasing from 110.84° in undoped ZnO films to 42.34°. The 5 wt. % Ba-doped ZnO films showed a high photocatalytic performance, reaching a 95.78% degradation of methylene blue after

5 hours of sunlight exposure. The reusability tests ensured the stability of our films after 5 successive cycles of recyclability within 5 h under sunlight irradiation, and we confirmed their stability by the SEM analysis after photocatalytic degradation of MB dye.

In the second parts of our experimental work, we discussed the impact of different deposition cycles (3, 6, 9, 12, and 15) on the structural, morphological, and optical properties of the 5 wt.% Ba-doped ZnO thin films synthesized via SILAR method. The XRD analysis revealed the polycrystalline nature with a hexagonal wurtzite structure of all deposited films. Crystallite sizes of the films enhanced at higher cycles. The SEM images illustrated a compact and uniform surface morphology at 15 cycles and the grain size increased from 29.71 nm to 44.79 nm. Moreover, EDX analysis depicted the presence of Zn, O, and Ba elements on the prepared films. The UV-Vis spectra demonstrated that the transmittance of Ba-doped ZnO films decreased with an increase in the number of deposition cycles, while the band gap energy also reduced from 3.68 eV to 3.25 eV at 03 and 15 cycles, respectively. Furthermore, the wettability tests confirmed the hydrophilic property of our films, with the highest wettability observed at 3 cycles, corresponding to the thinnest film thickness. The Ba-doped ZnO films deposited at 15 cycles number showed a major photocatalytic performance, achieving a 93.51% ($k = 0.5273\ h^{-1}$) and 54.31% ($k = 0.3218\ h^{-1}$) degradation of methylene blue and amoxicillin, respectively, after 5 hours of sunlight irradiation. Additionally, after examining the films post-photocatalytic process, it was observed that while the optical properties changed, the films maintained their structural integrity and exhibited strong performance, which is typical for photocatalytic applications. The reusability test conducted over three cycles demonstrated the excellent stability and recyclability of the prepared films.

In the third parts of our experimental work, we studied the influence of various annealing temperatures (300°C, 350°C, 400°C, and 450°C) on a series of 5 wt.% Ba-doped ZnO films, which were produced via the SILAR method with 15 deposition cycles. The XRD analysis presented the polycrystalline nature with a hexagonal wurtzite structure of all samples. It has been also found that the crystallinity and thickness values of films increased as annealing temperature increased. The SEM images showed that increasing the annealing temperature resulted in a more uniform and compact surface morphology. Additionally, annealing temperature influenced the optical properties, as film transparency increased with temperature from 300 °C to 450 °C. The annealed films displayed excellent photocatalytic activity for MB dye

under sunlight irradiation over 5 hours, with notable reusability potential. Specifically, the films annealed at 450°C achieved the highest degradation efficiency of 96.17%, which gradually declined to 94.89% after five consecutive cycles. These findings highlight the efficiency, durability, and reusability of the prepared thin films for photocatalytic applications.

Although this study focuses on laboratory-scale synthesis and characterization, future efforts could focus on the scaling-up of the Ba-doped ZnO thin films for industrial applications, including wastewater treatment, air purification, and self-cleaning surfaces. This would involve investigating the feasibility of large-scale production methods, cost-effectiveness, and the optimization of film deposition for large-area substrates. Additionally, refining the SILAR technique, including solvent and pH adjustments, could improve film morphology and photocatalytic performance.

Abstract

In this work, undoped and Ba-doped ZnO thin films were deposited on glass substrates by a simple and cost effectiveness successive ionic layer adsorption and reaction (SILAR) method. These films were investigated using various techniques. To optimize the quality of our films, we have studied the influence of dopant concentrations, deposition cycles number, and annealing temperature on film's structural, morphological, optical, and photocatalytic properties. All samples exhibited a polycrystalline nature with wurtzite hexagonal phase. The X-ray diffraction patterns shows that the 5 wt. % Ba-doped ZnO crystallization is better than undoped samples, with a (100) preferred orientation. SEM images revealed that the films were well adherent and uniform. UV-Visible depicted that the transmittance of the films increased as increasing of Ba-doping concentrations, demonstrating improved optical transparency. The 5 wt.% Ba-doped ZnO films displayed the highest photocatalytic efficiency, achieving 95.78% degradation of MB under sunlight irradiation over 5 hours. This sample showed exceptional stability and reusability, retaining its performance over five cycles.

On the other hand, 5 wt.% Ba-doped ZnO films deposited at different cycle numbers showed that an increase in deposition cycles led to better crystallinity at higher cycles. As a result, the photocatalytic efficiency improved to 93.51% at 15 cycles.

Furthermore, the results showed that the process of annealing temperature at 450°C enhanced the crystallinity, the optical properties, and the photocatalytic efficiency of Ba-doped ZnO films, achieving 96.17% degradation of MB, and which gradually decreased to 94.89% after five successive cycles.

Keywords: Ba-doped ZnO thin films, SILAR method, photocatalytic degradation, methylene blue.

Résumé

Dans ce travail, des films minces de ZnO non dopé et dopé au Ba ont été déposés sur des substrats en verre par une méthode simple et économique d'adsorption et de réaction successive des couches ioniques (SILAR). Ces films ont été étudiés à l'aide de diverses techniques. Afin d'optimiser la

qualité de nos films, nous avons étudié l'influence des concentrations de dopant, du nombre de cycles de dépôt et de la température de recuit sur les propriétés structurales, morphologiques, optiques et photocatalytiques des films. Tous les échantillons ont montré une nature polycristalline avec une phase hexagonale de type wurtzite. Les spectres de diffraction des rayons X ont montré que la cristallisation des films de ZnO dopés à 5 % en masse de Ba était meilleure que celle des échantillons non dopés, avec une orientation préférentielle le long du plan (100). Les images SEM ont révélé que les films étaient bien adhérents et uniformes. Les spectres UV-Vis ont montré que la transmittance des films augmentait avec l'augmentation de la concentration en Ba, démontrant ainsi une meilleure transparence optique. Les films de ZnO dopés à 5 % en Ba ont présenté la meilleure efficacité photocatalytique, atteignant une dégradation de 95,78 % de MB sous irradiation solaire pendant 5 heures. Cet échantillon a montré une stabilité et une réutilisabilité exceptionnelles, conservant ses performances sur cinq cycles.

D'autre part, les films de ZnO dopés à 5 % en Ba, déposés avec différents nombres de cycles, ont montré qu'une augmentation du nombre de cycles de dépôt conduisait à une meilleure cristallinité aux cycles plus élevés. En conséquence, l'efficacité photocatalytique a augmenté pour atteindre 93,51 % après 15 cycles.

De plus, les résultats ont montré que le processus de recuit à 450°C améliore la cristallinité, les propriétés optiques et l'efficacité photocatalytique des films de ZnO dopés au Ba, atteignant une dégradation de 96,17 % de MB, qui a progressivement diminué à 94,89 % après cinq cycles successifs.

Mots clés: Films minces de ZnO dopés au Ba, méthode de SILAR, dégradation photocatalytique, bleu de méthylène.